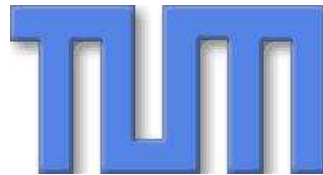# High Energy Astroparticle Physics with Cosmic Rays and Neutrinos

by

PASQUALE DARIO SERPICO

Technische Universität München
Physik Department
Institut für Theoretische Physik T30d
Univ.-Prof. Dr. Manfred Lindner

MAX-PLANCK-GESELLSCHAFT

Technische Universität München
Physik Department
Institut für Theoretische Physik T30d
Univ.-Prof. Dr. Manfred Lindner

High Energy Astroparticle Physics with Cosmic Rays and Neutrinos

PASQUALE DARIO SERPICO

Vollständiger Abdruck der von der Fakultät für Physik der Technischen Universität München zur Erlangung des akademischen Grades eines

Doktors der Naturwissenschaften (Dr. rer. nat.)

genehmigten Dissertation.

Vorsitzender: Univ.-Prof. Dr. L. Oberauer
Prüfer der Dissertation: 1. Univ.-Prof. Dr. M. Lindner
                         2. Hon.-Prof. Dr. G. Hasinger

Die Dissertation wurde am 23.01.2006 bei der Technischen Universität München eingereicht und durch die Fakultät für Physik am 03.04.2006 angenommen.

Summary

Current experiments in ultra-high energy cosmic ray and high energy neutrino physics may open new observational windows to the universe. In this dissertation I clarify the motivation and the challenges of ultra-high energy cosmic ray astronomy, and discuss in detail the opportunities for neutrino mixing studies at the next-generation neutrino telescopes.

In particular, I present a technique to properly evaluate the expected anisotropy in the ultra-high energy cosmic ray arrival distribution starting from a given astronomical catalogue of the local universe. By applying this method to the IRAS PSCz catalogue of galaxies, I establish the minimum statistics needed to significantly reject the hypothesis that ultra-high energy cosmic rays trace the baryonic distribution in the universe. A forecast for the Auger experiment is provided.

I also treat the influence of the Galactic magnetic field on the arrival directions of ultra-high energy cosmic rays. If the Galactic magnetic field was known with sufficient precision, it could be used as a spectrograph to discriminate among source models and primaries of ultra-high energy cosmic rays. I compare several Galactic magnetic field models and discuss for the example of the AGASA data how the significance of small scale clustering or correlations with proposed astrophysical sources are affected by the Galactic magnetic field.

Deflections of charged particles induced by the Galactic magnetic field and claims of anisotropies in cosmic ray data around 10^{18} eV could point to neutron beam sources in the primary flux of ultra-high energy cosmic rays. If neutron beams do exist, they might open interesting perspectives to probe neutrino mixing at neutrino telescopes. After an introduction to the field of high energy neutrinos, the new topic of neutrino flavour mixing studies at high energy telescopes is detailed, and other sources and observables suitable to that purpose are discussed.

Contents

Preface

E tirato dalla mia bramosa voglia, vago di vedere la gran commistione delle varie e strane forme fatte dalla artifiziosa natura [. . .] pervenni all' entrata di una gran caverna, dinanzi alla quale [. . .] subito si destarono in me due cose: paura e desiderio; paura per la minacciosa oscura spelonca, desiderio per vedere se là entro fussi alcuna miracolosa cosa.

Leonardo da Vinci

Since the time of Galilei and Newton, one of the fundamental pillars of modern physics is the realization that the terrestrial and cosmic systems obey the same basic laws. Astroparticle physics is the modern attempt to probe the properties of elementary fields by mean of astrophysical and cosmological systems or, vice versa, to apply the particle physics knowledge to understand astrophysical or cosmological issues. In the 21st century, the electromagnetic radiation still remains the main source of astronomical information. Extending the detectable band from visible light to the whole spectrum from radio-waves to gamma rays has represented the greatest astronomical achievement of the 20th century, with far-reaching consequences for physics as well. Using radiation of a different nature (cosmic rays, neutrinos, and eventually gravitational waves) could substantially change our view of astronomical objects, offering new celestial laboratories to explore fundamental physics.

This thesis deals with key aspects of the physics and astrophysics of high energy cosmic rays and neutrinos, and of their deep inter-connection. In Chapter 1 we summarize the current knowledge of cosmic ray astrophysics, the detection techniques, and the open issues in the field. In particular, the topic of "ultra-high energy cosmic ray astronomy" is introduced. Given the pervasive presence of magnetic fields in the cosmos, the feasibility of an astronomical program with charged particles at ultra-high energies is not guaranteed. This crucial question will be hopefully answered by the Pierre Auger Observatory, which is almost completed.

The first part of the thesis is devoted to explore some aspects of this issue. Cosmic rays at the highest observed energies (above 10^{19} eV) are expected

to suffer relatively small deflections in the cosmic magnetic fields. While the importance of the extragalactic magnetic fields is still debated, the existence of a large scale magnetic field in our Galaxy is an observational fact which has surely an important impact on charged particles' deflections. This in turn affects the statistical analysis of the small scale properties of the observed arrival directions. In Chapter 2 we compare several Galactic magnetic field models to evaluate the expected deflection patterns, and discuss for the example of the AGASA data how the significance of small scale clustering or correlations with given astrophysical sources are influenced by the Galactic magnetic field. The possibility to use the Galactic magnetic field as a "spectrograph" to discriminate among source models and primaries of ultra-high energy cosmic rays is analyzed. Such a diagnostic tool could sharpen our chances to use the highest energy particles of the universe to probe center-of-mass energies much larger than in any existing or planned accelerator, and might then help to find possible imprints of new physics. These issues were treated in our article

[I] M. Kachelrieß, P. D. Serpico and M. Teshima, "The Galactic magnetic field as spectrograph for ultra-high energy cosmic rays," astro-ph/0510444.

At energies above about 5×10^{19} eV the mean free path for proton interactions drops drastically, because the photo-pion production on the cosmic microwave background is energetically allowed. This implies that the volume of the universe that can be probed via cosmic rays is significantly reduced. An interesting consequence is that the pattern of the cosmic ray source distribution should be imprinted in the large scale anisotropies of the data, provided that cosmic magnetic fields are not too strong and that the heavy nuclei component of the cosmic ray flux is negligible. In Chapter 3 a careful treatment of a large scale catalogue of galaxies is performed to evaluate the expected signal if cosmic ray sources correlate with the luminous baryonic structure of the local universe. A chi-square approach is used to provide a forecast for testing this hypothesis at the Auger experiment. These calculations were presented in

[II] A. Cuoco, R. D' Abrusco, G. Longo, G. Miele and P. D. Serpico, "The footprint of large scale cosmic structure on the ultra-high energy cosmic ray distribution," JCAP **01**, 009 (2006) [astro-ph/0510765].

High energy astrophysical neutrinos are the topic of the second part of the thesis. The observations of ultra-high energy hadrons is a convincing

argument that extraterrestrial high energy neutrinos should exist. In Chapter 4 we review the field of high energy neutrinos, introducing the expected signals, the detection principles and the current and planned experiments. Given the important discoveries in the field of neutrino oscillations of recent years, it is worthwhile to explore what are the chances that these instruments and the new astrophysical targets they will disclose might have for neutrino mixing phenomenology. This issue is detailed in Chapter 5, which is based in particular on the papers

[III] P. D. Serpico and M. Kachelrieß, "Measuring the 1-3 mixing angle and the CP phase with neutrino telescopes," Phys. Rev. Lett. **94**, 211102 (2005) [hep-ph/0502088].

[IV] P. D. Serpico, "Probing the 2-3 leptonic mixing at high-energy neutrino telescopes," Phys. Rev. D **73**, 047301 (2006) [hep-ph/0511313].

The thesis ends with a concluding discussion in Chapter 6.

During the period spent as a Ph.D. student at the Max-Planck-Institut für Physik in Munich, I have also worked in other fields of astroparticle physics phenomenology, not covered in this dissertation. I briefly summarize these other lines of research.

Primordial nucleosynthesis and nuclear astrophysics
Following my laurea thesis in Naples and the preliminary results presented in [V], I have performed (in collaboration with the Naples astroparticle group) a detailed analysis of nuclear reaction uncertainties entering the primordial nucleosynthesis network, providing a new regression protocol and nuclear database [VI].

A collaboration with nuclear astrophysics experimental groups of Naples and Bochum (LUNA, ERNA) is ongoing to study the feasibility of laboratory measurements of some interesting reactions.

[V] A. Cuoco, F. Iocco, G. Mangano, G. Miele, O. Pisanti and P. D. Serpico, "Present status of primordial nucleosynthesis after WMAP: results from a new BBN code," Int. J. Mod. Phys. A **19**, 4431 (2004) [astro-ph/0307213]

[VI] P. D. Serpico, S. Esposito, F. Iocco, G. Mangano, G. Miele and O. Pisanti, "Nuclear Reaction Network for Primordial Nucleosynthesis: a detailed analysis of rates, uncertainties and light nuclei yields," JCAP **0412**, 010 (2004) [astro-ph/0408076].

Neutrino diffuse backgrounds from the early universe

Some attention has been paid to the cosmological neutrino backgrounds. We have characterized a new, diffuse cosmic source of neutrinos from the early universe: The neutrinos from the first generation of stars, the so-called PopIII [VII]. Unfortunately, a direct detection is at present out of question: Although this flux is comparable to the diffuse neutrino flux produced by the ordinary stars and core-collapse supernovae, due to the large cosmic redshift the typical energies are in the MeV and sub-MeV range where the solar and geophysical neutrino fluxes are much larger.

We also had a fresh look at the bounds to a non-zero chemical potential in the cosmic neutrino background [VIII], in particular via primordial helium. Its importance as one of the few tests of the cosmological standard assumption that sphaleron effects equilibrate the cosmic lepton and baryon asymmetries was emphasized.

In collaboration with members of the Valencia and Naples astroparticle groups, detailed calculations of the cosmic neutrino background spectral properties were performed and phenomenological consequences for primordial nucleosynthesis, cosmic microwave background and large scale structure have been derived [IX]. The effects of the neutrino oscillations in a 3×3 formalism and the QED plasma corrections to the reheating phenomenon following $e^\pm$ annihilation have been taken into account. A study of possible signatures of non-standard neutrino interactions (like flavour violating neutral currents) is in progress.

[VII] F. Iocco, G. Mangano, G. Miele, G. G. Raffelt and P. D. Serpico, "Diffuse Cosmic Neutrino Background from Population III Stars," Astropart. Phys. **23**, 303 (2005) [astro-ph/0411545].

[VIII] P. D. Serpico and G. G. Raffelt, "Lepton asymmetry and primordial nucleosynthesis in the era of precision cosmology," Phys. Rev. D **71**, 127301 (2005) [astro-ph/0506162].

[IX] G. Mangano, G. Miele, S. Pastor, T. Pinto, O. Pisanti and P. D. Serpico, "Relic neutrino decoupling including flavour oscillations," Nucl. Phys. B **729**, 221 (2005) [hep-ph/0506164].

Dark matter and axion physics

"Dark matter" and "dark energy" are among the most puzzling unsolved issues in cosmology and particle physics. SUSY neutralinos are the most promising dark matter candidates, but other possibilities can not be excluded. In [X], we have studied several astrophysical and cosmological consequences and bounds of an intriguing model of MeV-mass, scalar dark matter candidate proposed by C. Boehm and P. Fayet, and of a generalization of it.

The axion, a hypothetical particle which was originally proposed in order to solve the so-called CP-problem of strong interactions, is another prime candidate for dark matter. I am a member of the CAST collaboration, a CERN experiment for the direct search of solar axions [XI]. I have numerically recalculated the expected solar fluxes (including the transversal profile of the flux as a function of the impact parameter on the Solar disk) on the basis of the most recent solar model. I checked that the prediction does not depend significantly on the details of the solar models, as expected. The output of both calculations, available in electronic format, is actually used in the collaboration.

The nature of the dark energy is even more problematic for fundamental physics. As an alternative explanation to the cosmic acceleration shown by the SNIa data, C. Csaki, N. Kaloper and J. Terning have invoked the conversion of axion-like particles into photons in presence of intergalactic magnetic fields. In [XII] we have discussed a stringent constraint from the spectral shape of the cosmic microwave background, which excludes a large part of the parameter space for such a model. When combined with other constraints, it strongly disfavors the scenario, at least as leading mechanism to mimic cosmic acceleration.

[X] P. D. Serpico and G. G. Raffelt, "MeV-mass dark matter and primordial nucleosynthesis," Phys. Rev. D **70**, 043526 (2004) [astro-ph/0403417].

[XI] K. Zioutas *et al.* [CAST Collaboration], "First results from the CERN axion solar telescope (CAST)," Phys. Rev. Lett. **94**, 121301 (2005) [hep-ex/0411033].

[XII] A. Mirizzi, G. G. Raffelt and P. D. Serpico, "Photon axion conversion as a mechanism for supernova dimming: Limits from CMB spectral distortion," Phys. Rev. D **72**, 023501 (2005) [astro-ph/0506078].

Part I

Astronomy with ultra-high energy cosmic rays

Chapter 1

The status of cosmic rays

In this Chapter we introduce the topic of cosmic rays, with particular emphasis to the high and ultra-high energy regions. After an overview on the present status of the field (Sec. 1.1), we summarize the main features of the models of production and propagation of cosmic rays, with particular emphasis on the theoretical expectations and on the problems connected to the high energy tail of the spectrum (Sec. 1.2). In Section 1.3 we describe the basic features of the detection techniques employed. In Section 1.4 we conclude introducing the sub-topic of ultra-high energy cosmic ray astronomy, to which the first part of this dissertation is devoted. For more complete reviews of the field of ultra-high energy cosmic rays, we address the reader to the papers [Bha98, Nag00] or the monographies [Ber90, Gai90, Sta04, Sok04].

1.1 Introduction

Cosmic rays are a very wide topic, deeply related to many fields of physics, ranging from particle and nuclear physics to astrophysics. The present knowledge on elementary particles was triggered by cosmic rays, with the discovery of the positron in 1932, the muon in 1937, the pion in 1947, and later of the strange particles kaon and Λ-hyperon. Nowadays that the physics at accelerators is starting to fight against both technological and financial limitations, these natural laboratories enjoy renewed interest. Fundamental questions remain however unanswered in cosmic ray physics. From the astrophysical point of view, almost one century after their discovery, we have no definite clue to the origin, acceleration and propagation of cosmic rays, though we recognize that they carry information about our Galaxy, and probably also about the extragalactic space, at least at the highest observed energies.

In a nutshell, we know that cosmic rays at the sea level are mostly
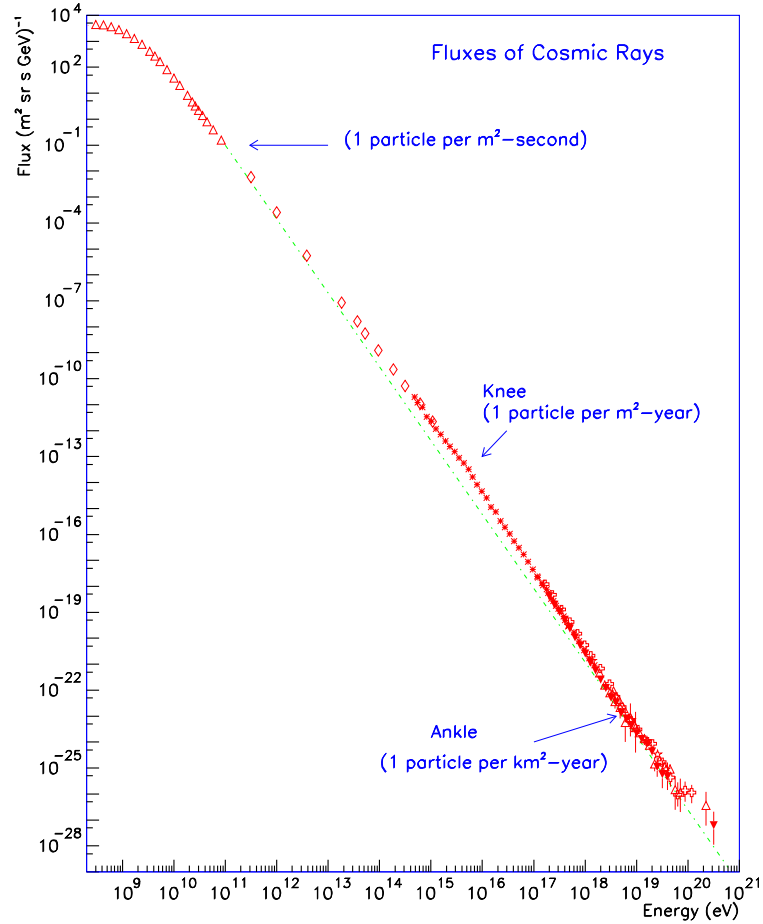
Fig. 1.1.— All particle cosmic ray energy spectrum as compiled by S. Swordy [Swo97]. The breaks of the power law spectrum at the knee and at the ankle are indicated.

$\mu^{\pm}, e^{\pm}, \gamma$, a few hadrons and many ν (the so-called atmospheric neutrinos) with an integrated flux of charged particles of about 200 m^{-2} s^{-1}. These are secondary particles generated in Earth's atmosphere by the so-called primary component, whose content at the top of the atmosphere is roughly 90% protons, 9% He nuclei, 1% of heavier nuclei up to iron, 1% $e^{\pm}$ and a small component of γ, of the order of 0.01%. Cosmic rays present an almost featureless energy-spectrum which extends over more than eleven decades up to at least 10^{20} eV, where the flux is lower than one particle km^{-2} century^{-1} (see Fig. 1.1). The main physical observables are the arrival directions, the chemical composition and energy spectra of the primaries, while at the highest energies also the arrival times provide interesting information.

The GeV and sub-GeV energy range is strongly influenced by the Solar magnetic modulation and also includes some contribution of Solar-injected particles. These particles constitute both numerically and energetically the bulk of the cosmic ray primaries, and their deflections in the Earth's magnetic field were historically crucial to understand the charged particle nature of Hess' "Kosmische Strahlung". Nowadays, this range still plays an interesting role for particle physics, in particular for indirect searches of dark matter via its annihilation products: anti-nuclei, positrons, gamma-rays, and neutrinos [Jun96, Beg98, Mau02]. The low energy range will not be treated further in this dissertation.

At higher energies the spectrum behaves like a power-law, $\mathrm{d}N/\mathrm{d}E \propto E^{-\gamma}$, with $\gamma \simeq 2.7$. The only distinct features are: i) A change in the index γ from 2.7 to 3.1 around 3 PeV (knee); ii) a possible second knee around 4–8×10^{17} eV; iii) a flattening again to $\gamma \simeq 2.7$ at about 5×10^{18} eV (ankle) (see Fig. 1.1). At the 29$^{\mathrm{th}}$ International Cosmic Ray Conference in 2005, the HiRes collaboration has also claimed strong evidence (almost $5\,\sigma$) in favour of a suppression of the flux at $E \gtrsim 5 \times 10^{19}$ eV (see also [Bem05]). This awaits further confirmation, but "the end of cosmic ray spectrum" at energies around 10^{20} eV is theoretically expected, as will be discussed in the following Section.

1.2 Production sites, acceleration and propagation

The nature of the sites and mechanisms of acceleration of cosmic rays is still an open question in high energy astrophysics, together with a full characterization of the background fields in which their propagation takes place. For the cosmic rays maybe up to the second knee, the standard paradigm invokes acceleration of the particles in shock waves in supernova remnants. A simple energy balance argument supports this scenario, once considering the parameters of Galactic size and supernova (SN) rate and energy release.

From a dynamical point of view, the acceleration is explained via the gradual energy transfer from the macroscopic waves of magnetized plasma to the particles filling the surrounding medium, through their repeated encounters. In this mechanism first proposed by Fermi [Fer49], the energy gain of the particles appears as a consequence of the relativistic boosts from the laboratory (lab) to the center-of-mass (CM) frame. According to the coherent or random nature of the motion of the magnetized clouds, an energy gain respectively linear or quadratic in the clouds' velocity β is achieved. Also, a non-thermal

power law is predicted and, in particular in the first order mechanism, with a spectral index slightly steeper than 2 and only weakly dependent on the details of the acceleration. Once taking into account propagation effects that steepen the spectrum, this model nicely reproduces the observed features of cosmic rays, though very little direct experimental evidence for the validity of the mechanism exists. Probably, the most interesting hints for hadronic acceleration come from the observations of very high energy gamma ray emission from supernova remnants which are "orphan" (invisible) in X-rays, thus disfavoring a leptonic emission process. Neutrinos from Galactic accelerators would be a smoking gun for hadronic acceleration, but as we will see in Chapter 4 they are difficult to detect, even in forthcoming experiments.

Both due to acceleration and confinement effects, the standard expectation is that the chemical composition becomes heavier at and after the knee, so that cosmic rays should turn from proton-dominated at $E \lesssim$ few $\times 10^{15}$ eV to iron dominated at $E \simeq 10^{17}$ eV. This is quite a generic prediction that however lacks unambiguous direct evidence. At the highest energies, say $E \gtrsim E_{\mathrm{ankle}}$, the Galactic magnetic field (GMF) can not confine the particles, which on the other hand do not correlate with Galactic structures. An extragalactic origin is then extremely likely for the so-called ultra-high energy cosmic rays (UHECRs). For astrophysical engines to confine and potentially accelerate particles, sufficiently strong and extended magnetic fields are required. The maximum energy attainable for a particle of charge $Z e$ is determined by the time it can be confined in the acceleration region, which in turn depends on the size L of the region and on the magnetic field strength B,

$$E_{\max} \sim \Gamma Z e B L = 10^{23} \, \text{eV} \, \Gamma \, Z \, \frac{B}{\text{Gauss}} \frac{L}{\text{kpc}}, \tag{1.1}$$

where Γ is a possible Lorentz boosting factor of the entire medium with respect to the observer. Equation (1.1) provides the so-called Hillas criterion [Hil84], which can be described graphically by plotting the magnetic field of possible sources against their typical size ("Hillas plot", see Fig. 1.2). Upper limits to the maximum attainable energies for a fixed primary charge are then represented by straight lines from the upper-left to the lower-right corner of the plane. Of course, other conditions should be fulfilled by a realistic accelerator: For example, the energy loss within the acceleration site implies a more stringent constraint than the Hillas criterion. Similar considerations also hold for other acceleration scenarios, like the one in a pulsar magnetosphere.

A plethora of possible acceleration sites has recently been reviewed [Tor04]. This zoo includes neutron stars, radio galaxies, quasar remnants, star-bursts, and colliding galaxies. However the most promising ones
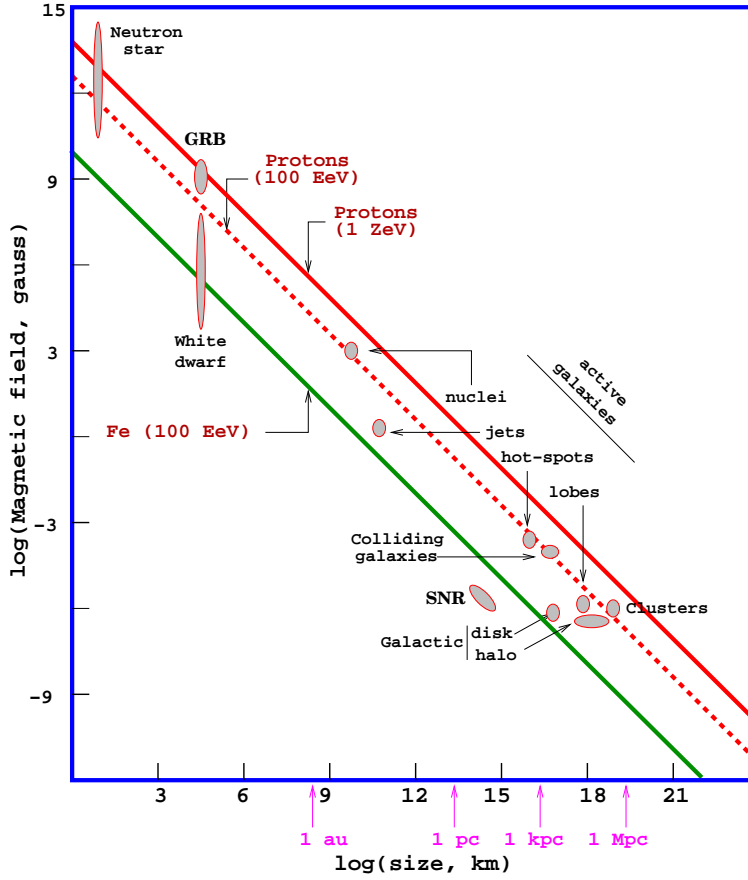
Fig. 1.2.— Hillas diagram showing size and magnetic field strengths of possible sites of particle acceleration [Anc02]. Eq. (1.1) implies that objects below the diagonal lines (from top to bottom), can not accelerate protons above 10^{21} eV, 10^{20} eV and iron nuclei above 10^{20} eV, respectively.

are active galactic nuclei (AGN) and gamma ray bursts (GRBs).

- AGN are the most powerful radiation emitters in the universe. Their observed photon spectrum ranges from radio waves to TeV energies. Their energy is presumably supplied by the gravitational accretion of matter around a super-massive black hole ($M \sim 10^8 M_\odot$) hidden in the AGN core. For an introduction to the physics and astrophysics of these objects see [Pet97, Kro99]. Protons could be accelerated by the first-order Fermi mechanism up to $E_{\max} \sim 10^{20}$ eV at accretion shocks at some distance from the central black hole [Pro92], or also

in the relativistic jets and external hot spots [Rac93]. Blazars—that are believed to be AGN pointing their relativistic jets towards us—and in particular their subclass of BL Lac objects, are among the best candidates for UHECR acceleration.

- During their short existence of a few seconds or less, GRBs are the brightest gamma ray sources in the universe. They have puzzled astrophysicists for a long time. Convincing observations have emerged in recent years proving that they have an extra-galactic origin, and that they are likely connected to cataclysmic processes involving the death of massive stars, at the least for the sub-class of long-duration bursts. Although we do not yet understand the internal mechanisms that generate GRB, the "relativistic fireball" model provides us with a successful phenomenology accommodating observations [Wax03]. It implies that an enormous amount of energy, about 10^{51} erg, must be released within a few seconds at most in a relativistically expanding plasma wind (the "fireball"). In the fireball's internal shocks, protons can be accelerated up to energies of order 10^{21} eV.

Independently of the mechanism responsible for extragalactic cosmic ray production, at $E \gtrsim 5 \times 10^{19}$ eV the universe becomes opaque to protons: The photo-meson interaction process $p + \gamma_{\mathrm{CMB}} \to \Delta \to \pi + N$ is now energetically allowed on the bulk of cosmic microwave background (CMB) photons. Above this threshold, the flux of any source located beyond a distance of about 100 Mpc should be greatly suppressed, a feature predicted in the Sixties by Greisen, Zatsepin, and Kuzmin and later named GZK-cutoff [Gre66, Zat66]. Heavier nuclei have a comparable mean free path with respect to photo-dissociations on CMB photons. Photons have an even shorter mean-free-path, because of pair-production on the tail of CMB and especially on the radio background (see Fig. 1.3). Nonetheless, extremely high energy cosmic rays of $E \gtrsim 10^{19.5}$ eV have been measured by several experiments (see Section 1.3). Moreover, the AGASA collaboration has claimed a clear extension of the spectrum beyond the expected GZK feature [Tak98], thus exacerbating the requirements for astrophysical accelerators. This has motivated the proposal of a whole class of non-standard physics scenarios to overcome the acceleration and/or propagation difficulties: neutrino messengers, super-heavy dark matter, topological defects, violation of Lorentz invariance, etc. (see [Kac04b] for an up-to-date overview on the status of such theories). Ongoing and forthcoming experiments are expected to shed light on the puzzle of the highest energy particles of the universe.
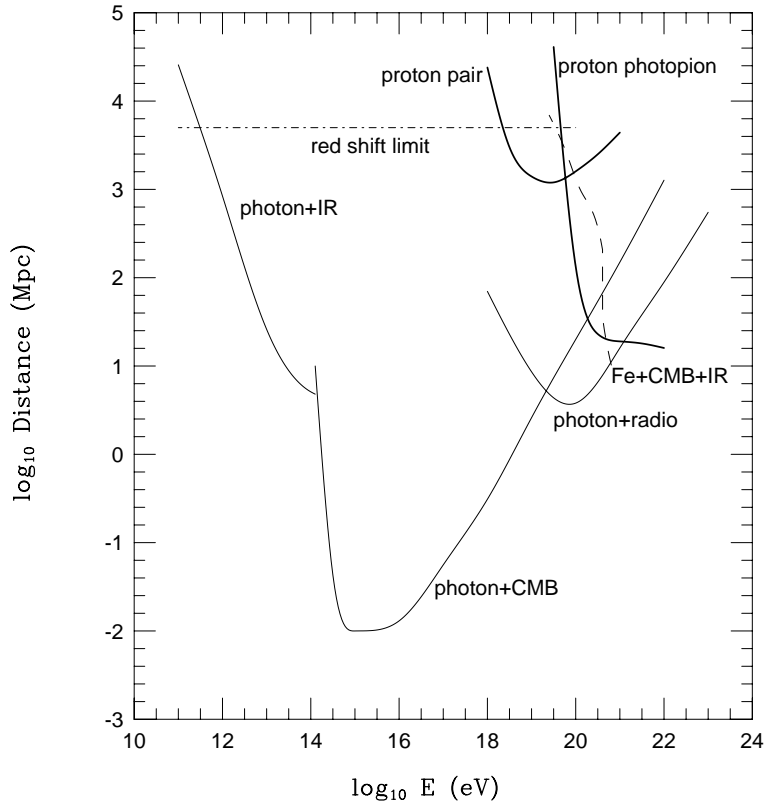
Fig. 1.3.— Attenuation distance of γ's, p's, and ^{56}Fe's in various background radiations as a function of energy [Tor04]. The three lowest and left-most thin solid curves refer to γ-rays, showing the attenuation by infra-red, microwave, and radio backgrounds. The upper, right-most thick solid curves refer to propagation of protons in the CMB, showing separately the effect of pair production and photo-pion production. The dashed-dotted line indicates the adiabatic attenuation length at the present cosmological epoch. The dashed curve illustrates the attenuation of iron nuclei.

1.3   Review of experimental methods

Cosmic rays can be measured via direct and indirect methods. Direct measurements identify the primary charge, mass and energy, by the use of spectrometers and calorimeters, for example. Since the atmosphere behaves as a shield, they must be performed at high altitude (high mountains, stratospheric balloons, satellites), and are thus limited in the exposure area and time. Because of the steeply falling spectrum, such experiments are only useful for $E \lesssim 10^{14}$ eV. It is a lucky coincidence that just at the energy where direct measurements of cosmic rays become inefficient, ground-based meth-

ods start working. Indeed, at energies larger than 10^{14} eV the primaries are studied indirectly through the measurement of the secondary particles produced in the atmosphere, that both works as a target and a calorimeter. In Section 1.3.1 we review some basic properties of these secondary particle cascades, in Section 1.3.2 we summarize the techniques used for their detection, while Section 1.3.3 is devoted to the very delicate issue of the determination of primary species. Historical and current experiments in the field of UHECRs are reviewed in Section 1.3.4.

1.3.1   Air shower cascades

After interacting with the atmosphere, the primary particle starts a cascade. At each generation the number of particles grows while the average energy decreases, until a maximum number of secondary particles N_{max} (nearly proportional to the primary energy E) is reached at a depth X_{max} in the atmosphere. Below the critical energy E_c, which depends on the particle species, the energy losses (mainly via ionization of atmospheric atoms) dominate over particle multiplication processes, and the shower size decreases as a function of depth. Most of the produced particles in each hadronic interaction are π and K mesons. K and $\pi^{\pm}$ decay into μ and ν, thus producing the most penetrating component of the atmospheric showers. The decays of π^0 into photons are the main responsible of the electromagnetic shower of γ and $e^{\pm}$, that constitute the majority of the particles of the shower. These atmospheric showers composed of millions (or billions!) of particles are known as extensive air showers (EAS). The longitudinal evolution of an EAS is a function of the nature and energy of the primary particle, and is naturally described in terms of the shower depth X, defined as

$$X \equiv \int_{h_{\mathrm{exp}}}^{\infty} \mathrm{d}h \, \frac{\mathrm{d}l}{\mathrm{d}h} \, \rho(h), \qquad (1.2)$$

where $\rho(h)$ is the atmospheric density profile, h_{exp} the altitude of the observational site, and $l(h)$ is the particle trajectory as a function of the altitude. For showers that are not too inclined with respect to the vertical direction, $\mathrm{d}l/\mathrm{d}h \simeq 1/\cos\theta_z$, θ_z being the zenith angle.

The electromagnetic longitudinal profile, i.e. the number of charged particles $N_{\pm}(X)$, is well described by the Greisen formula [Gre56],

$$N_{\pm}(X) = \frac{0.31}{\sqrt{T_{\mathrm{max}}}} e^T s^{-3T/2}, \qquad (1.3)$$

where $T \equiv X/X_{\pm}$ is the atmospheric slant depth measured in radiation lengths $X_{\pm} \simeq 37 \, \mathrm{g/cm^2}$ (i.e. the grammage needed to attenuate the energy of

an electromagnetic cascade by a factor $1/e$). The other parameters entering Eq. (1.3) are $T_{\max} \equiv X_{\max}/X_{\pm}$ and the shower age $s \equiv 3T/(T + 2T_{\max})$. Heitler's model of an electromagnetic cascade [Hei84] gives an intuitive understanding of basic properties of the shower, whose development is imagined as a sequence of generations. At each generation, a photon converts into an $e^{\pm}$ pair and each $e^{\pm}$ is assumed to emit a γ, the size of the shower thus doubling. The shower maximum is easily estimated as[1] $N_{\max} = E/E_c$ and requires a number of generations n given by $2^n = N_{\max}$, or $n = \log(E/E_c)/\log 2$. The maximum size occurs at $X_{\max} = n\,X_{\pm}\,\log 2$.

For a nucleon-induced cascade, most of the produced particles in each hadronic interaction are pions. Isospin symmetry suggests that at each generation $1/3$ of the energy goes immediately into the electromegnatic cascade (mainly via π^0 decay), and after n generations, only $(2/3)^n$ (usually less than 10%) of the energy remains in the hadronic channel, that eventually will go almost all in neutrinos and muons. A shower initiated by a nucleus of mass A almost behaves as A independent nucleonic showers each with an energy $1/A$ of the original one. This "superposition model" is useful to understand the features of a heavy nucleus cascade. The longitudinal profile for an hadronic cascade can not be calculated analytically, but it is well fitted by a Gaisser-Hillas functional form,

$$N_{\pm}(x) = N_{\max} \left(\frac{x}{w}\right)^w e^{w-x}, \qquad (1.4)$$

where $x \equiv (X - X_0)/\lambda$, $w \equiv (X_{\max} - X_0)/\lambda$, and $(N_{\max}, X_{\max}, X_0, \lambda)$ are four fit parameters. Often $\lambda = 70$ g/cm^2 is fixed, thus performing a three-parameter fit. More properly, what is measured is the energy deposition rate $\mathrm{d}E/\mathrm{d}X$, which however is proportional to the number of charged particles of the shower reported in Eq. (1.4).

The lateral distribution function of shower particles, denoted by $S(d)$, describes the particle density as a function of the distance d from the shower core. It depends on the average transverse momentum of the hadronic component, as well as on the multiple Coulomb scattering for the electromagnetic component. It is usually fitted with some analytical functions, crucially dependent on the shower age s. Note that azimuthal symmetry is implied by the use of the $S(d)$. This approximation fails for very inclined showers, where the effect of Earth's magnetic field, of the gradient of air density perpendicular to the shower axis, etc. can only be taken into account by simulations. For further details, see [Som04].

---

[1]Note however that the estimate considering the typical value $E_c \simeq 81$ MeV would overshoot by more than one order of magnitude the constant of proportionality suggested by simulations, $N_{\max} \sim E/(1.6\,\mathrm{GeV})$.

1.3.2   Detection techniques

Broadly speaking, EAS can be studied by detecting the secondary particles at ground level or by recording radiation from the shower front as it traverses the atmosphere. Actually modern EAS detectors tend to combine both techniques to sharpen the determination of shower parameters, ensure a better control over systematic errors, and allow inter-calibration of the techniques. This hybrid approach is actually the key tool in the experiments currently constructed, such as the Pierre Auger Observatory.

Surface Arrays

Direct detection of shower particles is the most commonly used method and involves constructing an array of sensors spread over a large area to sample particle densities as the shower arrives at the Earth's surface. Detection methods (all with duty cycles almost of 100%) include scintillator arrays and Cherenkov water tank arrays. Usually the energy, arrival time and directions of the secondary particles are recorded. After the discovery of EAS by Pierre Auger in 1938, the "modern" development of this technique was started at the Agassiz Station of the Harvard College Observatory, a work carried out between 1954 and 1957 [Cla57]. The existence of primary particles with energies greater than 10^{18} eV was established by the observation of one shower with more than 10^9 particles. Shielded or underground detectors are sometimes used in combination with surface array. They sense the muon fraction of the shower, which provides useful constraints on the chemical composition of the primaries (see Section 1.3.3).

The arrival times of the shower front at different surface stations allow one to reconstruct the shower axis. At least three non-collinear stations are required in the limit of planar geometry for the shower front. More stations are required for a characterization of its curvature. From the determination of the shower axis one can also infer the depth in the atmosphere X at which the shower is observed. The depth X is fixed by the height of the array above the sea level and the zenith angle of the event (see Eq. (1.2)).

The lateral distribution function $S(d)$ is another observable reconstructed in surface arrays. Although a detailed prediction of $S(d)$ is quite model-dependent, simulations allow to determine a certain distance d_E which optimizes the sensitivity of $S(d)$ to the primary energy, minimizing the model uncertainties and the dependence from the primary species. Then, while the shape of $S(d)$ is almost independent of energy, the value of $S(d_E)$ is often quoted as an energy-estimator. The distance d_E depends on the properties of the array, and in particular on the grid spacing (for example, $d_E \simeq 600$ m

for AGASA, and $d_E \simeq 1000$ m for Auger).

Atmospheric detectors

Atmospheric detectors measure the longitudinal development of the shower. Air Cherenkov detectors fall in this class, but for the purposes of UHECR studies nitrogen fluorescence detectors have proven to be much more powerful. These telescopes measure the fluorescence light emitted isotropically when atmospheric N_2 molecules are excited by the passage of charged particles. The emitted light is typically in the 300–400 nm ultraviolet range to which the atmosphere is quite transparent. Under favorable atmospheric conditions, EAS can be detected at distances as large as 20 km by telescopes of photo-multipliers covering a large effective area. However, observations can only be done in clear moon-less nights, resulting in an average 10% duty cycle. The implementation of the fluorescence technique has been pioneered in the desert of Utah, where the group from the University of Utah built a device containing two separate "Fly's Eyes" [Bal85a] that has monitored the sky from 1986 until 1993.

In a fluorescence detector, an air shower is seen as a spot of light moving downwards in the atmosphere at the speed of light. The track of the spot registered on the pixels of the mirrors defines a great circle in the sky, that together with the eye's location determines the shower-detector plane. If at least two telescopes at different locations see the event, then the geometry can be fully reconstructed (stereo reconstruction method). In principle, the energy determination in a fluorescence detector is straightforward and reduces to the determination of the total yield of emitted fluorescence light. The method has only a slight dependence on the hadronic primary assumed (error of about 2.5%), but in practice other systematics dominate over this limiting factor: The intrinsic fluctuation of the non-electromagnetic fraction of the energy, the dependence on the properties of the atmosphere, the lack of detailed knowledge of the absolute fluorescence efficiency, the partial degree of observation of the longitudinal development, contaminations from Cherenkov light, and so forth. The determination of the effective aperture of these instruments is another highly non-trivial issue [Pal05].

Finally, note that optical Cherenkov and fluorescence light are not the only radiation emitted during the shower development. Indeed, the column of ionized air produced by the shower can be also studied in radio-waves, by using radar echoes. This idea suggested already in 1940 [Bla40], has been recently re-explored [Gor00] as either an independent method to study air showers, or as a complement to existing fluorescence and surface

detectors. Recently, this technique has been successfully applied to EAS detection [Fal05], and the perspectives in forthcoming years seem very promising [Fal02, Fal04].

1.3.3   Chemical composition

While indirect detection of EAS is a relatively easy task, extracting precise information has proven exceedingly difficult because of the highly indirect method of measurement. Probably the most difficult parameter to extract is the primary particle species. The CR primary particles must be stable and, if charged, heavy enough not to lose too easily energy in the Galactic and intergalactic media. These conditions only allow nuclei (including protons), photons and neutrinos as standard model candidate primaries.

Neutrinos have very peculiar signatures at UHECR detectors, a topic that will be treated in some detail in Section 4.2.5. At present only upper limits on their flux have been obtained.

One way to distinguish in a statistical sense photon and hadron primaries is to compare the rate of vertical to inclined showers, a technique which exploits the attenuation of the electromagnetic shower component for large slant depths. This was the technique applied in [Ave00] using Haverah Park data to conclude that above 10^{19} eV, less than 48% of the primary UHECRs can be photons and above 4×10^{19} eV less than 50% can be photons (both bounds at the 95% confidence level, C.L.). At present, the most stringent upper limit on the photon fraction comes however from the study of X_{max} (see below): Auger preliminary data imply that no more than 26% of events at $E \geq 10^{19}$ eV can be induced by photons [Ris05].

The absence of clear photon or neutrino candidate events at present is not unexpected in astrophysical models for UHECRs, since ν and γ are only produced as secondary particles. On the other hand, this is already challenging for exotic models of UHECR production, such as the top-down scenarios, predicting a large photon fraction in the primaries, or Z-burst scenarios, where a large photon primary component is accompanied by a huge neutrino flux.

Up to now, all the indirect evidence suggests that UHECRs are mostly hadronic particles. Unfortunately distinguishing between a proton and a heavier nucleus shower is extremely difficult at the highest energies. A powerful way (at least in principle) to determine the primary species is achieved by measuring the correlation between different components, e.g. number of $e^{\pm}$ vs. number of $\mu^{\pm}$. Since muons are mainly produced via nuclear processes, it is clear that—for a fixed energy E—the relative number
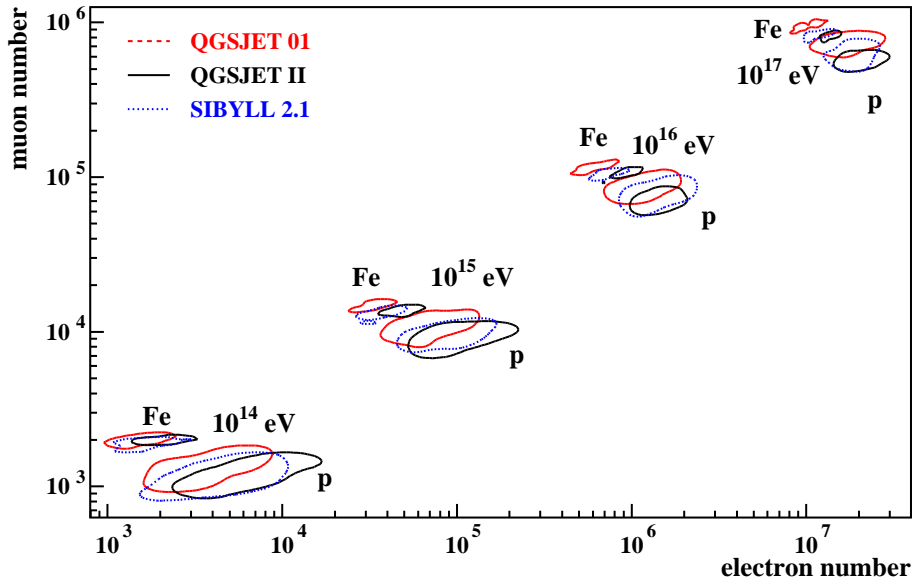
Fig. 1.4.— Number of muons vs. number of electrons at different lab energies, as resulting from proton and iron EAS simulations based on different hadronic interaction models [Eng05].

of muons for a hadronic primary is significantly larger than for a photon one. But more muons are also expected when a heavier nucleus instead of a proton triggers the shower. Indeed, the superposition model implies that heavy nuclei showers develop and attenuate earlier in the atmosphere, since they have less energy per nucleon. Nucleons of lower energies produce lower energy mesons, which decay more often than the higher energy ones, thus giving rise to more μ. Quantitatively, the number of muons grows with primary proton energy E roughly as $N_\mu^p = \alpha E^\beta$, with α and β only weakly dependent on the energy. The superposition model tells us that

$$N_\mu^A \simeq A \times \alpha (E/A)^\beta = A^{1-\beta} N_\mu^p. \qquad (1.5)$$

Simulations show that, at ultra-high energies, $\beta \simeq 0.93$ and thus that an iron nucleus produces a shower with around 30% more muons than a proton shower of the same energy. Unfortunately, the uncertainty of hadronic models makes this method very model-dependent, especially at high energies (see Fig. 1.4).

A more robust method for the estimate of the primary properties is based on the determination of the depth of maximum longitudinal development of the shower, $X_{\max}$. The quantity $X_{\max}$ increases with primary energy as more cascade generations are required to degrade the secondary particle energies;

for showers of a given total energy, heavier nuclei have smaller $X_{\max}$ because the shower is already subdivided into A nucleons when it enters the atmosphere. Specifically, the way the average depth of maximum $\langle X_{\max}\rangle$ changes with energy depends on the primary composition and particle interactions according to (see also Section 1.3.1)

$$\langle X_{\max}\rangle = D_e \ln\left(\frac{E}{E_0}\right),\qquad(1.6)$$

where D_e is the so-called elongation rate and E_0 is a characteristic energy that depends on the primary species [Lin81]. For a nucleus of mass number A, once again the superposition principle suggests the relation $E_0 \propto A$, that indeed is approximatively confirmed by simulations. In fluorescence detectors, $\langle X_{\max}\rangle$ and D_e can be determined directly from the longitudinal shower profiles, see Eq. (1.4); E_0 and thus the composition can be extracted after estimating E from the total fluorescence yield, i.e. the integral over X of the Eq. (1.4). Moreover, the fluctuation expected around the average depth $\langle X_{\max}\rangle$ are larger for protons than for heavy nuclei, whose showers are approximately an average of A single nucleon showers.

The status of present analyses (assuming for simplicity a bi-modal composition proton-iron) is summarized in the "estimated iron fraction" shown in Fig. 1.5 (see also [Wat04]). We can recognize some trend suggesting a transition to lower $\langle A\rangle$ moving from energies $E \simeq 10^{17}$ eV to $E \gtrsim 10^{19}$ eV, but it is clear that in view of the low statistics at the end of the spectrum and the wide variety of uncertainties in these experiments, one may conservatively say that this is not a closed issue.

A natural question suggested by the previous discussion is why the extraction of precise information on EAS primaries, and the chemical composition in particular, is so challenging. The ultimate reasons are that: i) the first generations of particles in the cascade are subject to inherent fluctuations and consequently this limits the event-by-event resolution of the experiments; ii) the center-of-mass energy of the first few cascade steps is well beyond any reached in collider experiments, as also shown in Fig. 1.6. Therefore, one needs to rely on hadronic interaction models that attempt to extrapolate our understanding of particle physics.

Reliable models are difficult to achieve, since the inelastic part of hadronic interactions of interest is dominated by hadronic emission at limited transverse momentum, $\langle p_T\rangle \sim 0.3$ GeV. Differently from the hard scattering at high p_T which can be predicted relatively well by perturbative QCD, no exact way is known to calculate the bulk of soft, non-perturbative interactions, and one has to rely on more or less phenomenological models. These mod-
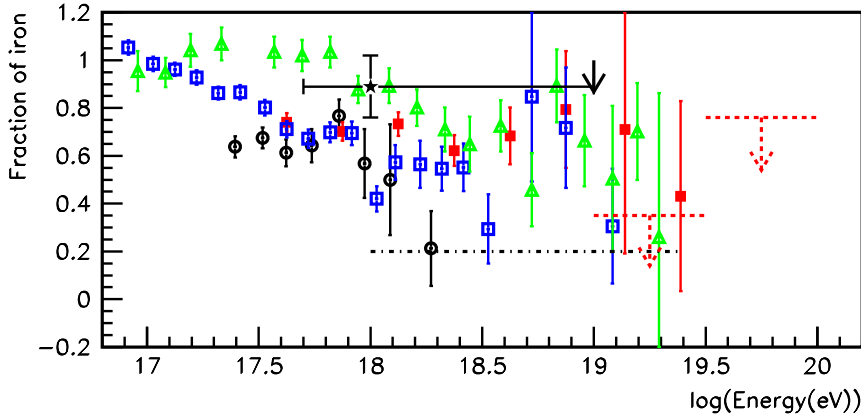
Fig. 1.5.— Iron fraction from various experiments [Anc04]: Fly's Eye (triangles), AGASA A100 (full squares), AGASA A1 (empty squares) using SIBYLL 1.6 and Haverah Park [Ave02], using QGSJET98 (circles). The mean composition determined in [Dov03] with the corresponding error for the Volcano Ranch energy range using QGSJET98 (star) is shown. The solid line arrow indicates the recent result using rise time measurements from Haverah Park [Ave03]. The dashed arrow lines represent upper limits obtained by the AGASA Collaboration with QGSJET98 [Shi03]. The dot-dashed horizontal line corresponds to results reported by the HiRes Collaboration [Arc03].

els are calibrated with the sparse accelerator data available in the forward region, and then extrapolated by one or two decades in the center of mass energy to interpret the EAS data. At present, the different approaches used to model the underlying physics of *pp* collisions show clear differences in multiplicity predictions which increase with rising energy [Anc04]. Experimental programs specifically devoted to the study of cross sections in the forward region are ongoing. For example, exploiting LHC, the most energetic accelerator nowadays in construction at CERN, experiments like LHCf [Sak05] or TOTEM [Egg03] should be able to validate the EAS models at least up to equivalent lab energies of 10^{17} eV (CM energy 14 TeV) for protons. A few years later, much larger energies should be attained in lead-lead ion collisions, and a dedicated heavy ion detector, ALICE, will also operate at this collider.

1.3.4 Status of present experiments

Several experiments have contributed to the study of UHECRs, that we list in the following:
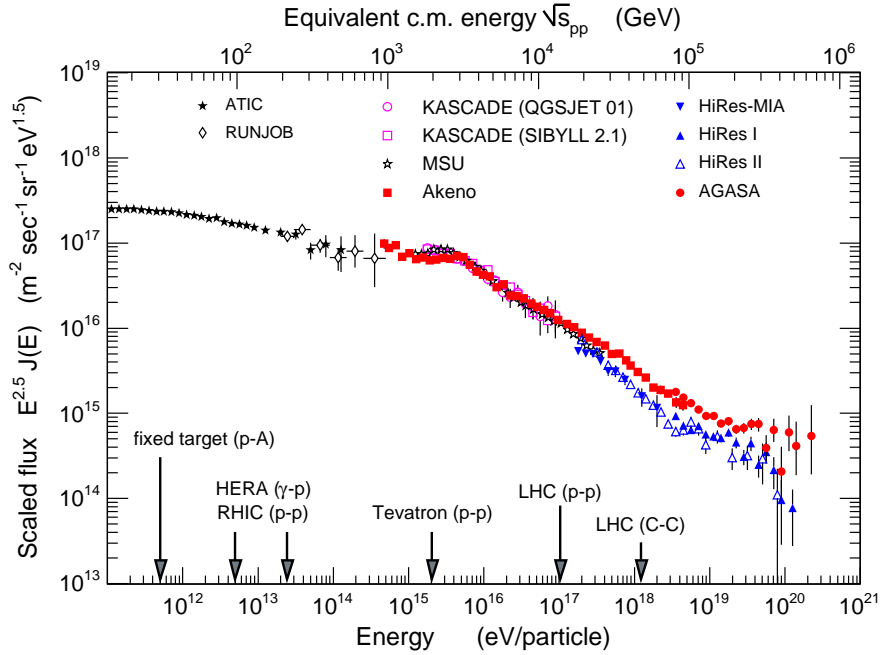
Fig. 1.6.— Primary cosmic ray flux scaled with $E^{2.5}$ compiled by R. Engel [Eng05]. Shown is a selection of recent and older measurements, included for reference. The energy scale reached in current and future accelerators is also shown for comparison.

- *Volcano Ranch* – (New Mexico, 1959 – 1963). This array consisted of 20 scintillator tubes installed in an hexagonal grid with spacing of 884 m, extending over an area of 8 km^2. It was the first experiment to detect an event of energy $\sim 10^{20}$ eV [Lin63] .

- *Sydney University Giant Air-shower Recorder [SUGAR]* – (Australia, 1968 – 1979) This experiment was made of 54 pairs of buried scintillators spaced each other by 50 m, for a total area covered of 100 km^2 [Win86a]. Until recently it has been the only giant detector for EAS in the southern hemisphere.

- *Haverah Park* – (Leeds, UK, 1968 – 1987) Made of water Cherenkov detectors of variable size, it extended over about 12 km^2 [Law91]. It has played a key role in the design of the surface detectors of the Pierre Auger Observatory.

- *Yakutsk* – (Siberia, 1974 – present). This experiment was a pioneer in the test of a multi-instrument approach to EAS detection. It consisted

of 50 air Cherenkov telescopes, 56 surface and 6 shielded scintillators, with a total covered area of about 12 km^2 [Efi91].

- *Akeno Giant Air Shower Array [AGASA]* – (Japan, 1990 – 2003) For longtime AGASA was the largest array in the world with an area of 100 km^2 [Chi91]. It consisted of 111 scintillator detectors on the ground and 27 detectors under absorbers for muons. Each surface detector was placed with a nearest-neighbor separation of about 1 km and the detectors were sequentially connected with a pair of optical fibers. The inner *Akeno* core was instrumented for observations of lower energy events.

- *Fly's Eye* – (Utah, USA, 1982-1993) This pioneering experiment in the fluorescence technique consisted of two stations containing telescopes equipped with photo-multipliers tubes (PMT) [Bal85a]. In 1991, it registered what is still the most energetic particle ever observed, with $E \sim 3 \times 10^{20}$ eV [Bir93].

- *HiRes* – (Utah, USA, 1997-2006) As an up-scaled version of Fly's Eye (14 telescopes in two sites) the High Resolution (HiRes) detector begun operations in May 1997 [Cor92, Abu00]. In monocular mode and taking into account a 10% duty cycle, the effective acceptance of this instrument is about 350 km^2 sr at 10^{19} eV and 1000 km^2 sr at 10^{20} eV— on average about 6 times the Fly's Eye acceptance—and the threshold energy is 10^{17} eV.

Among the previously mentioned experiments, only HiRes and Yakutsk are still taking data, though the latter has been "down-graded" to study a lower energy region. The solutions to many unanswered questions in UHECRs should come with two experiments of the next generation:

- *Pierre Auger Observatory* – [Cro92] (since 2004) The Pierre Auger Observatory (PAO), named after the French physicist that discovered and correctly interpreted EAS, is the largest collaboration ever formed for a cosmic ray experiment. It is an international project involving almost 300 scientists from institutes in four continents. The collaboration plans to build two sites: the southern site is near Malargüe, Argentina, just east of the Andes mountains; it has started operations while still in deployment phase in 2004, and should be completed and fully operational in 2006. A second observatory in the northern hemisphere (probably in southeastern Colorado, USA) could eventually be built to provide full sky coverage. Each site is expected to host about 1600 surface

Cherenkov tanks, covering an area of of 3000 km^2 on a triangular grid of 1.5 km size. Twenty-four fluorescence telescopes (grouped in four sites) sit on the border of the area, looking inside to maximize the number of events detected in hybrid mode.

- *Telescope Array* – [Ara03, Kah05] (beginning 2007) This Japanese-American project is the heir of the AGASA program. The collaboration plans to start observations in 2007, with surface detectors already in construction in the west desert of Utah, roughly one order of magnitude larger than AGASA, and three fluorescence eye stations to exploit the hybrid technique and reduce the systematic error. The main difference with respect to Auger is the coverage of northern sky, and the choice of plastic scintillators (as opposed to water Cherenkov tanks) for the 576 surface stations. An upgrade of the fluorescence component to ten stations is planned as a long term extension of the project.

Although not directly related to UHECRs, the study of the knee region is of particular importance to fix the issue of the chemical composition of cosmic rays, the validation of hadronic models, and the link with direct detection techniques, which in turn is crucial to determine the normalization of the spectrum. The most advanced experiment focusing on this region (and the only one running) is the KArlsruhe Shower Core and Array DEtector (*KASCADE*) [Ant03]. The scintillation detectors of the array (which is sensitive to both $e^\pm$ and muons) are housed in 252 stations on a grid with 13 m spacing, and a central hadronic sampling calorimeter is also installed. An upgrade of the project, named KASCADE-Grande, is ongoing. Present deconvolution techniques prove to be efficient enough to allow at least a rough reconstruction of the chemical composition of the flux, while the limiting factor clearly resides in the hadronic interaction models used in Monte Carlo simulations [Ant05].

1.4   Cosmic ray astronomy?

Almost a century after the discovery of cosmic rays, a satisfactory explanation of their origin is still lacking. The main difficulty is actually the loss of directional information due to the bending of their trajectories in cosmic magnetic fields. In the history of astronomical progress, the positional information has led the way in the astrophysical diagnostics. The loss of directional information prevents us from identifying cosmic ray sources, and as a consequence to shed light on their acceleration mechanisms in an unambiguous way. It is clear that starting the era of "cosmic ray astronomy"

would provide a new tool for astroparticle physics, with crucial consequences for important physics topics: The understanding of chemical composition of cosmic rays could in turn facilitate the study of QCD in the forward region at CM energies much larger than reachable at existing or planned accelerators; a clue to the dynamics of the most powerful astrophysical engines would offer a new tool for astroparticle physics; or maybe physics beyond the standard model would become necessary to explain the data.

But is the perspective of cosmic ray astronomy feasible? Given the few-μG intensity of regular and turbulent GMF, a diffusive confinement of cosmic rays of galactic origin is expected up to rigidity $\mathcal{R} \equiv pc/Ze \simeq$ few $\times 10^{17}$ V, p being the cosmic ray momentum, Ze its charge, and c the speed of light. Still at $\mathcal{R} \simeq$ few $\times 10^{18}$ V cosmic rays are strongly deflected, and no directional information can be extracted. In this region a transition from galactic to extragalactic cosmic rays is extremely likely. Around 10^{19} V the regime of relatively small deflections in the GMF starts. The transition decades $\mathcal{R} \simeq 10^{17}$–$10^{19}$ V, though not yet useful for "directional" astronomy, may still show a rich phenomenology (drifts, scintillation, lensing) which is an interesting research topic of its own [Rou03].

At energies above a few 10^{19} eV, protons propagating in the Galaxy retain most of their initial direction. Provided that extragalactic magnetic fields (EGMFs) are negligible, UHE protons (but not necessarily heavy nuclei) will allow us to probe the nature and properties of their cosmic sources. We have already mentioned the difficulties in determining the chemical composition of UHECRs, but it must be stressed that the structure and magnitude of the EGMFs are poorly known as well. Only recently were magnetic fields included in simulations of large scale structures (LSS) [Dol03, Sig04]. Qualitatively the simulations agree in finding that EGMFs are mainly localized in galaxy clusters and filaments, while voids should contain only primordial fields. However, the conclusions of [Dol03] and [Sig04] are quantitatively rather different and it is at present unclear whether deflections in extragalactic magnetic fields will prevent astronomy even with UHE protons or not. While numerical problems could explain the differences, it is important to stress that important physical processes at galaxy cluster scales are not yet implemented in the codes. The development of small scale fields is triggered by strong non-linear effects, and the practice to normalize the field intensity found in simulations to the level of the observed cluster field could be misleading, given the present accuracy.

Moreover, as a consequence of the steep CR power spectrum, UHECRs are extremely rare (a few particles km^{-2} century^{-1}) and their detection calls for the prolonged use of instruments with huge collecting areas. One further constraint arises from the GZK suppression described in Section 1.2. Until

now, the limited statistics available in the UHE regime has prevented from answering (in either way) the question raised in the title of this section, and actually the very detection of the GZK effect has not yet been firmly established.

However, ongoing projects like the Pierre Auger Observatory and the Telescope Array may finally open this new observational window. From now on let us assume that UHE astronomy is indeed possible, namely: i) Most of UHECRs are protons ii) EGMFs are negligibly small in most of the sky; iii) extragalactic astrophysical sources are responsible for UHECRs acceleration. The basic question is how one may support this scenario using the directional information in UHECRs. There are actually several approaches to test this hypothesis, which we now summarize.

1.4.1   Large scale anisotropies

Since cosmic rays can not propagate very far at trans-GZK energies, and their deflections are expected to be relatively small in most of the sky, anisotropy patterns are expected to show up in UHECRs, provided enough statistics is collected. Cosmic ray air shower detectors which experience stable operation over a period of a year or more have a uniform exposure in right ascension (R.A.). A traditional technique to search for large scale anisotropies is then to fit the R.A. distribution of events to a sine wave with period $2\pi/m$ (m^{th} harmonic) to determine the components (x, y) of the Rayleigh vector [Lin75]

$$x = \frac{2}{N}\sum_{i=1}^{N}\cos(m\,\alpha_i)\,,\quad y = \frac{2}{N}\sum_{i=1}^{N}\sin(m\,\alpha_i)\,,\qquad(1.7)$$

where α_i is the R.A. of the i-th event. The mth harmonic amplitude of N data is given by the Rayleigh vector length $\mathcal{R} = (x^2 + y^2)^{1/2}$. The expected length of such a vector for values randomly sampled from a uniform phase distribution is $\mathcal{R}_0 = 2/\sqrt{N}$. The chance probability of obtaining an amplitude with length larger than that measured is $p(\geq \mathcal{R}) = e^{-k_0}$, where $k_0 = \mathcal{R}^2/\mathcal{R}_0^2$. Until now, all experiments to date have reported results consistent with an isotropic sky on large scales [Edg78, Win86b, Cas90, Tak99].

On the other hand, these analyses are completely blind to intensity variations which depend only on declination, δ. Combining anisotropy searches in R.A. over a range of declinations could dilute the results, since significant but out of phase Rayleigh vectors from different declination bands can cancel each other out. Moreover, analysis methods that consider distributions in one celestial coordinate, while integrating over the second, have proved to be potentially misleading [Wdo84]. In general, an analysis in terms of both celestial

coordinates, possibly based on an exposure to the full celestial sphere, would be much more reliable. A study [Anc03a] of the angular power spectrum of the distribution of trans-GZK cosmic rays ($E > 10^{19.6}$ eV) as seen by the AGASA and SUGAR experiments shows no departures from either homogeneity or isotropy on an angular scale greater than $10°$. Analogously, HiRes data are also statistically consistent with an isotropic distribution [Abb03].

All this does not obviously imply an isotropic distribution, but it merely means that available data are too sparse to claim a statistically significant measurement of anisotropy. Actually, we will see within a specific example in Chapter 3 that at least a factor 5 improvement with respect to present statistics is needed to perform significant tests of large scale anisotropy.

1.4.2   Small scale clustering

Although there seems to be a remarkable agreement among experiments on the large scale isotropy of the data, this is certainly not the case considering the two-point auto-correlation function on a small angular scale, i.e. at a scale comparable with the angular resolution of the experiment. The analyses carried out by the AGASA Collaboration indicate that the clustering of events on the celestial sky occurrs at considerably higher than chance coincidence at separation angles less than the angular resolution $\theta_{\min} = 2.5°$ [Hay96, Hay00]. AGASA finds indeed four doublets and one triplet among the 57 events reported with mean energy above $10^{19.6}$ eV, with probability of observing these clusters by chance coincidence for an isotropic distribution estimated to be smaller than 1% (see Fig. 1.7).
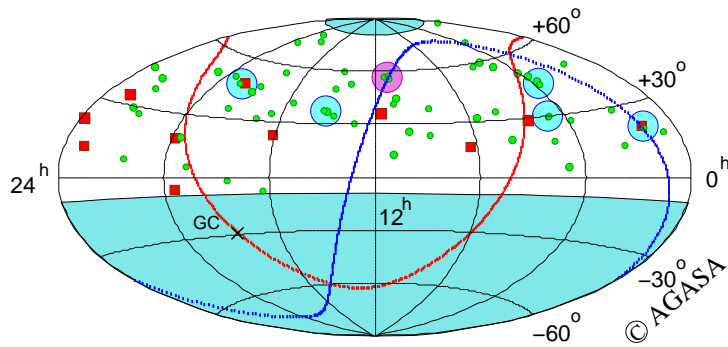

Fig. 1.7.— Arrival directions of cosmic rays with energies above 4×10^{19} eV in equatorial coordinates. Red squares and green circles represent cosmic rays with energies of $> 10^{20}$ eV , and $(4 - 10) \times 10^{19}$ eV, respectively. Circles enclose the multiplets.

A data set including events from other experiments has also been studied [Uch99]: six doublets and two triplets out of 92 events with energies above $10^{19.6}$ eV were found. The angular two-point correlation function of a combined data sample of AGASA ($E > 4.8 \times 10^{19}$ eV) and Yakutsk ($E > 2.4 \times 10^{19}$ eV) was analyzed [Tin01a]. For a uniform distribution of sources, the probability of chance clustering is reported to be as small as 4×10^{-6}. Far from confirming what seemed a fascinating discovery, the analysis reported by the HiRes Collaboration showed that the data are consistent with no small scale anisotropy among the highest energy events [Abb04a, Abb04b], though this finding is still compatible with expectations [Yos04b, Kac04a]. The preliminary data of the Auger Observatory, though being searched only for single sources, gave negative result as well [Rev05].

The discovery of such clusters would be a tremendous breakthrough for the field, but the case for them is not yet proven. To calculate a meaningful statistical significance in such an analysis, it is important to define the search procedure a priori in order to ensure it is not inadvertently devised especially to suit the particular data set after having studied it. In the analyses carried out by the AGASA Collaboration [Hay96, Hay00], for instance, the angular bin size was not defined ahead of time. Very recently, with the aim to avoid accidental bias on the number of trials performed in selecting the angular bin, the original claim of the AGASA Collaboration [Hay96] was re-examined considering only the events observed after the claim [Fin04]. This study showed that the evidence for clustering in the AGASA data set is weaker than was previously claimed, and consistent with the null hypothesis of isotropically distributed arrival directions.

Summing up, the clustering on small angular scale at the upper end of the spectrum remains an open question, and the increase in statistics and improved resolution attainable with the PAO is awaited to solve the issue. We will see in Chapter 2 that the presence of a regular GMF affects the estimate of the chance probability for these analyses in a non-negligible way, especially for experiments observing the Galactic Center (GC) like Auger South.

1.4.3   Correlations

An unambiguous alignment beyond random expectations between UHECRs and a given class of astrophysical accelerator candidates would certainly constitute a great discovery.

In the past, some claims that this could be indeed the case have been raised. In 1998, Farrar and Biermann pointed out the existence of a directional correlation between compact radio-quasar and UHECRs: all events at

the high end of the spectrum observed by that time, with energy at least 1σ above $10^{19.9}$ eV, were aligned with high redshifted quasars, a phenomenon with a chance probability of occurrence less than 0.5% [Far98]. Since then, this correlation has been analyzed several times [Hof99, Far99, Sig00, Vir02]. Using an updated event list (twice the size of the previous) from the Haverah Park [Ave00] and the AGASA [Hay00] experiments, Sigl et al. [Sig00] showed that the statistical significance of the alignment is lowered to 27%. Other authors, however, favored the earlier alignment [Vir02], but their correlation signal comes from events with large uncertainty both in energy and in position: they considered events from the SUGAR experiment, although it is not clear whether all these events are above the GZK cutoff. After the Haverah Park energy estimates have been re-assessed [Ave01], the original correlation has to be dropped altogether: for the cosmic rays in question, the energy of the 2 events observed by this array with incident zenith angle $< 45°$, that was previously quoted as $> 10^{19.9}$ eV at 1σ, is now shifted by 30% downwards, below the energy cut chosen by Farrar and Biermann. Hence, independently of the statistical test used, when considering only the highest energy ($> 10^{19.9}$ eV at 1σ) events the correlation between UHECRs and quasars is consistent with a random distribution at the 1σ level.

Tinyakov and Tkachev [Tin01b, Tin01c, Tin03] reported a correlation between the arrival directions of UHECRs and BL Lacs. Specifically, the 22 BL Lacs chosen were those identified as such in the (9th-Edition) Veron-Cetty and Veron (2000) [Ver00] catalogue of Quasars and Active Galactic Nuclei, with redshift $z > 0.1$ or unknown, magnitude $m < 18$, and radio flux at 6 GHz $F_6 > 0.17$ Jy. The CR sample of Tinyakov and Tkachev consists of 26 events measured by the Yakutsk experiment with energy $> 10^{19.38}$ eV [Afa96], and 39 events measured by the AGASA experiment with energy $> 10^{19.68}$ eV [Hay00]. The evidence supporting their claim is based on 6 events reported by the AGASA Collaboration (all with average energy $< 10^{19.9}$ eV), and 2 events recorded with the Yakutsk experiment (both with average energy $< 10^{19.6}$ eV), which were found to be within 2.5° of 5 BL Lacs contained in the restricted sample of 22 sources. The chance probability for this coincidence set-up was claimed to be 2×10^{-5}. Here also the data set used to make the initial assertion is also used to test the hypothesis. What is further subject to critique is that the imposed cuts on the BL Lac catalogue were chosen so as to maximize the signal-to-noise ratio, compensating *a posteriori* the different cut adjustments by inclusion of a penalty factor [Eva03]. Without such arbitrary cuts, the significance of the correlation signal is reduced to the 1σ level. Even accepting this approach, the estimated value of the penalty factor is subject to debate [Eva03, Tin03].

In order to test the hypothetical correlation between UHECRs and BL

Lacs, Torres *et al.* [Tor03a] performed a blind analysis using the Haverah Park [Sta95] and Volcano Ranch [Lin80] data samples. Such analysis shows no positional coincidences between these two samples up to an angular bin $> 5°$, an angular scale that is well beyond the error in arrival determination of these experiments ($\simeq 3°$) [Uch99].

Additionally, Gorbunov *et al.* [Gob02] claimed that a set of γ-ray loud BL Lacs can be selected by intersecting the EGRET, the UHECRs, and the BL Lac catalogs (all conveniently cut). The only requirement considered for an object to be physically associated with an EGRET source is that the angular distance between the best estimated position of the pair does not exceed $2 \times R_{95}$, where R_{95} is the 95% C.L. contour of the EGRET detection. However, identifying EGRET sources with BL Lacs (or any other object) just by positional pairing within twice the EGRET error grossly underestimates the goodness of existing γ-ray data: Only a few percent of the sources should indeed appear beyond the 95% contour radius R_{95}. Without such oversimplification, the correlation is not very significant [Tor03a].

Finally, another interesting result is the correlation between BL Lacs objects and the HiRes catalogue at energies between 1 and 4×10^{19} eV, with a second and less significant excess at much lower energies [Gob04, Abb05, Fin05]. Since this is a different claim, the significance can only be evaluated by an independent analysis on new data. Once again, however, it is clear that the question of correlations with BL Lacs is all but closed.

1.4.4 Single cluster studies

It has been recently observed [Far05a] that two events registered by HiRes above 3×10^{19} eV fall within 2.5° of the AGASA triplet above 4×10^{19} eV. The different thresholds could however well coincide within the energy-scale systematics errors. This "quintuplet" is intriguing, since it arises from a combined sample of only 94 events. Note also that one of the highest energy data of the Yakutsk catalogue coincides with the above-mentioned cluster, within the experimental resolution. It is virtually impossible to properly evaluate the chance probability of such a configuration, given the a posteriori cuts and the adjustments done to maximize the multiplicity of the cluster. On the other hand, it is an interesting exercise to assume that the signal is associated with a physical source of UHECRs, and explore the consequences of such an Ansatz.

In [Far05b] it is observed that the direction of the multiplet is exceptional in having a likely merging pair of galaxy clusters at about 200 Mpc, with an unusually low foreground density. It is thus conceivable that large scale shocks or another product of the merging galaxy clusters may accelerate

the UHECRs, or the merging galaxy clusters may be coincidental and the UHECRs may be accelerated in a rare event of an un-exceptional progenitor. Low magnetic deflections in the foreground void may explain why this is the only identified point-like cluster despite present UHECR statistics.

In [Tro05] the same cluster is studied with respect to possible deflections of particles in regular magnetic fields. Best-fit positions of a potential source of these clustered particles are found, with account of the errors in energy estimation, both in the frameworks of particular models of the Galactic magnetic field and treating the direction and the amount of deflection as free parameters. The study suggests that an unknown regular component of either Galactic or extragalactic magnetic field may dominate over modelled components in the direction of the cluster.

Obviously, such analyses should been taken with a grain of salt, relying on a yet unproven assumption. On the other hand, they are suggestive of the amount of information (on galactic and extragalactic magnetic fields, on the accelerating engine, etc.) that could be derived from a clear identification of a single UHECR source.

Evidently, the crucial issue of UHECR astronomy is still in its infancy, and even the tools to start this field are currently being developped. Some ideas to study the feasibility of a UHECRs astronomy program are reported in the following two Chapters. Chapter 2 deals with the possibility to use the Galactic magnetic field as a spectrograph for UHECRs. This is relevant for the case of small scale clustering of events induced by relatively few, bright sources. Chapter 3 describes the formalism to properly evaluate the expected anisotropy in the UHECR arrival distribution starting from a given astronomical catalogue of the local universe. This is particularly relevant if a large number of "weak" sources, possibly correlating with the luminous baryon matter, is the origin of UHECRs. In both cases, the emphasis is mainly on methodological aspects, though specific applications will be considered: In the first case to the published AGASA data, in the second one to a forecast for the Auger South experimental site.

Chapter 2

The Galactic magnetic field as spectrograph for ultra-high energy cosmic rays

In the previous Chapter, we have seen that EAS experiments can in principle measure the chemical composition of the CR flux. However, predictions of different hadronic interaction models differ substantially at the highest energies, and it is a theoretically and experimentally challenging task to differentiate between proton and heavy nuclei primaries. Other signs for proton or nuclear primaries are therefore highly desirable. The authors of [Ber05] advocated as the cleanest signature for extragalactic protons a dip in the CR flux around 10^{19} eV, caused by energy losses of protons due to e^+e^- pair production on cosmic microwave photons. This dip can be seen in the experimental data of AGASA, Fly's Eye, HiRes and Yakutsk and is an indication both for the extragalactic origin of UHECRs and, since it is unique for protons (see e.g. [All05a]), for the dominance of protons at these energies.

Complementary information on the charge of the primary may be obtained by anisotropy and/or positional studies of CR. The existence of magnetic fields in space suggests that they might be used as a natural spectrograph. This is a very old and powerful idea in cosmic-ray physics, at least for the Earth's magnetic field. Historically, the discovery of the latitude effect [Com32] proved that a significant fraction of cosmic rays was made of charged particles, and the east-west asymmetry [Ros34] demonstrated the predominance of positively charged primaries (for an early review see [Joh38]). Some decades later, Zatsepin and Gerasimova [Zat51, Ger60] suggested that the photo-disintegration of CRs by solar photons could allow to determine the mass of the primary nuclei between 10^{17} and 10^{18} eV by comparing the energies of the survivor and the fragment, usually a nu-

cleon. They would generate almost simultaneous air showers in the Earth's atmosphere, spatially separated by a distance controlled by the solar system magnetic field[1]. Recent reanalyses of this proposal show that, though challenging for the low rates of detectable pairs of events [Med98], there is some hope to gain insights on the primary charge, eventually exploiting the additional information of the angular orientation of the plane of the pair of events [Epe98].

It is natural to ask if the weaker magnetic fields known to exist on larger scales like the GMF might play a similar role at even higher energies, thus providing important information about the charge composition and the sources of the UHECRs. A signature of proton primaries may be the small scale clustering of UHECR arrival directions. The small number of sources able to accelerate beyond 10^{19} eV should result in small scale clustering of arrival directions of UHECRs if deflections in magnetic fields can be neglected. For nuclei with higher electric charge Ze, the deflections in the GMF alone dilute a small scale clustering signal even at the highest energies observed. We have explained in Section 1.4.2 that the existence of such clusters is one of the hot topics in present research on UHECRs.

In this Chapter we will quantify the effect of the GMF on the arrival direction of UHECRs and a possible clustering signal. In the following, we will assume optimistically that extragalactic magnetic field deflections are small in most of the extragalactic sky. Although not being firmly established, this condition is a necessary pre-requisite for any program of UHECR astronomy. In Sec. 2.1, we review the main features of three GMF models presented previously in the literature. In Sec. 2.2, we discuss in some details the role of the GMF for the propagation of UHECRs and the method we use to assess the significance of a possible small scale clustering in UHECRs data. In Sec. 2.3, we apply these concepts to the AGASA data set of events with energy $E \geq 4 \times 10^{19}$ eV, first to autocorrelation studies and then to test correlations with a class of astrophysical source candidates. In Sec. 2.4, we present conclusive remarks.

2.1   Galactic magnetic field models

The first evidence for a Galactic magnetic field was found more than 50 years ago from the observation of linear polarization of starlight [Hit49]. Meanwhile, quite detailed information about the GMF has been extracted mainly

---

[1]In the light of the improved knowledge of the intensity of the interplanetary field, the kinematic splitting of the fragment, considered in the original proposal, was later recognized as a sub-leading effect.

from Faraday rotation measurements of extragalactic sources or Galactic pulsars [Zwi97]. However, it is not yet possible to reconstruct the GMF solely from observations (for an attempt see [Stp01]), and instead we will employ phenomenological models for the GMF.

The GMF can be divided into a large scale regular and a (typically) small scale turbulent component, with rather different properties and probably also origin. The root-mean-square deflection $\delta_{\rm rms}$ of a CR traversing the distance L in a turbulent field with mean amplitude $B_{\rm rms}$ is [Har02a]

$$\delta_{\rm rms} = \frac{ZeB_{\rm rms}}{E}\sqrt{\frac{LL_c}{2}} \simeq 0.085° \frac{Z}{E_{20}}\frac{B_{\rm rms}}{\mu{\rm G}}\sqrt{\frac{L}{\rm kpc}\frac{L_c}{50{\rm pc}}}\,, \qquad (2.1)$$

where L_c denotes the coherence length of the field, E_{20} is the energy in units of 10^{20} eV, and $L \gg L_c$ has been assumed. Recently, it has been noted that the latter condition may not be fulfilled, at least for some directions in the sky [Tin04]. However, their analysis based directly on the observed turbulent power spectrum confirmed that the deflections in the random field are typically one order of magnitude smaller than those in the regular one. Therefore, henceforth we shall neglect the turbulent component of the GMF.

The regular GMF resembles the matter structure of the Galaxy and has different properties in the disk and the halo. In the disk, the field is essentially toroidal, i.e. only its radial (B_r) and azimuthal (B_θ) components are non-vanishing. The disk field can be classified according to its symmetry properties and sign reversals: antisymmetric and symmetric configurations with respect to the transformation of the azimuthal angle $\theta \to \theta + \pi$ are called bisymmetrical (BSS) and axisymmetrical (ASS), respectively. According to the symmetry property with respect to a reflection at the disk plane ($z \to -z$), the notation A or S is used: in the first case, the field reverses sign at $z = 0$ (odd field), while in the second case it does not (even field). Theoretical motivations and observations in external galaxies [Sol92] associate the presence of field reversals far away from the GC to a BSS geometry. In our Galaxy, there are probably from three to five reversals. The closest one is at a distance of 0.3–0.6 kpc towards the GC, where the higher values seem to be confirmed from the new wavelet data-analysis used in [Stp01, Fri00], and about 0.6 kpc is the value suggested in the review [Bec00]. Moreover, there is increasing evidence for positive z parity (configuration S) of the GMF near the Sun [Fri00, Bec00, Bec96].

In galactic coordinates, the field components in the disk can be parameterized as

$$B_r = B(r,\theta)\sin p\,, \qquad B_\theta = B(r,\theta)\cos p\,, \qquad (2.2)$$

where p is the pitch angle and $R_0 \simeq 8.5$ kpc is the galactocentric distance of
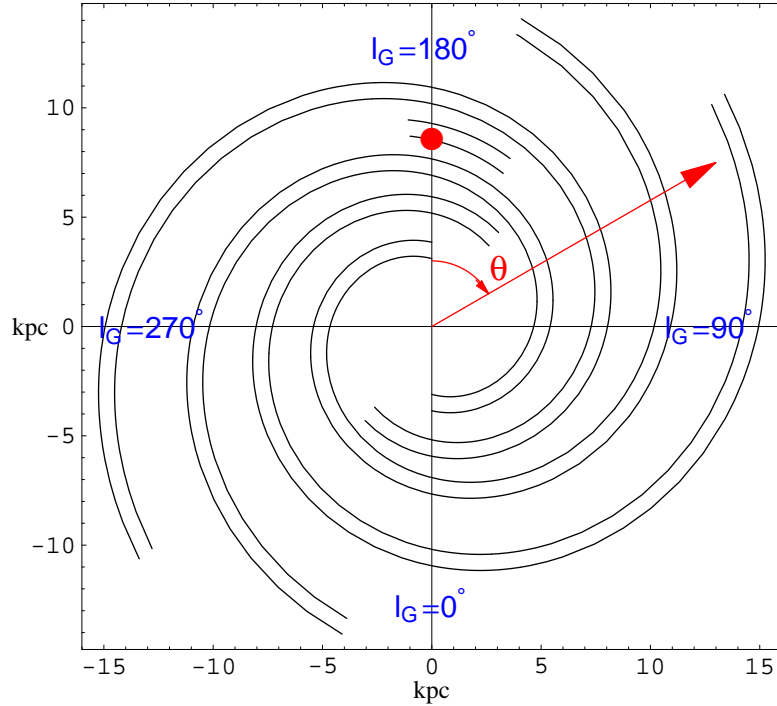
Fig. 2.1.— The galactocentric frame used, together with the Solar position (filled circle) along the y-axis and the orientation of the galactic polar angle θ. The corresponding galactic longitudes are also shown, as well as the galactic spiral arm model as given in [Wai92].

the Sun, cf. Fig. 2.1. Estimates for the pitch angle vary between $p = -8° \pm 2°$ from pulsar [Han01] and starlight polarization data, but other observations pointing to values of p between $-13°$ and $-18°$ also exist [Bec00].

The function $B(r, \theta)$ is traditionally modeled reminiscent of the spiral structure of the matter distribution in the Galaxy as

$$B(r,\theta) = b(r) \cos \left[\theta - \frac{1}{\tan p} \ln \left(\frac{r}{\xi_0} \right) \right] . \tag{2.3}$$

In terms of the distance d to the closest sign reversal, ξ_0 can be expressed as $\xi_0 = (R_0 + d) \exp(-\frac{\pi}{2} \tan p)$.

The radial profile function $b(r)$ is generally assumed to fall off as r^{-1} [Sta97, Tin01c], consistent with pulsar measurements [Ran94]. The behaviour of the disk field in the inner region of the Galaxy is less well known, but clearly the field has to be regularized for $r < r_{min}$. For $r \geq r_{max}$, the field is turned off. In the following, we will fix $r_{max} = 20$ kpc. The vertical profile

of the field outside the plane $z = 0$ is modeled by

$$B(r, \theta, z) = f(z)B(r, \theta).$$ (2.4)

Despite remaining uncertainties, the regular magnetic field in the thin disk is yet much better known than other components, namely the halo (or thick disk) field and a possible dipole field. The first could dominate at large Galactic latitudes and the second may be of crucial importance near the center of the Galaxy. Because of the huge volume occupied by the halo field, it may play a dominant role for UHECR deflections, while the possibly much higher strength of the field in the center of the Galaxy might prevent us to access some directions in the UHECR extragalactic sky (see Sec. 2.2).

For the halo field, an extrapolation of the thin disk field into the galactic halo with a scale height of a few kpc has often been assumed [Sta97, Tin01c]. This minimal choice is in agreement with radio surveys of the thick disk [Beu85] and mimics the expected behaviour of a "Galactic wind" diffusing into the halo. However, Faraday rotation maps [Han01, Han97] of the inner Galaxy ($-90° < l_G < 90°$) and of high latitudes ($|b_G| > 8°$) favor a roughly toroidal component in the halo, of opposite sign above and below the plane (odd z parity or configuration A) and with an intensity of 1–2 μG [Han99]. Moreover, there is some evidence for a B_z component of about $0.2\,\mu$G at the solar distance [Han94] that could derive from a dipolar structure at the GC [Han02]. In the filaments already detected, the field strength almost reaches the mG scale [Bec00]. Even if this intriguing picture is roughly consistent with the one expected if an A0 dynamo mechanism operates in the Galactic halo, it needs observational confirmation. For example, there is no general consensus about the existence of such high-intensity magnetic fields in the central region of the Galaxy [Roy04, LaR05].

In the following, we review three phenomenological models that parameterize the regular GMF. These models are characterized by different symmetries, choices of the functions $b(r)$ and $f(z)$ and additional parameters.

TT model

Tinyakov and Tkachev (TT) examined if correlations of UHECR arrival directions with BL Lacs improve after correcting for deflections in the GMF [Tin01c]. They assumed $b(r) \propto r^{-1}$ for $r > r_{min} = 4$ kpc, and $b(r) = $ const. for $r \leq r_{min}$. The field $b(r)$ was normalized to 1.4 μG at the Solar position. The pitch angle was chosen as $p = -8°$ and the parameter d fixed to -0.5 kpc. They compared a BSS-A and a BSS-S model and found that for the former model the correlations with BL Lacs increased.

This model has an exponential suppression law,

$$f(z) = \text{sign}(z) \exp(-|z|/z_0) \,, \tag{2.5}$$

with $z_0 = 1.5$ kpc chosen as a typical halo size. No dipole component was assumed.

HMR model

Harari, Mollerach and Roulet (HMR) used a BSS-S model with cosh profiles for both the disk and the halo field with scale heights of $z_1 = 0.3$ kpc and $z_2 = 4$ kpc respectively [Har99],

$$f(z) = \frac{1}{2\cosh(z/z_1)} + \frac{1}{2\cosh(z/z_2)} \,. \tag{2.6}$$

Thus the disk and halo field share the same spiral-like geometrical pattern. The function $b(r)$ was chosen as $b(r) = 3R_0/r \tanh^3(r/r_1) \,\mu\text{G}$ with $r_1 = 2$ kpc, hence reducing to $b(r) \propto r^{-1}$ for $r \gg r_1$ while vanishing at the GC. The pitch angle was fixed to $p = -10°$, and $\xi_0 = 10.55$ kpc. This model represents a slightly modified and smoothed version of the BSS model discussed by Stanev in [Sta97]. Apart for the vertical profile $f(z)$, the main differences with respect to the TT model are the z parity and the $r \to 0$ behaviour of the field.

PS model

In [Prz03], Prouza and Smida (PS) used for the disk field the same BSS-S configuration as in [Sta97], with a single exponential scale height z_0 and $b(r)$ as described in Sec. 2.1. In the slightly modified version we use here, we fix $z_0 = 0.2$ kpc, $p = -8°$, $d = -0.5$ kpc and normalize the local field to $2\,\mu\text{G}$. Apart from the larger field-strength, the main difference with the TT model is the parity of the disk field, which we take here to be even as in [Prz03].

Additionally, we consider a toroidal thick disk/halo contribution,

$$\begin{aligned} B_{Tx} &= -B_T \,\text{sign}(z) \cos\theta \,, \\ B_{Ty} &= B_T \,\text{sign}(z) \sin\theta \,, \end{aligned} \tag{2.7}$$

where

$$B_T = \frac{B_{T,\text{max}}(r)}{1 + \left(\frac{|z| - h_T}{w_T}\right)^2} \,, \tag{2.8}$$

$h_T = 1.5$ kpc is the height of the maximum above the plane and $w_T = 0.3$ kpc is its Lorentzian width. In contrast to [Prz03], we choose

$$B_{T,\max}(r) = 1.5\,\mu\mathrm{G}\left[\Theta(R_0 - r) + \Theta(r - R_0)e^{\frac{R_0 - r}{R_0}}\right]\,, \qquad (2.9)$$

so that the halo contribution becomes negligible for $r \gg R_0$. Note that there is no evidence for such a field outside the solar circle [Han97].

Finally, a dipole field is added as in Ref. [Prz03, Yos03],

$$\begin{aligned}
B_x &= -3\mu_G \cos\phi \sin\phi \sin\theta / R^3\,, \\
B_y &= -3\mu_G \cos\phi \sin\phi \cos\theta / R^3\,, \\
B_z &= \mu_G(1 - 3\cos^2\phi)/R^3\,,
\end{aligned} \qquad (2.10)$$

where $R \equiv \sqrt{r^2 + z^2} = \sqrt{x^2 + y^2 + z^2}$, $\cos\phi \equiv z/R$ and μ_G is the magnetic moment of the Galactic dipole with $\mu_G = 123\,\mu\mathrm{G}\,\mathrm{kpc}^3$ in order to reproduce $B_z \simeq +0.2\,\mu\mathrm{G}$ near the Solar system [Han94]. To avoid a singularity in the center, we set $B_z = -100\,\mu\mathrm{G}$ inside a sphere of 500 pc radius centered at the GC. Note that in [Prz03] values as large as 1 mG were used for the hard core of the dipole field. However, data from low frequency non-thermal radio emissions of electrons [LaR05] favor a value of about $10\,\mu\mathrm{G}$ down to a 10 pc scale, giving the conservative bound of $100\,\mu\mathrm{G}$ which we actually use.

Finally, we warn the reader that these models are intended to provide only a rough approximation to the true structure of the GMF. At small scales (about tens of pc), stronger fields at the level of tens of μG have been detected in irregular regions associated with star formation and molecular clouds complexes. These local fields are omitted in the usual GMF models, but could be responsible for significant—though local—effects in some directions in the Galactic plane. Moreover, the GMF models are not self-consistent because the condition $\nabla \cdot \mathbf{B} = 0$ is not fulfilled by any of the disk fields discussed. Using the Ansatz of Eq. (2.3) for $B(r, \theta)$, $\nabla \cdot \mathbf{B} = 0$ can only be satisfied by $b(r) = \mathrm{constant}$, or a non-vanishing z-component of the disk field.

2.2 Galactic magnetic field and UHECR propagation

2.2.1 Isotropic cosmic ray flux

A generalized version of the Liouville theorem was shown to be valid for CRs propagating in magnetic fields soon after the discovery of the geomagnetic

effect [Lem33, Swa33]. The Liouville theorem ensures the constancy of the phase space volume along the particle trajectories: when the density of CR trajectories is increased by the GMF, the angular spread of their velocities increases also, so that the CRs arrive from a larger solid angle. Both effects compensate each other in the flux per unit solid angle, and as a consequence an isotropic flux remains isotropic to an observer behind a magnetized environment. For UHECRs, this theorem has been numerically tested [Alv01]. In that work, particles were injected isotropically from randomly distributed sources at different galactocentric distances. Even after the propagation in the GMF, the sky on Earth appears isotropic (see left panel of Fig. 6 in [Alv01]). Following the particles backwards to their original sources, the effective exposure of an experiment to the extragalactic sky is strongly modified by the GMF (see their Fig. 6, right panel). However, even for an isotropic flux outside the Galaxy, the GMF introduces anisotropies if blind regions on the external sky exist for an observer.

A simple analytic estimate of this effect can be given for a dipole field. Given the azimuthal symmetry, the Størmer theory (see Refs. [Joh38, Stø55], or [She04] for a modern generalization) can be applied to determine the rigidity cutoff $\mathcal{R}_S$ below which no particle can reach the Earth. Since the Earth is at zero galacto-magnetic latitude, we obtain

$$\mathcal{R}_S = \frac{\mu_G}{2R_0^2} \frac{1}{[1 + \sqrt{1 - \sin\epsilon}]^2} \,. \tag{2.11}$$

Here, $\mathcal{R}_S$ depends on the arrival direction of the cosmic ray via the function ϵ, that we do not need to specify here. Assuming that the tiny vertical component detected at the solar system of $0.2\,\mu$G is due to a dipole field, we get $\mu_G \simeq 120\,\mu$G and then $\mathcal{R}_S$ would vary in the range 10^{17} to 10^{18} V. Obviously, the geometry of the GMF is more complicated than a simple dipole. Nevertheless, one expects qualitatively similar results for more realistic models of the GMF. A naive estimates of the Larmor radius,

$$r_L = \frac{p}{ZeB} \simeq \frac{\mathcal{R}}{3 \times 10^{15}\text{V}} \frac{\mu\text{G}}{B} \text{ pc} \tag{2.12}$$

shows that, given $B \simeq$ few μG, for $\mathcal{R} \lesssim 10^{17}$ V particles are likely to be trapped in the Galactic magnetic disk with a thickness-scale of 100 pc. We confirmed this estimate numerically, although precise quantitative statements depend on the GMF model. Note that the argument can be turned around: for a given rigidity cutoff $\mathcal{R}_S$, large scale anisotropies should be seen around $E \sim Ze\,\mathcal{R}_S$, if an extragalactic component dominates at this energy. Thus, models that invoke a dominating extragalactic proton component already at $E \simeq 4 \times 10^{17}$ eV (see e.g. Ref. [Ahl05]) or extragalactic iron nuclei at $E \lesssim 10^{19}$ eV might be inconsistent with the observed isotropy of the CR flux.

2.2.2 Anisotropic flux due to finite number of sources

If the AGASA small scale clusters are not just a statistical fluctuation, the UHECR flux is, at least on small scales, anisotropic. In this case, the CR flux can be magnified or demagnified by magnetic lensing phenomena, and the application of the Liouville theorem is non-trivial [Har00]. The magnification effects of the GMF change the experimental exposure and a well-defined procedure is needed to assess the significance of any detected anisotropy.

Ideally, one may test the significance of observed anisotropies by comparing the values of the statistical estimator based on the N_d data with a large number $\mathcal{N}$ of simulated N_d-points samples of the null-hypothesis. For each set, one should consider the propagation in the GMF, convolve with the experimental exposure, and finally reject the null-hypothesis with a given significance. Instead, we will use for practical reasons the usual back-tracking technique [Kar71]. It consists in following the CR trajectory backwards in time, by reversing the charge $Z\,e$ and the arrival direction vector of the particle, thus using the final conditions (at the Earth) to determine the initial ones (before entering the GMF).

Since we deal with ultra-relativistic particles, the equations of motion can be written in the form

$$\frac{\mathrm{d}\mathbf{v}}{\mathrm{d}t} = \frac{\mathbf{v} \times \mathbf{B}}{\mathcal{R}}\,, \tag{2.13}$$

where $\mathbf{v}$ is a vector of modulus practically equal to $c = 1$. The integration is stopped when the particle reaches a distance of 50 kpc from the GC. Note that the energy losses of UHECRs on galactic scales (~ 10 kpc) are negligible, provided the trajectory is not very far from a rectilinear one. In Fig. 2.2, we show the map thus obtained, for the three models considered and a rigidity of 4×10^{19} V. Note that the deflection δ of a particle of rigidity E/Ze in a field of strength B coherent over the scale L is approximately given by

$$\delta \simeq 0.53° \frac{Z}{E_{20}} \frac{B}{\mu\mathrm{G}} \frac{L}{\mathrm{kpc}}\,. \tag{2.14}$$

To obtain an estimate for the average deflection of CRs in different sky regions, labelled as in Table 2.1, we have followed backwards 50000 randomly chosen CRs of rigidity $\mathcal{R} = 10^{20}$ V, for which the hypothesis of a quasi-rectilinear trajectory is well fulfilled. In Table 2.2, we show the average value and the variance of $\mathcal{R}_{20}\delta$ (i.e., in units of 10^{20} V) for the three models of the regular GMF discussed in the Section 2.1, calculated separately for eight different sky regions. The quantity $\mathcal{R}\delta$ depends only on the GMF model and scales almost linearly with the field strength B. The largest difference between the three GMF models occurs in the region Al: in the PS model, the
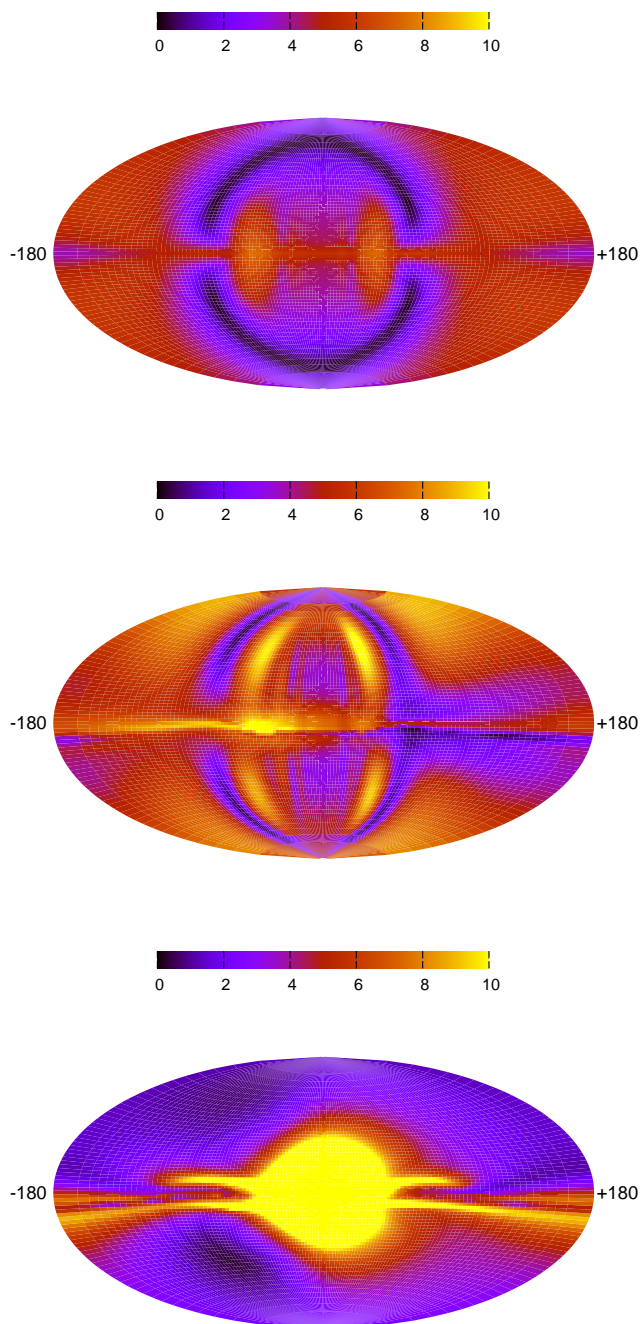
Fig. 2.2.— Deflection maps for the TT (top), HMR (middle), and PS (bottom) models of the GMF, for a rigidity of 4×10^{19} V. The deflection scale is in degrees, and the maps refer to the direction as observed at the Earth. All maps use a Hammer-Aitoff projection of galactic coordinates.

only one with a dipole field, huge deflections arise close to the GC, which is an almost inaccessible zone. In the regions Bh, Ch, and Dh the stronger halo fields of the TT and especially the HMR model cause larger deflections than in the PS model. In the l-regions, apart for Al, the deflections of the three models are all of the order $1°$–$2°$, and comparable to each other within 1σ. Since the CR in these directions mainly travel through the disk, in order to escape the galaxy they have to cross the regions where the field geometry and intensity is better known, and a better agreement among the models exists.

$b_G \backslash l_G$	$315 \le l_G < 45$	$45 \le l_G < 135$	$135 \le l_G < 225$	$225 \le l_G < 315$
$|b_G| \ge 30$	Ah	Bh	Ch	Dh
$|b_G| < 30$	Al	Bl	Cl	Dl

Table 2.1: The labels used for the eight different regions of the sky referred to in the text. Angles are in degrees.

region	$\mathcal{R}_{20}\,\delta$ (PS)	$\mathcal{R}_{20}\,\delta$ (TT)	$\mathcal{R}_{20}\,\delta$ (HMR)
Ah	$1.8° \pm 1.0°$	$0.9° \pm 0.5°$	$2.1° \pm 0.8°$
Bh	$1.3° \pm 0.4°$	$1.3° \pm 0.6°$	$2.2° \pm 0.8°$
Ch	$0.9° \pm 0.4°$	$2.0° \pm 0.3°$	$2.7° \pm 0.5°$
Dh	$0.5° \pm 0.2°$	$1.1° \pm 0.6°$	$2.1° \pm 0.9°$
Al	$14° \pm 21°$	$1.9° \pm 0.4°$	$2.2° \pm 0.7°$
Bl	$2.0° \pm 0.9°$	$1.7° \pm 0.5°$	$1.2° \pm 0.4°$
Cl	$1.7° \pm 1.1°$	$1.9° \pm 0.5°$	$1.8° \pm 0.3°$
Dl	$1.6° \pm 1.0°$	$1.6° \pm 0.5°$	$2.3° \pm 0.6°$

Table 2.2: The rigidity times average deflections $\mathcal{R}_{20}\,\delta$ in the eight different regions labelled in Table 2.1.

If one excludes the central regions of the Galaxy, the average deflection is $\delta \simeq 2°/\mathcal{R}_{20}$, and the differences for the magnitude of the deflections are of the order of 50% among the models. Thus only for the highest energy events and proton primaries the role of the GMF is negligible compared to the angular resolution δ_{exp} of CR experiments. The latter is as good as $\delta_{\mathrm{exp}} \simeq 0.6°$ for the HiRes experiment [Abb04a] and for Auger hybrid events [Bon05].
For lower $\mathcal{R}$, correcting for deflections in the GMF would be crucial to exploit fully the angular resolution of UHECR experiments. Note also that, even in the ideal case of a perfectly known GMF, a reconstruction of the

original arrival directions would require a relatively good energy resolution: an uncertainty of, say, 30% in the energy scale around 5×10^{19} eV would lead to errors $\gtrsim 1°$ in the reconstructed position of proton primaries in most of the sky.

Apart for deflections, (de-) focusing effects of the GMF effectively modify the exposure to the extragalactic sky. This modification of the exposure can be calculated by back-tracking a large number of events and looking at the obtained map of event numbers per solid angle outside of our Galaxy. For the purpose of illustration, we show in Fig. 2.3 some relative exposure maps obtained for fixed rigidity for the three chosen GMF models. They were obtained with the technique described in [Har99], and essentially represent the ratio $\omega_B(l,b) = d\Omega_\infty(l',b')/d\Omega_\oplus(l,b)$, where $d\Omega_\oplus$ is an infinitesimal small cone at Earth (around the direction l,b) transported along the trajectory of a charged particle to the border of the Galaxy $d\Omega_\infty$ (around the new position $l'(l,b), b'(l,b)$). If $\omega_B(l,b)$ deviates significantly from one, the corrected exposure has to be used in (auto-) correlation studies. Note how this effect is present in all the models at least for cosmic rays observed at the Earth along the Galactic plane.

A remark on the role of the turbulent GMF is in order. A comparison of Eq. (2.1) and Eq. (2.14) shows that deflections in the turbulent GMF are sub-leading. However, this does not ensure automatically that magnetic lensing by the random field is irrelevant at high energies, because lensing depends on the gradient of the field and the critical energy for amplification is proportional to $L_c^{-1/2}$. The detailed analysis of Ref. [Har02a] showed indeed that small-scale turbulence can produce relatively large magnification effects, and suggested that it may even be responsible for (some of) the multiplets seen by AGASA above 4×10^{19} eV. We argue that neglecting the turbulent GMF is justified in view of the current experimental energy and angular resolution as well as of the limited event number. First, possible lensing effects by the random GMF are weakened by the presence of a regular field component [Har02a]: Already without regular field, the magnification peaks are quite narrow in energy space, $\Delta E/E \sim 20\%$, and thus their width $\Delta E/E$ is comparable to the energy resolution of CR experiments. The presence of the regular GMF narrows further these magnification peaks. Second, the experimental angular resolution introduces an additional averaging effect. Thus it is seems unlikely that lensing effects of the turbulent GMF lead at present to distinctive effects taking into account the current experimental limitations. Phenomenologically, our analysis is the same both if the multiplets are due to intrinsically strong UHECRs sources or due to turbulent lensing. While for a single cluster analysis the role of turbulent

lensing might be crucial, we expect that in a global analysis the random GMF introduces a small scale (and strongly energy dependent) correction of the sky map on the top of the magnifications effects of the regular GMF.

The extension of the back-tracking method to very low rigidities, say around 10^{18} V, or to distances comparable to the interaction length of the CR primaries [Tam05] is rather risky. In the former case, as we have previously motivated and is nicely illustrated in the Figures of [Yos04a, Med97], blind regions start to appear, that in the back-tracking method correspond to particles trapped in the GMF. Since the motion of the CR is very folded and chaotic, one has to follow trajectories up to Mpc lengths [Yos04a]. This scale is of the same order of the interaction length of protons in the Galaxy, thus implying that a non-negligible fraction of particles (the "almost-trapped ones" which finally escape) starts to interact inside the Galaxy. In the latter case, trajectories have also in the straight line approximation about the same length or are smaller than the interaction length with diffuse photon backgrounds. In both cases, the Liouville theorem is violated and one can not rely on the back-tracking method for quantitative statistical studies.

2.3 AGASA data sample

In order to make the general considerations of the previous section more concrete, we will discuss here some applications to the AGASA data. The AGASA experiment has published the arrival directions of their data until May 2000 with zenith angle $< 45°$ and energy above 4×10^{19} eV [Hay00]. This data set consists of $N = 57$ CRs and contains a clustered component with four pairs and one triplet within $2.5°$ [Tak99] that has been interpreted as first signature of point sources of UHECRs. The reconstruction of the original CR arrival directions and the estimate of their errors is obviously an important first step in the identification of astrophysical CR sources.

In Fig. 2.4, we show the measured directions of all CRs in the AGASA data with $E \geq 10^{20}$ eV together with their reconstructed arrival direction at the border of the Galaxy for the case of Carbon primaries. In the southern Galactic hemisphere, the TT model often produces opposite deflections with respect to the HMR and PS models because of its antisymmetric field configuration. A longitudinal shift is often appreciable in the PS model, as a consequence of the dipolar component we added. The larger deflection found in the TT and HMR models for high latitudes is explained by the stronger regular halo field in these models. The best chances for source identification arise obviously by looking at directions opposite to the GC. On the other
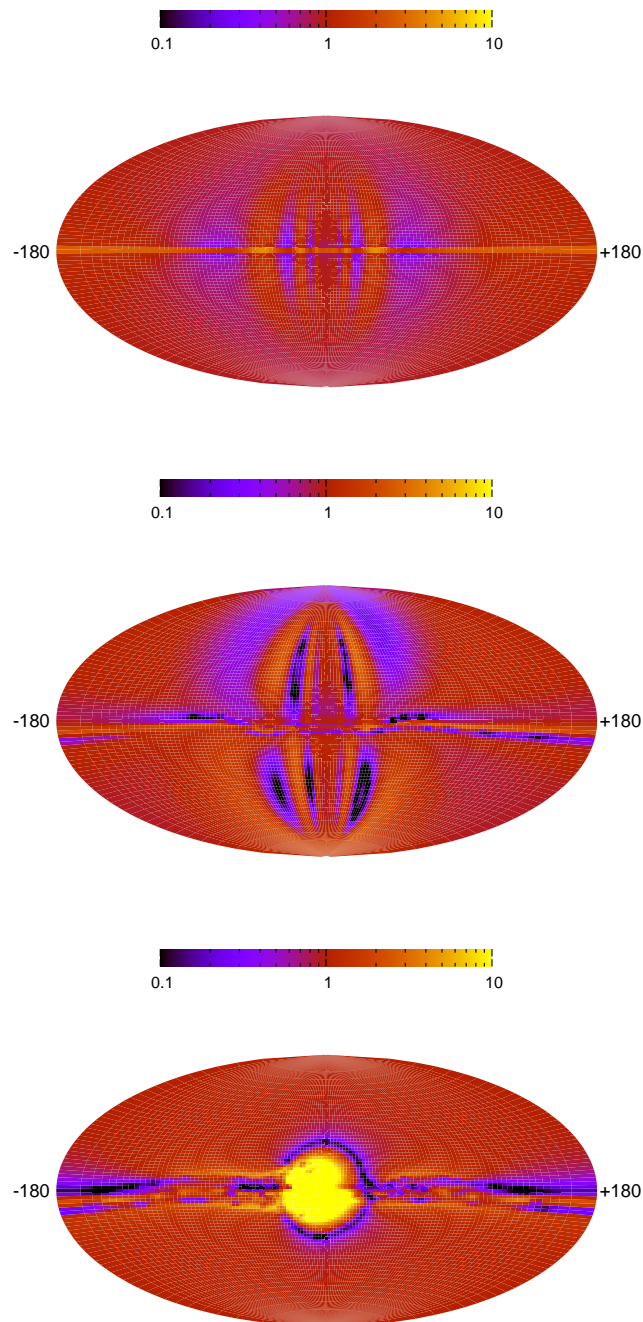
Fig. 2.3.— The extragalactic "exposure" maps for the TT (top), HMR (middle), and PS (bottom) model for a rigidity of 4×10^{19} V. All maps use a Hammer-Aitoff projection of galactic coordinates.

hand, observations towards the GC have a certain importance to use the UHECRs as diagnostic tool for the GMF [Har02b, Med03, Alv05a].
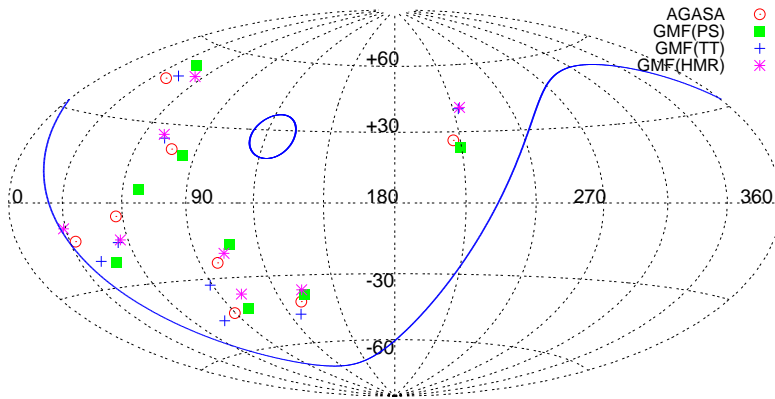
Fig. 2.4.— The AGASA data set of CRs with estimated energy exceeding 10^{20} eV together with their reconstructed positions assuming Carbon primaries and the three GMF models discussed in the text. The line bounds the region visible to AGASA for zenith angles $\leq 45°$.

Before turning to the statistical analysis, we briefly recall the estimators we will use in the following. The autocorrelation function w_1 is defined as

$$w_1 = \sum_{i=1}^{N_d} \sum_{j=1}^{i-1} \Theta(\ell - \ell_{ij}),\qquad(2.15)$$

where ℓ_{ij} is the angular distance between the two cosmic rays i and j, ℓ the chosen bin size, Θ the step function, and N_d is the number of CRs considered. Analogously, one can define the correlation function w_s as

$$w_s = \sum_{i=1}^{N_d} \sum_{a=1}^{N_s} \Theta(\ell - \ell_{ia}),\qquad(2.16)$$

where ℓ_{ia} is the angular distance between the CR i and the candidate source a and N_s is the number of source objects considered.

2.3.1 Autocorrelation analysis

We now discuss how the small scale clustering observed by AGASA is modified by the GMF. Note from Fig. 2.3 that even for protons the magnification of the exposure is already significant at the energy of 4×10^{19} eV.

Neglecting the influence of the GMF, one generates a large number of Monte Carlo sets of CRs, each consisting of N_d CRs distributed according to the geometrical exposure ω_{exp} of AGASA. The fraction of Monte Carlo sets that has a value of the first bin of the autocorrelation function w_1 larger or equal to the observed one, w_1^*, is called the chance probability P of the signal. For a nonzero GMF one uses the back-tracking method: the observed arrival directions at the Earth are back-tracked following a particle with the opposite charge to the boundary of the GMF. Then the value w of the autocorrelation function is calculated. Since also the exposure is changed by the GMF, the CRs of the Monte Carlo sets have to be generated now using as exposure $\omega_{\mathrm{tot}}(E, l, b) = \omega_{\mathrm{exp}}(l, b)\omega_B(E, l, b)$. This is automatically fulfilled if one back-tracks uniformly distributed Monte Carlo sets in the same GMF. For very large statistics, however, it is numerically more convenient to explicitly calculate $\omega_B(E, l, b)$ and generate the Monte Carlo sets accordingly. The resulting chance probability is called P in Table 2.3. For illustration, we show also the chance probability P_0 calculated using only the experimental exposure (or $\omega_B = 1$) that overestimates that clusters come from the same source.

Correcting for the GMF reduces for all three GMF models the value of w_1. While however for the TT and HMR models two doublet above 5×10^{19} eV disappear, the PS model loses one low-energy doublet. Thus, either some of the pairs are created by the focusing effect of the GMF, or the GMF and especially its halo component is not well enough reproduced by the models. In the latter case, "true pairs" are destroyed by the the incorrect reconstruction of their trajectories in the GMF. Troitsky discussed in detail the effect of the GMF on the AGASA triplet and found that current GMF models defocus it [Tro05]. If the clustering is physical, this could be explained by a wrong modeling of the GMF in that high-latitude region. Alternatively, our assumptions of negligible deflections in the extragalactic magnetic field and of protons as primaries could be wrong. Note that the effect of the GMF induced exposure to the extragalactic sky is not in general negligible. The fact that P_0 is only somewhat smaller than P hints that only a small fraction of clusters might be caused by magnetic lensing (in the regular field). For the AGASA data set this is expected, because the field of view of this experiment peaks away from the inner regions of the Galactic plane, and the GC in particular. Finally, we note that the energy threshold for which the chance of clustering is minimal decreases for the TT model. This change is however rather small and a larger data set is needed for any definite conclusion.

In Table 2.4 the same analysis is performed for the TT model only, but assuming also $Z = +2, -1$. In no case an improvement with respect to the $Z = 0$ case is appreciable.

Model		no GMF		TT		HMR		PS	
$E_{20}^{\min}$	N_d	w_1	$P[\%]$	w_1	$P\,(P_0)\,[\%]$	w_1	$P\,(P_0)\,[\%]$	w_1	$P\,(P_0)\,[\%]$
0.50	32	4	0.22	2	8.9 (8.5)	2	9.5 (8.5)	4	0.27 (0.22)
0.45	43	6	0.05	4	1.5 (1.4)	4	1.8 (1.4)	6	0.10 (0.05)
0.40	57	7	0.18	6	0.8 (0.7)	5	3.3 (2.4)	6	1.09 (0.72)

Table 2.3: Number N of CRs with energy $E \geq E_{20}^{\min}$ (in units of $10^{20}\,\mathrm{eV}$) and zenith angle $\theta \leq 45°$; the values of the first bin of the autocorrelation function w_1, and the chance probability $P(w_1 \geq w_1^*)$ from an isotropic test distribution are shown for the two cases with (P) and without (P_0) correction of the exposure, respectively. Proton primaries are assumed.

Model		$Z=0$		$Z=+1$		$Z=+2$		$Z=-1$	
$E_{20}^{\min}$	N_d	w_1	$P[\%]$	w_1	$P[\%]$	w_1	$P[\%]$	w_1	$P[\%]$
0.50	32	4	0.22	2	8.9	1	41	4	0.27
0.45	43	6	0.05	4	1.5	4	1.8	6	0.10
0.40	57	7	0.18	6	0.8	5	3.5	6	1.08

Table 2.4: As in Table 2.3, but for different charges (TT model).

2.3.2 Correlations with BL Lacs

Tinyakov and Tkachev examined if correlations of UHECRs arrival directions with BL Lacs improve after correcting for deflections in the GMF [Tin01c] . The significance of the correlation found is still debated, and we choose this example only to illustrate how correlation of UHECR arrival directions with sources can be used to test the GMF model and the primary charge. We use from the BL Lac catalogue [Ver03] all confirmed BL Lacs with magnitude smaller than 18 (187 objects in the entire sky).

Model		no GMF		TT		HMR		PS	
$E_{20}^{\min}$	N_d	w_s	$P[\%]$	w_s	$P\,(P_0)\,[\%]$	w_s	$P\,(P_0)\,[\%]$	w_s	$P\,(P_0)\,[\%]$
0.50	32	8	8.8	8	9.7 (8.8)	4	65 (64)	7	17 (17)
0.45	43	11	4.7	14	0.6 (0.5)	7	49 (39)	7	39 (39)
0.40	57	13	6.6	20	0.05 (.05)	11	20 (18)	7	67 (67)

Table 2.5: As in Table 2.3, but for the correlation function and the BL Lac catalogue discussed in the text.

In Table 2.5, we show the chance probability to observe a stronger correlation taking into account the three different GMF models and assuming proton

primaries. A remarkable improvement of the correlation signal is found only for the TT model, while for the two other models the correlation becomes weaker. In Table 2.6, the same analysis is performed for $Z = +2$ and -1, and the TT model. An improvement with respect to the $Z = 0$ case is only found for protons, i.e. for $Z = +1$. This example shows clearly that UHECRs observations have the potential to restrict the GMF models, which on the other hand might allow to determine the charge of the CR primaries.

Model		$Z=0$		$Z=+1$		$Z=+2$		$Z=-1$	
$E_{20}^{\min}$	N_d	$w_{\rm s}$	$P[\%]$	$w_{\rm s}$	$P[\%]$	$w_{\rm s}$	$P[\%]$	$w_{\rm s}$	$P[\%]$
0.50	32	8	8.8	8	9.7	7	20	6	27
0.45	43	11	4.7	14	0.6	12	3.4	7	36
0.40	57	13	6.6	20	0.05	13	9.9	8	50

Table 2.6: As in Table 2.5, but for different charges (TT model).

2.4   Conclusion and perspectives

In this Chapter we have discussed in detail the effect of the regular component of the Galactic magnetic field on the propagation of UHECR. We have reviewed the current observational knowledge about the GMF and have compared three models discussed previously in the literature. Both in small-scale clustering and correlation studies, the GMF might be used as a sort of natural spectrograph for UHECR, thus helping in identifying sources, restricting the GMF models as well as the chemical composition of the primaries. Notice that the latter point is an important prerequisite to use UHECR data to study strong interaction at energy scales otherwise inaccessible to laboratory experiments.

As a qualitative consequence of the existence of a regular GMF and despite current uncertainties in the GMF models, we have argued that the observed isotropy of cosmic ray flux e.g. around a few 10^{17} eV disfavors a transition to an extragalactic flux of protons at too low energies, say below $10^{17.5}$ eV.

At higher energies, the cosmic rays should enter the ballistic regime. We have provided in tabular and pictorial form an estimate of the typical deflection suffered by UHECRs in the small deflection limit and of its variability from model to model. These results imply that, if the angular resolution of current experiments has to be fully exploited, deflections in the GMF cannot be neglected even for $E = 10^{20}$ eV protons, especially for trajectories along

the Galactic plane or crossing the GC region. Since the magnitude as well as the direction of the deflections are very model-dependent, it is difficult to correct for deflections with the present knowledge about the GMF.

We have also emphasized that, to the purpose of statistical analyses like auto-correlation/cross-correlation studies, the GMF can effectively act in distorting the exposure of the experiment to the extragalactic sky, and we provided some maps of this "exposure-modification" effect. As a consequence, to estimate the chance probability e.g. of small-scale clustering, one should take into account the role of the GMF. We showed that this effect is already appreciable in the data published by AGASA, although its field of view do not include the central regions of the Galaxy. Especially for experiments in the southern hemisphere like Auger, one might think to exclude some part of their data from auto-correlation and correlation studies, as long as no reliable model for the GMF is established. Note that the required cuts are quite drastic. For instance, fixing $E_{\min} = 4 \times 10^{19}$ eV and considering only sky regions where $|\omega_B - 1| < 0.2$ would exclude

TT: $-5° < b_G < 5°$ for all l_G and $-60° < b_G < 60°$ for $-94° < l_G < 75°$,
PS: $-25° < b_G < 22°$ for all l_G and $-38° < b_G < 40°$ for $-33° < l_G < 35°$,
HMR: $-11° < b_G < 8°$ for all l_G and all b_G for $-90° < l_G < 90°$.

Note that in the HMR model more than half of the sky would be excluded. Moreover, at least the overlap of the excluded regions of different models should be considered as long as no GMF model can be clearly favored. A very minimal cut for all three models and for $E_{\min} = 4 \times 10^{19}$ eV is $-5° < b_G < +5°$ for all l_G and $-40° < b_G < +40°$ for $-35° < l_G < 35°$.

If regions where $|\omega_B - 1|$ is large are not excluded, then magnification effects have to be taken into account to assess properly the significance of auto-correlation and correlation studies. As an example, we have performed an autocorrelation analysis of the AGASA data set including GMF effects. Although the present statistics does not allow to draw strong conclusions, we have not found any signal of improvement after the correction for GMF. This could point to an insufficient knowledge of the field or to a significantly heterogeneous chemical composition of the primaries. Finally, the AGASA signal might only be a chance fluctuation.

A reasonable prescription may then be to perform statistical analysis taking into account several models of GMF and several primary charges. In the most pessimistic case, this would allow to quantify in an approximate way the contribution of the GMF to the overall uncertainty. On the other hand, a strong improvement in the significance of a statistical estimator might favor a certain GMF model and/or primary charge assignment. For example,

by repeating the study of Ref. [Tin01c] we have found that the significant correlation of BL Lacs with UHECRs is strongly dependent on the GMF and primary adopted, and is present only in the TT model of the GMF for $Z = 1$. Although this evidence needs confirmation with a larger data set of UHECRs, it may be the start of the era of UHECR astronomy.

Chapter 3

The footprint of large scale structures on the ultra-high energy cosmic rays

The study of small scale clustering is not the only tool available to start UHECR astronomy. Independently from the observation of small scale clustering, one could still look for large scale anisotropies in the data, eventually correlating with some known configuration of astrophysical source candidates. In this context, the most natural scenario to be tested is that UHECRs correlate with the luminous matter in the "local" universe. This is particularly expected for candidates like gamma ray bursts (hosted more likely in star formation regions) or colliding galaxies, but it is also a sufficiently generic hypothesis to deserve an interest of its own.

Aims of this Chapter are: i) to describe a method to evaluate the expected anisotropy in the UHECR sky starting from a given catalogue of the local universe, taking into account the selection function, the blind regions as well as the energy-loss effects; ii) to assess the minimum statistics needed to significantly reject the null hypothesis, in particular providing a forecast for the Auger experiment. Previous attempts to address a similar issue can be found in [Wax96, Smi02, Sin03]. Later in the Chapter we will come back to a comparison with their approaches and results.

We use the IRAS PSCz galaxy catalogue [Sau00]. This catalogue has several limitations, but it is good enough to illustrate the main features of the issue, while still providing some meaningful information. In this Chapter we stress mainly methodological issues. An extension of the analysis to the much more detailed 2MASS [Jar00, Jar04] and SDSS [Yor00, Ade05] galaxy catalogues is presently investigated.

The Chapter is structured as follows: the catalogue and the related issues

are discussed in Section 3.1. In Section 3.2 we describe the technique used for our analysis. The results are discussed in Section 3.3, where we compare our findings with those obtained in previous works. In Section 3.4 we give a brief overview on ongoing research and experimental activities, and draw our conclusions.

3.1   Astronomical data

3.1.1   The catalogue

Two properties are required to make a galaxy catalogue suitable for the type of analysis discussed here. First, a great sky coverage is critical for comparing the predictions with the fraction of sky observed by the UHECR experiments (the Auger experiment is observing all the Southern hemisphere and part of the Northern one). Second, the energy-loss effect in UHECR propagation requires a knowledge of the redshifts for at least a fair subsample of the galaxies in the catalogue. Selection effects both in fluxes and in redshifts play a crucial role in understanding the final outcome of the simulations.

Unfortunately, in practical terms these two requirements turn out to be almost complementary and no available catalogue matches both needs simultaneously. A fair compromise is offered by the IRAS PSCz catalogue [Sau00] which contains about 15000 galaxies and related redshifts with a well understood completeness function down to $z \sim 0.1$ (i.e. down to a redshift which is comparable to the attenuation length introduced by the GZK effect) and a sky coverage of about 84%. The incomplete sky coverage is mainly due to the so called zone of avoidance centered on the galactic plane and caused by the galactic extinction and to a few, narrow stripes which were not observed with enough sensitivity by the IRAS satellite (see Fig. 3.1). These regions are excluded from our analysis with the use of the binary mask available with the PSCz catalogue itself.

3.1.2   The selection function

No available galaxy catalogue is complete in volume and therefore completeness estimates derived from the selection effects in flux are needed. More in detail, the relevant quantity to be derived is the fraction of galaxies actually observed at the various redshifts, a quantity also known as the redshift selection function $\phi(z)$ [Pee80]. A convenient way to express $\phi(z)$ is in terms of the galaxy luminosity function (i.e. the distribution of galaxy luminosities)
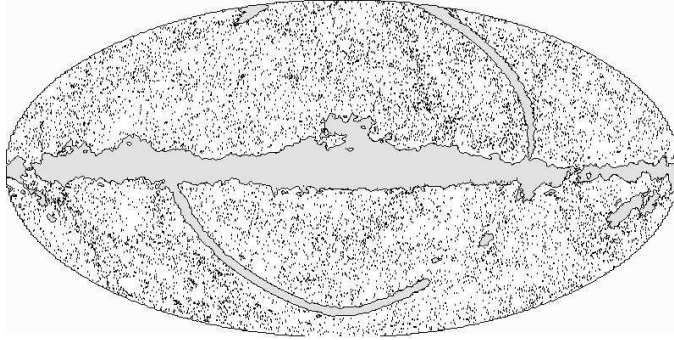
Fig. 3.1.— PSCz catalogue source distribution and related mask in galactic coordinates.

$\Phi(L)$ as

$$\phi(z) = \frac{\int_{L_{\min}(z)}^{\infty} d\,L\ \Phi(L)}{\int_{0}^{\infty} d\,L\ \Phi(L)}. \tag{3.1}$$

Here $L_{\min}(z)$ is the minimum luminosity detected by the survey as function of redshift. For a flux-limited survey with limiting flux $f_{\lim}$, $L_{\min}(z)$ is given by definition in terms of the luminosity distance $d_L(z)$ as

$$L_{\min}(z) = 4\pi d_L^2(z) f_{\lim}. \tag{3.2}$$

The luminosity distance depends on the cosmology assumed, though for redshifts $z \lesssim 0.1$ it can be approximated by $d_L(z) \simeq z/H_0$. Generally $\phi(z)$ is inferred from the catalogue data itself in a self-consistent way, using the observational galaxy luminosity distribution to estimate $\Phi(L)$; for details see [San79, Efs88] and the references in the PSCz article [Sau00]. The quantity $n(z)/\phi(z)$ represents the experimental distribution corrected for the selection effects, which must be used in the computations. A detailed discussion of this issue can be found in [Bln00]. Furthermore, we wish to stress that for $z \ll 1$ evolution effects are negligible and the local universe galaxy luminosity function can be safely used. In the case of deeper surveys like SDSS, cosmological effects can not be neglected and our approach can still be employed even though a series of corrections (e.g. evolutionary effects or scale-dependent luminosity) must be taken into account [Teg03]. These corrections are needed since luminous galaxies, which dominate the sample at large scales, cluster more than faint ones [Dav88]. In the case of the PSCz catalogue the selection function is given as [Sau00]

$$\phi(r) = \phi_* \left(\frac{r}{r_*}\right)^{1-\alpha} \left[1 + \left(\frac{r}{r_*}\right)^{\gamma}\right]^{-\left(\frac{\beta}{\gamma}\right)}, \tag{3.3}$$
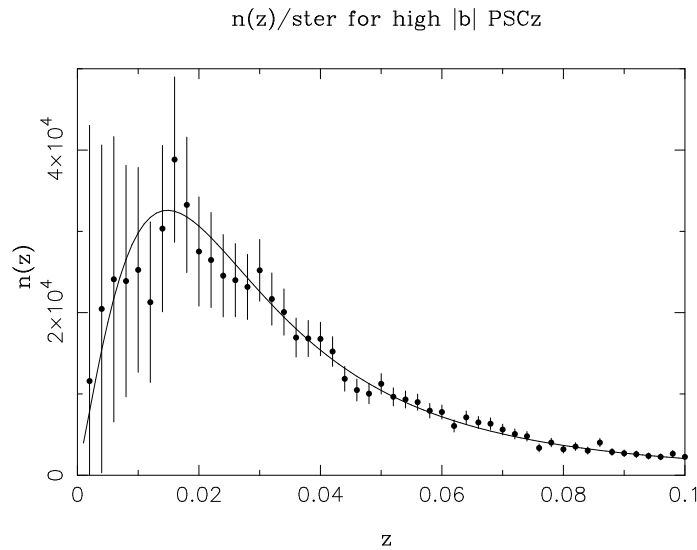
Fig. 3.2.— Experimental redshift distribution of the PSCz catalogue galaxies and prediction for an homogeneous universe from the selection function $\phi(z)$ [Sau00]. Both are normalized in order to represent the number of sources per unit of redshift per steradian.

with the parameters $\phi_* = 0.0077$, $\alpha = 1.82$, $r_* = 86.4$, $\gamma = 1.56$, $\beta = 4.43$ that respectively describe the normalization, the slope at low redshift, the break distance in $h^{-1}\mathrm{Mpc}$, its sharpness and the additional slope beyond the break (see Fig. 3.2).

It is clear, however, that even taking into account the selection function we can not use the catalogue up to the highest redshifts ($z \simeq 0.3$), due to the rapid loss of statistics. At high z, the intrinsic statistical fluctuation due to the selection effect starts to dominate over the true matter fluctuations, producing artificial clusterings not corresponding to real structures ("shot noise" effect). This problem is generally treated constructing from the point sources catalogue a smoothed density field $\rho(\hat{\Omega}, z)$ with a variable smoothing length that effectively increases with redshift, remaining always of size comparable to the mean distance on the sphere of the sources of the catalogue. We minimize this effect by conservatively setting the maximum redshift at $z = 0.06$ (corresponding to $180\, h^{-1}\mathrm{Mpc}$) where we have still good statistics while keeping the shot noise effect under control. With this threshold we are left with about $11,500$ sources of the catalogue. Furthermore, for the purposes of the present analysis, the weight of the sources rapidly decreases with redshift due to the energy losses induced by the GZK effect. In the energy range $E \geq 5 \times 10^{19}\,\mathrm{eV}$, the contribution from sources beyond $z = 0.06$ is sub-

dominant, thus allowing us to assume for the objects beyond $z = 0.06$ an effectively isotropic source contribution.

3.2 The formalism

In the following we describe in some detail the steps involved in our formalism. In Sec. 3.2.1 we summarize our treatment for energy losses, in Sec. 3.2.2 the way the effective UHECR map is constructed, and in Sec. 3.2.3 the statistical analysis we perform.

3.2.1 UHECR propagation

Our first goal is to obtain the underlying probability distribution $f_{\rm LSS}(\hat{\Omega}, E)$ to observe a UHECR with energy higher than E from the direction $\hat{\Omega}$. For simplicity here and throughout the Chapter we shall assume that each source of our catalogue has the same probability to emit a UHECR, according to some spectrum at the source $g(E_i)$. In principle, one would expect a correlation of this probability with one or more properties of the source: its star formation rate, radio-emission, size, etc. The authors of [Sin03] tested for a correlation $L_{\rm UHECR} \propto L_{\rm FIR}^{\kappa}$, $L_{\rm UHECR}$ being the luminosity in UHECRs, $L_{\rm FIR}$ the one in far-infrared region probed in the IRAS catalogue, and κ a phenomenological parameter. The results of their analysis do not change appreciably as long as $0 \lesssim \kappa \lesssim 1$. We can then expect that our limit of $\kappa = 0$ might well work for a broader range in parameter space. The method we discuss can be however easily generalized to such a case, and eventually also to a multi-parametric modelling of the correlation.

In an ideal world where a volume-complete catalogue were available and no energy losses for UHECRs were present, each source should then be simply weighted by the geometrical flux suppression $\propto d_L^{-2}$. The selection function already implies a change of the weight into $\phi^{-1} d_L^{-2}$. Moreover, while propagating to us, high energy protons lose energy as a result of the cosmological redshift and of the production of $e^{\pm}$ pairs and pions (the dominant process) caused by interactions with the CMB. For simplicity, we shall work in the continuous-loss approximation [Ber88]. Then, a proton of energy E_i at the source at $z = z_i$ will be degraded at the Earth ($z = 0$) to an energy E_f given by the energy-loss equation

$$\frac{1}{E}\frac{{\rm d}E}{{\rm d}z} = -\frac{{\rm d}t}{{\rm d}z} \times (\beta_{\rm rsh} + \beta_{\pi} + \beta_{e^{\pm}}). \tag{3.4}$$

We are neglecting here diffuse backgrounds other than CMB, and assuming straight-line trajectories, coherently with the hypothesis of weak EGMF.

Equation (3.4) has to be integrated from z_i, where the initial Cauchy condition $E(z = z_i) = E_i$ is imposed, to $z = 0$. The different terms in Eq. (3.4) are explicitly shown below

$$-\frac{\mathrm{d}t}{\mathrm{d}z} = \left[(1+z)H_0\sqrt{(1+z)^3\,\Omega_M + \Omega_\Lambda}\right]^{-1}, \tag{3.5}$$

$$\beta_{\mathrm{rsh}}(z) = H_0\sqrt{(1+z)^3\,\Omega_M + \Omega_\Lambda}, \tag{3.6}$$

$$\beta_{e^\pm}(z, E) \simeq \frac{\alpha^3 Z^2}{4\pi^2}\frac{m_e^2 m_p^2}{E^3}\int_2^\infty \mathrm{d}\xi \frac{\varphi(\xi)}{\exp\left[\frac{m_e m_p \xi}{2ET_0(1+z)}\right] - 1}, \tag{3.7}$$

$$\beta_\pi(z, E) \simeq \begin{cases} C_\pi(1+z)^3 & E \geq E_{\mathrm{match}}, \\ A_\pi(1+z)^3 e^{-\frac{B_\pi}{E(1+z)}} & E \leq E_{\mathrm{match}}, \end{cases} \tag{3.8}$$

where H_0 is the Hubble constant and Ω_M and Ω_Λ are respectively the matter and cosmological constant densities in terms of the critical one, m_e and m_p are respectively the electron and proton masses, T_0 the present CMB temperature, and α the fine-structure constant. We assume $H_0 = 71\,\mathrm{km\ s^{-1}}$ $\mathrm{Mpc^{-1}}$, $\Omega_M = 0.27$, and $\Omega_\Lambda = 0.73$ [Spe03]. Since we are probing the relatively near universe, the results will not depend much on the cosmological model adopted, but mainly on the value assumed for H_0. More quantitatively, the r.h.s of Eq. (3.4) changes linearly with H_0^{-1} (apart for the negligible term β_{rsh}), while even an extreme change from the model ($\Omega_M = 0.27$; $\Omega_\Lambda = 0.73$) to ($\Omega_M = 1$; $\Omega_\Lambda = 0.0$) (the latter ruled out by present data) would only modify the energy loss term by 6% at $z = 0.06$, the highest redshift we consider. The parametrization for β_π as well as the values $\{A_\pi, B_\pi, C_\pi\} = \{3.66 \times 10^{-8}\mathrm{yr^{-1}}, 2.87 \times 10^{20}\,\mathrm{eV}, 2.42 \times 10^{-8}\mathrm{yr^{-1}}\}$ are taken from [Anc96], and $E_{\mathrm{match}}(z) = 6.86\,e^{-0.807\,z} \times 10^{20}\,\mathrm{eV}$ is used to ensure continuity to $\beta_\pi(z, E)$. A useful parametrization of the auxiliary function $\varphi(\xi)$ can be found in [Cho92], which we follow for the treatment of the pair production energy loss. In practice, we have evolved cosmic rays over a logarithmic grid in E_i from 10^{19} to 10^{23} eV, and in z from 0.001 to 0.3. The values at a specific source site has been obtained by a smooth interpolation.

Note that in our calculation i) the propagation is performed to attribute an "energy-loss weight" to each z in order to derive a realistic probability distribution $f_{\mathrm{LSS}}(\hat{\Omega}, E)$; ii) we are going to smooth the result over regions of several degrees in the sky (see below), thus performing a sort of weighted average over redshifts as well. Since this smoothing effect is by far dominant over the single source stochastic fluctuation induced by pion production, the average effect accounted for by using a continuous energy-loss approach is a suitable approximation. In summary, the propagation effects provide us an invertible final-energy function $E_f(E_i, z)$ giving the energy at the Earth for

a particle injected with energy E_i at a redshift z.

3.2.2 Map making

Given an arbitrary injection spectrum $g(E_i)$, the observed events at the Earth would distribute, apart for a normalization factor, according to the spectrum $g(E_i(E_f, z))dE_i/dE_f$. In particular we will consider in the following a typical power-law $g(E_i) \propto E_i^{-s}$, but this assumption may be easily generalized. Summing up on all the sources in the catalogue it is easy to obtain the expected differential flux map on Earth

$$F(\hat{\Omega}, E_f) \propto \sum_k \frac{1}{\phi(z_k)} \frac{\delta(\hat{\Omega} - \hat{\Omega}_k)}{4\pi d_L^2(z_k)} E_i^{-s}(E_f, z_k) \frac{\mathrm{d}E_i}{\mathrm{d}E_f}(E_f, z_k), \qquad (3.9)$$

where the selection function and the geometrical flux suppression have been taken into account. However, given the low statistics of events available at this high energies, a more useful quantity to employ is the integrated flux above some energy threshold E_{cut}, that can be more easily compared with the integrated UHECR flux above the cut E_{cut}. Integrating the previous expression we have

$$
\begin{aligned}
f_{\mathrm{LSS}}(\hat{\Omega}, E_{\mathrm{cut}}) &\propto \sum_k \frac{1}{\phi(z_k)} \frac{\delta(\hat{\Omega} - \hat{\Omega}_k)}{4\pi d_L^2(z_k)} \int_{E_i(E_{\mathrm{cut}}, z_k)}^{\infty} E^{-s} \mathrm{d}E \\
&= \sum_k f_{\mathrm{LSS}}(k)\, \delta(\hat{\Omega} - \hat{\Omega}_k),
\end{aligned}
\qquad (3.10)
$$

that can be effectively seen as if at every source k of the catalogue a weight $f_{\mathrm{LSS}}(k)$ is assigned that takes into account geometrical effects (d_L^{-2}), selection effects (ϕ^{-1}), and physics of energy losses through the integral in $\mathrm{d}E$; in this "GZK integral" the upper limit of integration is taken to be infinite, though the result is practically independent on the upper cut used, provided it is much larger than 10^{20} eV.

It is interesting to compare the similar result expected for an uniform source distribution with constant density; in this case we have (in the limit $z \ll 1$)

$$f_{\mathrm{LSS}}(\hat{\Omega}, E_{\mathrm{cut}}) \propto \int \mathrm{d}z \frac{[E_i(E_{\mathrm{cut}}, z)]^{-s+1}}{s-1} \equiv \int \mathrm{d}z\, p(z, E_{\mathrm{cut}}, s), \qquad (3.11)$$

where the integral in $\mathrm{d}E$ has been explicitly performed and the flux suppression weight is cancelled by the geometrical volume factor. The integrand $p(z, E_{\mathrm{cut}}, s)$ containing the details of the energy losses also provides an effective cut at high z. The integrand—normalized to have unit area—can be

interpreted as the distribution of the injection distances of CR observed at the Earth. It also suggests the definition of the so called "GZK sphere" as the sphere from which originates most (say 99%) of the observed CR flux on Earth above an energy threshold $E_{\rm cut}$. In Figure 3.3 we plot the distribution p for different values of $E_{\rm cut}$ and s. We see that around a particular threshold $z_{\rm GZK}$ the distribution falls to zero: The dependence of $z_{\rm GZK}$ on $E_{\rm cut}$ is quite critical as expected, while there is also a softer dependence on s. This suggests naturally the choice $E_{\rm cut} = 5 \times 10^{19}$ eV for the chosen value $z_{\rm GZK} \simeq 0.06$; at the same time, the energy cut chosen is not too restrictive, ensuring indeed that significant statistics might be achieved in a few years.

For this $E_{\rm cut}$ the isotropic contribution to the flux is sub-dominant; however we can take it exactly into account and the weight of the isotropic part is given by

$$w_{\rm iso} = \frac{\int_{z_{\rm GZK}}^{\infty} {\rm d}z\, p(z, E_{\rm cut})}{\int_0^{z_{\rm GZK}} {\rm d}z\, p(z, E_{\rm cut})} \sum_k f_{\rm LSS}(k). \tag{3.12}$$

Finally, to represent graphically the result, the spike-like map (3.10) is effectively smoothed through a Gaussian filter as

$$f_{\rm LSS}(\hat{\Omega}, E_{\rm cut}) \propto \sum_k f_{\rm LSS}(k) \exp\left(-\frac{d_s^2[\hat{\Omega}, \hat{\Omega}_k]}{2\sigma^2}\right) + \frac{w_{\rm iso}}{4\pi} 2\pi\sigma^2 \mu(\hat{\Omega}). \tag{3.13}$$

In the previous equation, σ is the width of the gaussian filter, d_s is the spherical distance between the coordinates $\hat{\Omega}$ and $\hat{\Omega}_k$, and $\mu(\hat{\Omega})$ is the catalogue mask (see Sec. 3.1.1) such that $\mu(\hat{\Omega}) = 0$ if $\hat{\Omega}$ belongs to the mask region and $\mu(\hat{\Omega}) = 1$ otherwise.

3.2.3　Statistical analysis

Given the extremely poor UHECR statistics, we limit ourselves to address the basic issue of determining the minimum number of events needed to significantly reject "the null hypothesis". To this purpose, it is well known that a χ^2-test is an efficient estimator. Notice that a χ^2-test needs a binning of the events, but differently from the K-S test performed in [Sin03] or the Smirnov-Cramer-von Mises test of [Smi02], it has no ambiguity due to the 2-dimensional nature of the problem. A similar approach was used in [Wax96], with which later we will compare our results. A criterion guiding us in the choice of the bin size is the following: with N UHECRs events available and M bins, one would expect $\mathcal{O}(N/M)$ events per bin. To allow a reliable application of the χ^2-test, one has to impose $N/M \geq 10$. Each cell should then cover at least a solid angle of $\Delta_M \sim 10 \times \Delta_{\rm tot}/N$, $\Delta_{\rm tot}$ being the solid angle accessible to the experiment. For $\Delta_{\rm tot} \sim 2\pi$ (50% of full sky coverage),
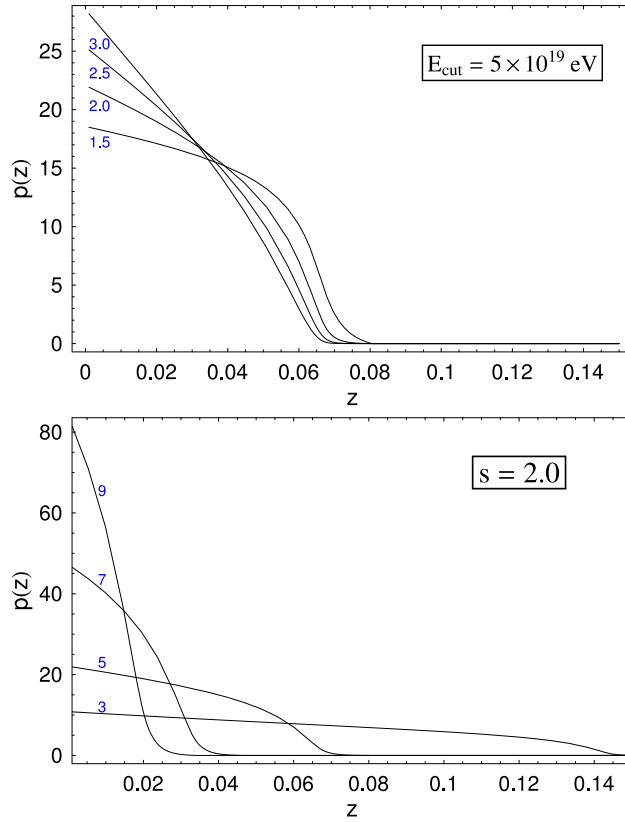
Fig. 3.3.— Distribution of the injection distances of CR observed at the Earth for fixed $E_{cut} = 5 \times 10^{19}$ eV (top) and $s = 1.5, 2.0, 2.5, 3.0$ and for fixed spectral index $s = 2.0$ (bottom) and varying $E_{cut} = 3, 5, 7, 9 \times 10^{19}$ eV.

one estimates a square window of side $454°/\sqrt{N}$, i.e. $45°$ for 100 events, $14°$ for 1000 events. Since the former number is of the order of present world statistics, and the latter is the achievement expected by Auger in a few years of operation, a binning in windows of size $15°$ represents a reasonable choice for our forecast. This choice is also suggested by the typical size of the observable structures, a point we will comment on further at the end of this Section. Notice that the GMF, that induces at these energies typical deflections of about $4°$, can be safely neglected for this kind of analysis. The same remark holds for the angular resolution of the experiment.

Obviously, for a specific experimental set-up one must include the proper exposure ω_{exp}, to convolve with the previously found f_{LSS}. The function ω_{exp} depends on the declination δ, right ascension R.A., and, in general, also of energy. For observations having uniform coverage in R.A., like AGASA or
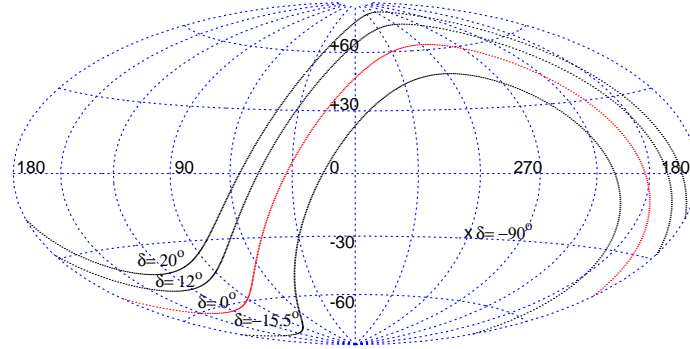
Fig. 3.4.— Galactic coordinate reference frame and contours enclosing 68%, 95% and 99% of the Auger exposure function, with the corresponding declinations. The celestial equator ($\delta = 0°$) and south pole ($\delta = -90°$) are also shown.

Auger ground based arrays, one can easily parameterize the relative exposure as [Som00]

$$\omega_{\mathrm{exp}}(\delta) \propto \cos\theta_0 \sin\alpha_m \cos\delta + \alpha_m \sin\theta_0 \sin\delta, \qquad (3.14)$$

where θ_0 is the latitude of the experiment ($\theta_0 \approx -35°$ for Auger South), α_m is given by

$$\alpha_m = \begin{cases} 0\,, & \text{if } \xi > 1 \\ \pi\,, & \text{if } \xi < -1 \\ \arccos^{-1}\xi\,, & \text{otherwise} \end{cases} \qquad (3.15)$$

and

$$\xi \equiv \frac{\cos\theta_{\max} - \sin\theta_0 \ \sin\delta}{\cos\theta_0 \ \cos\delta}\,, \qquad (3.16)$$

$\theta_{\max}$ being the maximal zenith angle cut applied (we assume $\theta_{\max} = 60°$ for Auger). Contour plots for the Auger exposure function in Galactic coordinates are shown in Fig. 3.4.

For a given experiment and catalogue, the null hypothesis we want to test is that the events observed are sampled—apart from a trivial geometrical factor—according to the distribution $f_{\mathrm{LSS}}\,\omega_{\mathrm{exp}}\,\mu$. Since we are performing a forecast analysis, we will consider test realizations of N events sampled according to a random distribution on the (accessible) sphere, i.e. according

to $\omega_{\mathrm{exp}}\,\mu$, and determine the C.L. with which the hypothesis is rejected as a function of N. For each realization of N events we calculate the two functions

$$\mathcal{X}^2_{\mathrm{iso}}(N) = \frac{1}{M-1}\sum_{i=1}^{M}\frac{(o_i - \epsilon_i[f_{\mathrm{iso}}])^2}{\epsilon_i[f_{\mathrm{iso}}]}, \tag{3.17}$$

$$\mathcal{X}^2_{\mathrm{LSS}}(N) = \frac{1}{M-1}\sum_{i=1}^{M}\frac{(o_i - \epsilon_i[f_{\mathrm{LSS}}])^2}{\epsilon_i[f_{\mathrm{LSS}}]}, \tag{3.18}$$

where o_i is the number of "random" counts in the i-th bin Ω_i, and $\epsilon_i[f_{\mathrm{LSS}}]$ and $\epsilon_i[f_{\mathrm{iso}}]$ are the theoretically expected number of events in Ω_i respectively for the LSS and isotropic distribution. In formulae (see Eq. (3.10)),

$$\epsilon_i[f_{\mathrm{LSS}}] = N\alpha\frac{\sum_{j\in\Omega_i} f_{\mathrm{LSS}}(j)\omega_{\mathrm{exp}}(\delta_j)\mu(j) + w_{\mathrm{iso}}/4\pi\,S[\Omega_i]}{\sum_j f_{\mathrm{LSS}}(j)\omega_{\mathrm{exp}}(\delta_j)\mu(j) + w_{\mathrm{iso}}/4\pi\,S_\omega}, \tag{3.19}$$

$$\epsilon_i[f_{\mathrm{iso}}] = N\alpha\frac{S[\Omega_i]}{S_\omega}, \tag{3.20}$$

where $S[\Omega_i] = \int_{\Omega_i}d\Omega\,\omega_{\mathrm{exp}}\mu$ is the spherical surface (exposure- and mask-corrected) subtended by the angular bin Ω_i, and similarly $S_\omega = \int_{4\pi}d\Omega\,\omega_{exp}\mu$. The mock data set is then sampled $\mathcal{N}$ times in order to establish empirically the distributions of $\mathcal{X}^2_{\mathrm{LSS}}$ and $\mathcal{X}^2_{\mathrm{iso}}$, and the resulting distribution is studied as function of N (plus eventually s, E_{cut}, etc.). The parameter

$$\alpha \equiv \frac{\int d\Omega\,\omega_{\mathrm{exp}}(\delta)\mu(\Omega)}{\int d\Omega\,\omega_{\mathrm{exp}}(\delta)} \tag{3.21}$$

is a mask-correction factor that takes into account the number of points belonging to the mask region and excluded from the counts o_i. Note that the random distribution is generated with N events in the all sky-view of the experiment, but, effectively, only the region outside the mask is included in the statistical analysis leaving us with effective $N\alpha$ events to study. This is a limiting factor due to quality of the catalogue. With a better sky coverage the statistics is improved and the number of events required to asses the model can be reduced.

As our last point, we return to the problem of the choice of the bin size. To assess its importance we studied the dependence of the results on this parameter. For a cell side larger than about $25°$ the analysis loses much of its power, and a very high N is required to distinguish the models and obtain meaningful conclusions. This is somewhat expected looking at the map results that we obtain, where typical structures have dimensions of about $15°$–$20°$: a greater cell size results effectively in a too large smoothing and a consequent lost of information. On the other hand, a cell size below $4°$–$6°$ makes the use

of a χ^2 analysis not very reliable, because of the low number of events in each bin expected for realistic exposure times. In the quite large interval 6°–20° for the choice of the cell size, however, the result is almost independent of the bin size, that makes us confident on the reliability of our conclusions.

3.3 Results

In Fig. 3.5 we plot the smoothed maps in galactic coordinates of the expected integrated flux of UHECRs above the energy threshold $E_{\mathrm{cut}} = 3, 5, 7, 9 \times 10^{19}$ eV and for slope parameter $s = 2.0$; the isotropic part has been taken into account and the ratio of the isotropic to anisotropic part $w_{\mathrm{iso}} / \sum_k f_{\mathrm{LSS}}(k)$ is respectively $83\%, 3.6\%, \ll 1\%, \ll 1\%$.

Only for $E_{\mathrm{cut}} = 3 \times 10^{19}$ eV the isotropic background constitutes a relevant fraction, since the GZK suppression of distant sources is not yet present. For the case of interest $E_{\mathrm{cut}} = 5 \times 10^{19}$ eV the contribution of w_{iso} is almost negligible, while it practically disappears for $E_{\mathrm{cut}} \gtrsim 7 \times 10^{19}$ eV. Varying the slope for $s = 1.5, 2.0, 2.5, 3.0$ while keeping $E_{\mathrm{cut}} = 5 \times 10^{19}$ eV fixed produces respectively the relative weights $8.0\%, 3.6\%, 1.8\%, 0.9\%$, so that only for very hard spectra w_{iso} would play a non-negligible role (see also Fig. 3.3).

Due to the GZK-effect, as it was expected, the nearest structures are also the most prominent features in the maps. The most relevant structure present in every slide is the Local Supercluster. It extends along $l \simeq 140°$ and $l \simeq 300°$ and includes the Virgo cluster at $l = 284°, b = +75°$ and the Ursa Major cloud at $l = 145°, b = +65°$, both located at $z \simeq 0.01$. The lack of structures at latitudes from $l \simeq 0°$ to $l \simeq 120°$ corresponds to the Local Void. At higher redshifts the main contributions come from the Perseus-Pisces supercluster ($l = 160°, b = -20°$) and the Pavo-Indus supercluster ($l = 340°, b = -40°$), both at $z \simeq 0.02$, and the very massive Shapley Concentration ($l = 250°, b = +20°$) at $z \simeq 0.05$. For a more detailed list of features in the map, see the key in Fig. 3.6.

The E_{cut}-dependence is clearly evident in the maps: as expected, increasing E_{cut} results in a map that closely reflects the very local universe (up to $z \simeq 0.03$–0.04) and its large anisotropy; conversely, for $E_{\mathrm{cut}} \simeq 3$–$4 \times 10^{19}$ eV, the resulting flux is quite isotropic and the structures emerge as fluctuations from a background, since the GZK suppression is not yet effective. This can be seen also comparing the near structures with the most distant ones in the catalogue: While the Local Supercluster is well visible in all slides, the signal from the Perseus-Pisces super-cluster and the Shapley concentration is of comparable intensity only in the two top panels, while becoming highly attenuated for $E_{\mathrm{cut}} = 7 \times 10^{19}$ eV, and almost vanishing for $E_{\mathrm{cut}} = 9 \times 10^{19}$ eV.
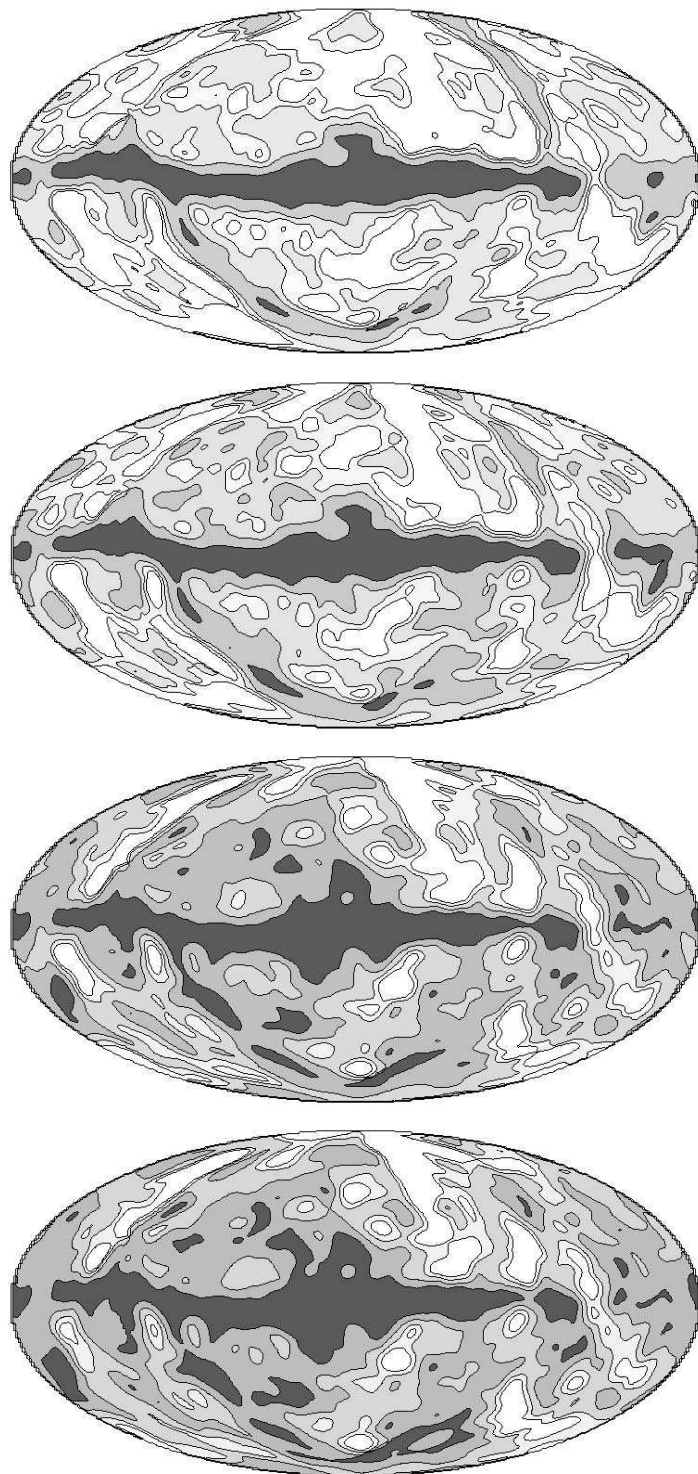
Fig. 3.5.— Equal area Hammer-Aitoff projections of the smoothed UHECRs arrival directions distribution (Eq. (3.13)) in galactic coordinates obtained for fixed $s = 2.0$ and, from the upper to the lower panel, for $E_{cut} = 3, 5, 7, 9 \times 10^{19}$ eV. The smoothing angle is $\sigma = 3°$. The contours enclose 95%, 68%, 38%, 20% of the corresponding distribution.
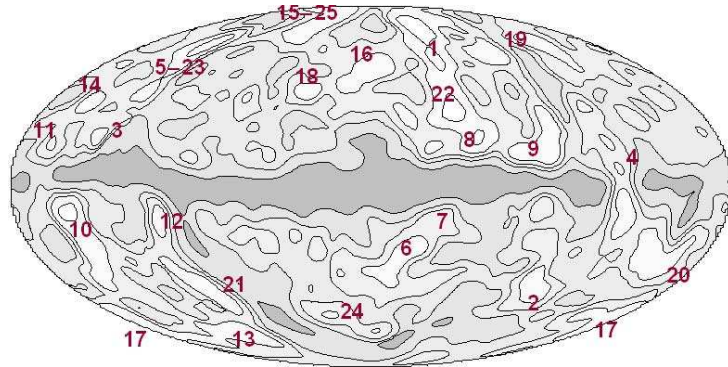
Fig. 3.6.— Detailed key of the structures visible in the UHECR maps; arbitrary contour levels. Labels correspond to: (1) Southern extension of Virgo and Local Supercluster; (2)Fornax-Eridani Cluster; (3) Cassiopea Cluster; (4) Puppis Cluster; (5) Ursa Major Cloud; (6-7) Pavo-Indus and "Great Attractor" region; (8) Centaurus Super-Cluster; (9) Hydra Super-Cluster; (10) Perseus Super-Cluster; (11) Abell 569; (12) Pegasus Cluster; (13-17) Pisces Cluster; (14) Abell 634; (15) Coma Cluster; (16-18) Hercules Supercluster; (19) Leo Supercluster; (20) Columba Cluster; (21) Cetus Cluster; (22) Shapley Concentration; (23) Ursa Major Supercluster; (24) Sculptor Supercluster; (25) Bootes Supercluster.

A similar trend is observed for increasing s at fixed E_{cut}, though the dependence is almost one order of magnitude weaker.

Looking at the contour levels in the maps we can have a precise idea of the absolute intensity of the "fluctuations" induced by the LSS; in particular, for the case of interest of $E_{\mathrm{cut}} = 5 \times 10^{19}$ eV the structures emerge only at the level of 20%–30% of the total flux, the 68% of the flux actually enclosing almost all the sky. For $E_{\mathrm{cut}} = 7$–9×10^{19} eV, on the contrary, the local structures are significantly more pronounced, but in this case we have to face the low statistics available at these energies. Then in a low-statistics regime it is not an easy task to disentangle the LSS and the isotropic distributions.

The structures which are more likely to be detected by Auger (see also Fig. 3.4) are the Shapley concentration, the Southern extension of the Virgo cluster, the Local Supercluster and the Pavo-Indus super-cluster. Other structures, such as the Perseus-Pisces supercluster and the full Virgo cluster are visible only from the Northern hemisphere and are therefore within the reach of experiments like Telescope Array [Ara03], or the planned North extension of the Pierre Auger Observatory. Moreover, the sky region obscured by the heavy extinction in the direction of the Galactic Plane reflects a lack of information about features possibly "hidden" there. Unfortunately, this region

falls just in the middle of the Auger field of view, thus reducing—for a given statistics N—the significance of the check of the null hypothesis. Numerically, this translates into a smaller value of the factor α of Eq. (3.21) with respect to a hypothetical "twin" Northern Auger experiment.

A quantitative statistical analysis confirms the previous qualitative considerations. In Table 3.1 we report the probability to reject the isotropic hypothesis at 90% and 99% C.L. when UHECRs follow the LSS distribution as a function of the injection spectral index and of the observed number of events. In Figure 3.7 we show the distributions of the functions $\mathcal{X}^2_{\mathrm{iso}}$ and $\mathcal{X}^2_{\mathrm{LSS}}$ introduced in the previous Section for $s = 2.0, 3.0$ and $N = 200, 1000$. It is clear that a few hundred events are hardly enough to reliably distinguish the two models, while $N = 800$–1000 should be more than sufficient to reject the hypothesis at 2–3 σ, independently of the injection spectrum. Steeper spectra however slightly reduce the number of events needed for a given C.L. discrimination. It is also interesting to note that, using different techniques and unconstrained LSS simulations, it was found that a comparable statistics is needed to probe a magnetized local universe [Sig04].

With respect to the previous literature on the subject, our analysis is the closest to the one of [Wax96]. Apart for technical details, the greatest differences with respect to this work arise because of the improved determination of crucial cosmological parameters in the last decade. Just to mention a few, the Hubble constant used in [Wax96] was 100 km s^{-1} Mpc^{-1}, against the presently determined value of 71^{+4}_{-3} km s^{-1} Mpc^{-1}. This changes by 30% the value of the quantity z_{GZK} (see Section 3.2.2). Moreover, the catalogue [Fis95] that was used in [Wax96] contains about 1/3 of the objects we are consider-

$N \setminus s$	1.5	2.0	2.5	3.0
50	(42:6)	(47:8)	(52:10)	(52:10)
100	(55:9)	(60:12)	(66:14)	(69:16)
200	(72:27)	(78:33)	(84:40)	(86:43)
400	(92:61)	(95:72)	(97:80)	(98:83)
600	(98:85)	(99:91)	(100:96)	(100:97)
800	(100:95)	(100:98)	(100:99)	(100:100)
1000	(100:98)	(100:100)	(100:100)	(100:100)

Table 3.1: The probability (in %) to reject the isotropic hypothesis at (90%:99%) C.L. when UHECRs follow the LSS distribution, as a function of the injection spectral index and of the observed number of events, fixing $E_{\mathrm{cut}} = 5 \times 10^{19}$ eV.
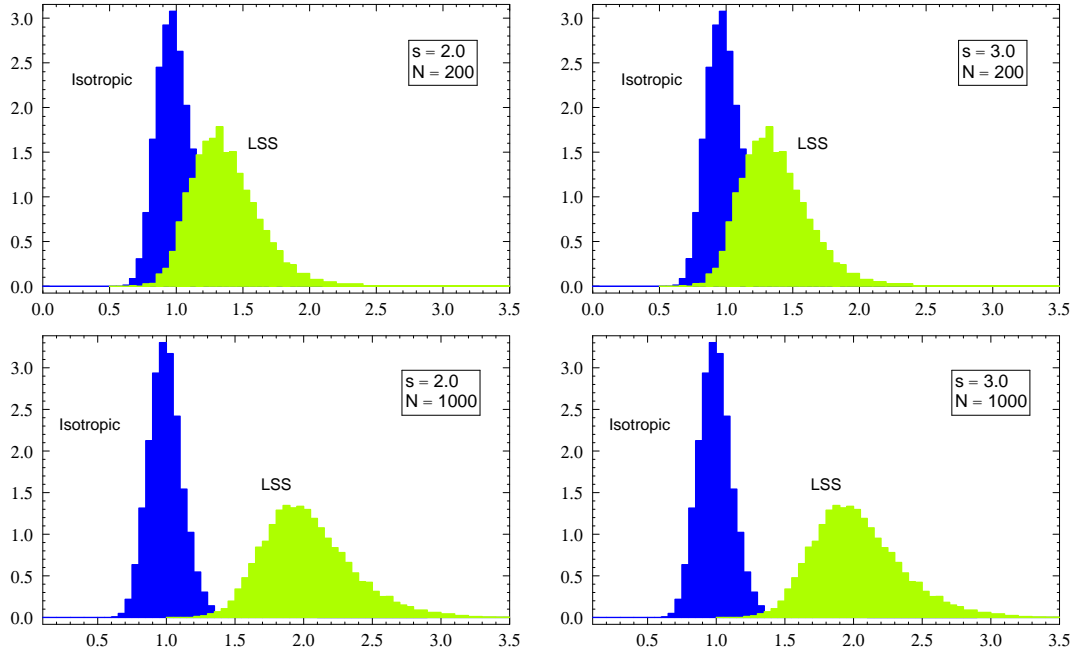
Fig. 3.7.— The probability distributions of the estimators $\mathcal{X}^2_{\mathrm{iso}}$ and $\mathcal{X}^2_{\mathrm{LSS}}$ for the cases $s = 2.0, 3.0$ and for $N = 200, 1000$ events, fixing $E_{\mathrm{cut}} = 5 \times 10^{19}$ eV. The distribution are the results of 10000 Monte-Carlo simulation like described in the text.

ing, has looser selection criteria and larger contaminations [Sau00]. Finally, the specific location of the Southern Auger observatory was not taken into account. All together, when considering these factors, we find quite good agreement with their results.

Some discrepancy arises instead with the results of [Sin03], whose maps appear to be dominated by statistical fluctuations, which mostly wash away physical structures. This has probably to be ascribed to two effects, the energy cut $E_{\mathrm{cut}} = 4 \times 10^{19}$ eV and the inclusion of high redshift object (up to $z \simeq 0.3$) of the catalogue [Sau00] in their analysis. Their choice of $E_{\mathrm{cut}} = 4 \times 10^{19}$ eV implies indeed $z_{\mathrm{GZK}} \simeq 0.1$, i.e. a cutoff in a redshift range where shot noise distortions are no longer negligible. The same remarks hold for [Smi02], which also suffers of other missing corrections [Sin03]. Also, in both cases, the emphasis is mainly in the analysis of the already existing AGASA data than in a forecast study. Our results however clearly show that AGASA statistics (only 32 events at $E \geq 5 \times 10^{19}$ eV in the published data set [Hay00], some of which falling inside the mask) is too limited to draw any firm conclusion.

3.4 Summary and conclusion

In this Chapter we have described the technical steps needed to properly evaluate the expected anisotropy in the UHECR sky starting from a given catalogue of the local universe, taking into account the selection function, the blind regions, and the energy-loss effects. By applying this method to the catalogue [Sau00], we have established the minimum statistics needed to significantly reject the null hypothesis, in particular providing a forecast for the Auger experiment. We showed with a χ^2 approach that several hundred events are required to start testing the model at Auger South. The most prominent structures eventually visible for this experiment were also identified.

Differently from other statistical tools based e.g. on auto-correlation analysis, the approach sketched above requires an Ansatz on the source candidates. The distribution of the luminous baryonic matter considered here can be thought as a generic expectation deserving interest of its own, but it is also expected to correlate with many sources proposed in the literature. In any case, if many astrophysical sources are involved in UHECR production, it is likely that they should better correlate with the local baryonic matter distribution than with an isotropic background.

Until now, the lack of UHECR statistics and the inadequacy of the astronomical catalogues has seriously limited the usefulness of these kinds of analyses. However, progress is expected in both directions in forthcoming years. From the point of view of UHECR observatories, the Southern site of Auger is almost completed, and already taking data: From January 2004 to June 2005, it has reached a cumulative exposure of 1750 km^2 sr yr, observing 10 events over $10^{19.7}$ eV = 5×10^{19} eV (www.auger.org/icrc2005/spectrum.html), Notice that statistical and systematic errors are still quite large, and a downshift in the $\log_{10} E$ scale of 0.1 would for example change the previous figure to 17 events. Once completed, the total area covered will be 3000 km^2, thus improving by one order of magnitude present statistics in a couple of years [Bet05]. The idea to build a Northern Auger site strongly depends on the possibility to perform UHECR astronomy, for which full sky coverage is of primary importance. In any case, starting from 2007, the Telescope Array should offer almost an order of magnitude larger aperture per year than AGASA in the Northern sky, with a better control over the systematics thanks to a hybrid technique similar to the one employed in Auger.

The other big step is expected in astronomical catalogues. The 2MASS survey [Jar00] has resolved more than 1.5 million galaxies in the near-infrared, and has been explicitly designed to provide an accurate photometric and astrometric knowledge of the nearby Universe. The observation in the near IR

is particularly sensitive to the stellar component, and as a consequence to the luminous baryons. Although the redshifts of the sources have to be obtained via photometric methods, the larger error on the distance estimates (about 20% from the 3-band 2MASS photometry [Jar04]) is more than compensated by the larger statistics. Independently of the large sky coverage, deep surveys like SDSS [Ade05] undoubtedly have an important role in mapping the local universe as well. For example, the information encoded in such catalogues can be used to validate methods, like the neural networks [Col03], used to obtain photometric redshifts. An even better situation is expected from future projects like SDSS II (`www.sdss.org`). Finally, a by-product of these surveys is the discovery and characterization of active galactic nuclei [Bes05a, Bes05b], which in turn could have interesting applications in the search for the sources of UHECRs.

Part II

Neutrino telescopes and mixing angles studies

Chapter 4

High energy neutrinos

High energy neutrinos (HEν) are generated in cosmic objects by the decay of charged pions and other hadrons resulting from collisions of accelerated particles with atomic nuclei or with photons. This basic fact already explains the link between HEν and cosmic rays. The interest in opening the "HEν-window" is related to the impressive penetrating power of neutrinos, allowing to look inside dense media as well as distant cosmological epochs. Since they propagate in straight lines like photons, they may provide the ultimate answer to the puzzle of the sources of cosmic rays. A comparison with the photon horizon, plotted in Fig. 4.1, clearly shows that astrophysical high energy phenomena, beyond the electroweak scale, or remote epochs—back to the era when the universe was only 1 second old—can only be explored by means of neutrinos. The great potential for significant discoveries, the increase of the neutrino cross section, charged leptons range, and angular resolution with energy, and the opportunity to use large natural target media (water, ice, atmosphere) make the prospects for neutrino astronomy much better at high energies. In this Chapter, we shall briefly review the source candidates and the basic production processes associated with HEν (Sec. 4.1), and we shall describe the detection techniques currently pursued (Sec. 4.2). Finally, the status of present and planned experiments will be discussed (Sec. 4.3). More detailed introductions to the field can be found in specific reviews [Lea00, Hal02, McD03].

4.1   Sources of high energy neutrinos

The processes responsible for the atmospheric neutrino flux also occur wherever cosmic rays interact with matter or radiation. These could be defined as secondary sources of HEν, in the sense that they are not related to the
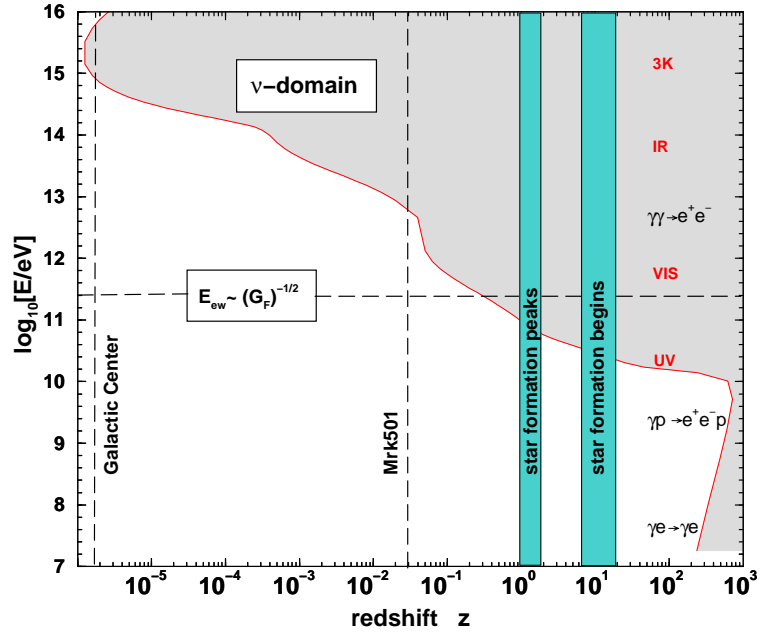
Fig. 4.1.— Gamma-ray horizon (for a Hubble constant of $H_0=60$ km s^{-1} Mpc^{-1} and a cold dark matter cosmology) due to various absorption processes (predominantly photon-photon pair production in the extragalactic radiation field). The shaded area is invisible for gamma-ray astronomy [Lea00].

hosts of high energy phenomena, but only with the propagation of cosmic rays. Nonetheless, they are promising targets for observation whenever the density is significantly lower than the one of the terrestrial atmosphere. This implies indeed that the produced light mesons more often decay than interact. Also, many of the muons from the meson decays will decay before losing a large amount of energy. The resulting spectra are then harder than the atmospheric flux at sufficiently high energy, and these neutrinos might therefore dominate over the atmospheric ones in all or part of the sky, although they come from far away. As examples of secondary sources, we mention the Solar corona neutrinos (see Sec. 4.1.1), the Galactic diffuse neutrinos (Sec. 4.1.2), and the Cosmogenic neutrinos (Sec. 4.1.3). The former two are dominated by proton-proton collisions (*pp* neutrinos), while the latter arises because of proton-photon interactions over the threshold for the Δ-resonance (*pγ* neutrinos).

Since the UHECR production mechanism is not yet known, the previous ones are the only guaranteed neutrino sources for which reliable calculations

of the fluxes are possible, given the good knowledge of the astrophysical environments involved. However, in any scenario of UHECR production one finds other sources of neutrinos, typically of extragalactic origin (Sec. 4.1.4) or associated to new physics (Sec. 4.1.5). If only astrophysical accelerators are involved, the mechanisms commonly invoked for neutrino production are just the pp and $p\gamma$ processes mentioned above for secondary sources, but with a target within or just outside the sources of high energy cosmic rays. For exotic models, the most popular channels of neutrino production are annihilations (or decays) of new (meta-)stable heavy particles X, e.g.

$$X + \bar{X} \rightarrow \begin{cases} \nu + \bar{\nu}, \\ l + \bar{l} \rightarrow \text{decay products}, \\ W^+ + W^- \rightarrow \text{decay products}, \\ q + \bar{q} \rightarrow \pi^\pm, K, \ldots \rightarrow \text{decay products}, \end{cases}$$

where the branching ratios of the different channels depend on the characteristics of the model.

Maybe bright objects in the HEν sky exist that are not even relevant for photon or cosmic ray astrophysics. For example, Nature could have constructed "thick" sources in the heavens, where a target medium absorbs all parent protons as well as the muons, electrons and gamma rays from $\pi^0 \rightarrow \gamma + \gamma$. This type of source would be hidden to any other high energy astronomical observation. This example serves as a reminder that history testifies that we have not been particularly successful at predicting the phenomena invariably revealed by new ways of viewing the heavens. Surprises can be expected!

Since pp and $p\gamma$ processes are in any case very important, it is worthwhile to spend a few words on them, assuming for simplicity that only pions are involved in the final state.

- pp collisions

  Following simple relativistic kinematics, for the CM energy of a proton-proton collision to exceed the energy threshold for pion production, the accelerated proton must have an energy above

$$E_p^{\min} = \frac{(2m_p + m_\pi)^2 - 2m_p^2}{2m_p} = 1.23 \, \text{GeV}, \tag{4.1}$$

  in the lab frame. Average energies of neutrinos and photons are related to each other and correlated with the proton energies, since both are decay products of the pions produced in inelastic collisions. A typical

value for the inelastic pp cross section σ_{pp} is 30 mb, with an inelasticity[1] κ_{pp} and pion multiplicity N_π^{pp} at TeV lab energies of $\langle \kappa_{pp} \rangle \simeq 0.4 - 0.5$ and $N_\pi^{pp} \simeq 15$, only slowly varying with energy. Then

$$\langle E_\pi \rangle = \frac{\langle \kappa_{pp} \rangle E_p}{N_\pi^{pp}}, \quad \langle E_\gamma \rangle \simeq \frac{\langle E_\pi \rangle}{2}, \quad \langle E_\nu \rangle \simeq \frac{\langle E_\pi \rangle}{4}, \qquad (4.2)$$

where we have used the fact that each charged pion decays into four leptons, and each neutral one into two photons. Isospin symmetry implies that roughly 2/3 of produced pions are charged.

- $p\gamma$ collisions

  Pions can also be generated in $p\gamma$ collisions, the main channel being in this case the Δ-baryon resonance, $p\gamma \to \Delta \to \pi N$. For this process to take place, the CM energy of the interaction must exceed the Δ-mass, 1.23 GeV. This corresponds to an energy in the lab frame of

$$E_p^{\min} = \frac{m_\Delta^2 - m_p^2}{4 E_\gamma} \simeq \left(\frac{1\,\text{MeV}}{E_\gamma} \right) \times 160\,\text{GeV}. \qquad (4.3)$$

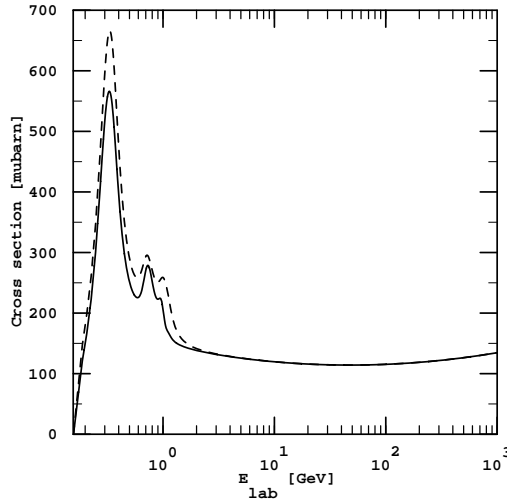This is clearly a much higher energy threshold than in the case of

Fig. 4.2.— The total photo-pion production cross section for protons (solid line) and neutrons (dashed line) as a function of the photon energy in the nucleon rest frame, E_{lab} [Bha98].

---

[1]The inelasticity is the fraction of the primary particle's energy which is transferred to the products.

pp collisions. For example, to generate TeV photons by this mechanism, radiation clouds surrounding the accelerator must contain photons of MeV energies. Such clouds are known to exist around at least some line-emitting blazars. In the case of $p\gamma$ collisions, the cross section at the Δ resonance region rises rapidly to $\sigma_{p\gamma} \simeq 550~\mu$b, with a multiplicity $N_\pi^{pp} \simeq 1$, while at higher energies the non-resonant multi-pion region starts, with a $\sigma_{p\gamma} \simeq 125~\mu$b, and $N_\pi^{pp} \simeq 3$ for CM energies $\sqrt{s} \simeq 2$ GeV; in between heavier hadronic resonances dominate (Fig. 4.2). The main decay channels in the resonant region are $p\pi^0$ and $n\pi^+$, and close to threshold the average inelasticity is $\langle\kappa_{p\gamma}\rangle \simeq 2m_\pi/m_p \simeq 0.2\text{–}0.3$. Relations analogous to Eq. (4.2) hold, but note that—at least in the resonant region, and if neutrons do not interact significantly before escaping or decaying—isospin equipartition is not realized: $N_{\pi^-} \ll N_{\pi^+} \simeq N_{\pi^0}$.

It is clear from the two examples above that whenever charged pions are involved in neutrino production, an associated production of gamma-rays takes place with $\langle E_\gamma \rangle \simeq 2\langle E_\nu \rangle$, while the relative flux of ν to γ depends on the production mechanism. One finds

$$\frac{\mathrm{d}F_\gamma}{\mathrm{d}E_\gamma}(E_\gamma = E_{\pi^0}/2) = 2\frac{\mathrm{d}E_{\pi^0}}{\mathrm{d}E_\gamma}\frac{\mathrm{d}F_{\pi^0}}{\mathrm{d}E_{\pi^0}}(E_{\pi^0}) = 4\frac{\mathrm{d}F_{\pi^0}}{\mathrm{d}E_{\pi^0}}(E_{\pi^0}), \qquad (4.4)$$

$$\frac{\mathrm{d}F_{\nu_e}}{\mathrm{d}E_{\nu_e}}(E_{\nu_e} = E_\pi/4) = \frac{\mathrm{d}E_\pi}{\mathrm{d}E_{\nu_e}}\frac{\mathrm{d}F_\pi}{\mathrm{d}E_\pi}(E_\pi) = 4\frac{\mathrm{d}F_\pi}{\mathrm{d}E_\pi}(E_\pi), \qquad (4.5)$$

$$\frac{\mathrm{d}F_{\nu_\mu}}{\mathrm{d}E_{\nu_\mu}}(E_{\nu_\mu} = E_\pi/4) = 2\frac{\mathrm{d}E_\pi}{\mathrm{d}E_{\nu_e}}\frac{\mathrm{d}F_\pi}{\mathrm{d}E_\pi}(E_\pi) = 8\frac{\mathrm{d}F_\pi}{\mathrm{d}E_\pi}(E_\pi), \qquad (4.6)$$

where π indicates indistinctly the charged pions. Neutrino oscillations will conspire to produce about equal amounts of ν_e, ν_μ and ν_τ. Each neutrino flavour flux will be roughly 1/3 of the total neutrino flux given by

$$\frac{\mathrm{d}F_\nu}{\mathrm{d}E_\nu}(E_\nu = E_\pi/4) = 12\frac{\mathrm{d}F_\pi}{\mathrm{d}E_\pi}(E_\pi). \qquad (4.7)$$

Introducing the "isospin" factor I

$$\frac{\mathrm{d}F_\pi}{\mathrm{d}E_\pi}(E_\pi) \equiv I\frac{\mathrm{d}F_{\pi^0}}{\mathrm{d}E_{\pi^0}}(E_{\pi^0}), \qquad (4.8)$$

we end up with

$$\frac{\mathrm{d}F_\nu}{\mathrm{d}E_\nu}(E_\nu = E_\gamma/2) = 3\,I\,\frac{\mathrm{d}F_\gamma}{\mathrm{d}E_\gamma}(E_\gamma), \qquad (4.9)$$

relating neutrino and γ fluxes. Typical values are $I \simeq 1$ for $p\gamma$ and $I \simeq 2$ for pp. Eq. (4.9) can be used to constrain the expected neutrino flux, whenever the γ signal can be estimated. Actually, very high energy γ-rays rapidly degrade on cosmological scales via $e^{\pm}$ pair production on the diffuse photon backgrounds, cascading down as shown in Fig. 4.1.

A bolometric relation can however be derived. If one plugs into Eq. (4.9) a typical power-law spectrum $\mathrm{d}F_\gamma/\mathrm{d}E_\gamma = k(E_0/E)^s$, one gets $\mathrm{d}F_\nu/\mathrm{d}E_\nu = 3\,k\,I(E_0/2E)^s$ and by integrating both sides over $\mathrm{d}E$ from the respective minima energies $(2\,E_\nu^{\mathrm{min}} = E_\gamma^{\mathrm{min}})$ to ∞, one gets the result

$$\int \frac{\mathrm{d}F_\gamma}{\mathrm{d}E_\gamma}(E)\mathrm{d}E = \frac{2}{3\,I} \int \frac{\mathrm{d}F_\nu}{\mathrm{d}E_\nu}(E)\mathrm{d}E \tag{4.10}$$

and analogously

$$\int E\frac{\mathrm{d}F_\gamma}{\mathrm{d}E_\gamma}(E)\mathrm{d}E = \frac{4}{3\,I} \int E\frac{\mathrm{d}F_\nu}{\mathrm{d}E_\nu}(E)\mathrm{d}E \tag{4.11}$$

for the total energy. The exact coefficient of proportionality depends however on the spectral shape, as one can easily check by using e.g. a broken power-law or a decreasing exponential. Equation (4.11) can be used to obtain very conservative upper bounds on the HEν flux [Ber75], e.g. using EGRET diffuse extragalactic gamma-ray flux detection in the 30 MeV–50 GeV range [Str04]. This is the only robust theoretical limit for sources thick to photo-hadron interactions, and depends only weakly on the spectral shape [Man01, Lea00]. However, for most astrophysical sources (Fermi acceleration injection spectra, optically thin, etc.) a much tighter bound applies, the so-called Waxman-Bahcall limit [Wax98]: starting from relations like Eqs. (4.2) and (4.7), they constrain the HEν flux using the observed UHECR flux.

In the literature, much effort has been dedicated to study pp and $p\gamma$ processes, but other "standard physics" sources are possible as well. For nuclear primaries of mass number A, pion production via $A\,p$, AA and $A\gamma$ mechanisms are possible, eventually as single nucleon excitations. However, neutrinos can be produced in this case in interactions of much lower center of mass energy, namely via weak decays of instable nuclei following spallation or photo-dissociation interactions [Rac96]. The threshold for such a process is easily estimated. For example, for $A\gamma$ reactions one gets

$$E_{A\gamma}^{\mathrm{thr}} = \frac{(m_A + B)^2 - m_A^2}{4E_\gamma} \simeq \left(\frac{B}{E_\gamma}\right) \times \frac{A}{2}\,\mathrm{GeV}, \tag{4.12}$$

where B is the binding energy of a nucleon to the nucleus of atomic number A, ranging from about 2.2 MeV (^{2}H) to about 8.8 MeV (^{56}Fe). The energy per

nucleon $E^{\text{thr}}_{A\gamma}/A$ should be compared with the energy required for photo-pion production as a single-nucleon resonance, as given in Eq. (4.3).

Another almost overlooked possibility are purely leptonic processes. The most important channel is the process $\gamma\gamma \to \mu^+\mu^-$ that could provide a non-negligible fraction of neutrinos from GRBs [Raz05]. Of course, in a GRB the high energy photons are produced via π^0 decays, and in any case they are ultimately connected with hadronic accelerators. However, there have been speculations about the possibility of leptonic processes like $e\gamma \to e\mu^+\mu^-$ as neutrino sources associated with exotic objects decaying/annihilating at high redshift (topological defects, relic particles, etc.) [Kus00, Pos01]. Unfortunately, these early claims relied on a wrong extrapolation of the cross section for the $e\gamma$ muon-pair production [Ath01a]. Nonetheless, it is worth noting that apart from neutrino production, the process $\gamma\gamma \to \mu^+\mu^-$ could have some relevance for the energy losses of ultra high energy photons, possibly on the poorly known optical and infra-red diffuse backgrounds.

4.1.1 Solar corona neutrinos

Cosmic ray interactions in the Solar atmosphere produce HEν [Sec91, Ing96b]. The direction of these neutrinos is strongly correlated with the primary cosmic ray direction, so that only neutrinos produced in the far side of the Sun can reach the Earth. This also means that they must pass through the interior of the Sun, or at least skim its atmosphere. However, the density at the first interaction point is lower in the Solar atmosphere than in the terrestrial one, and the resulting neutrino spectra have a slope similar to that of the original cosmic-ray spectrum (whereas the neutrino spectra due to showers in the Earth's atmosphere are steeper than the cosmic ray spectrum by approximately one power). Only at the TeV-scale shadowing effects due to interactions within the Sun start to become relevant. The most recent calculations of the Solar corona neutrino flux use Monte Carlo codes based on the Lund model for particle interactions, including diffractive production processes, obtained a HEν flux from the Sun which significantly exceeds the atmospheric background above a few TeV in an experimental aperture of one square degree [Ing96b]. The expected event rate is of the order of 20 events per year above 100 GeV in a km^3-detector. Oscillations between the Sun and the Earth change the received flavour ratios. The importance of $\nu_\mu \to \nu_\tau$ vacuum oscillations has been stressed in [Het99], where a rate of about five τ leptons above 100 GeV per year in a km^3 detector was estimated. A characterization of oscillations of Solar corona neutrinos, relying on the updated knowledge of mixing parameters and including solar matter effects is still lacking.

4.1.2   Galactic diffuse neutrinos

Even though the interstellar medium of the Milky Way has a very low density (around 1 nucleon/cm^3) cosmic rays interact with it in high energy collisions and produce secondary particles [Dom93, Ber92, Ing96a, Can05]. The very low density of the interstellar medium implies that the interaction lengths of the secondary mesons and muons is long compared to their decay length, so they will decay before losing energy. The attenuation due to absorption is also negligible in such a low density environment, despite the galactic size of about 10 kpc. The fluxes of high energy neutrinos and photons from the interstellar medium are therefore larger than those from the atmosphere, although the initial production rate is smaller. A measurement of these fluxes could potentially give valuable information about the distribution of matter and cosmic rays in the galaxy, and is thus important to determine the origin of the cosmic rays. Unfortunately, the flux is expected to be quite low. Along the Galactic disk, and particularly towards the GC, the expected flux starts exceeding the atmospheric one at energies $E \gtrsim 0.1$ PeV, while in the direction orthogonal to the Galactic plane the flux is lower by about two orders of magnitude. The corresponding event rate in a detector of 3×10^4 m^2, like the currently running AMANDA, is of about 0.5/year in a cone of opening angle 10° directed towards the center of the Milky Way [Ing96a].

4.1.3   Cosmogenic neutrinos

Very high energy cosmic rays generate neutrinos in interactions with the CMB [Ber69, Ste79, Eng01]. Given CMB photon energies, the threshold for the photo-pion process is around 4×10^{19} eV (see Eq. 4.3). This so-called Cosmogenic flux, of the order of 8×10^{-9} E_ν^{-2} GeV^{-1} cm^{-2} s^{-1} sr^{-1} above 10^{17} eV, is among the most likely sources of high energy neutrinos, and the most straightforward to predict. A detailed observation of this flux would be of crucial importance, in particular as a diagnostic tool for UHECRs. The knowledge of both the spectra of cosmogenic neutrinos and of UHECRs would allow us to determine the UHECR injection spectrum, to identify the evolution model for their sources [Sec05] and also gain insight about their chemical composition [Hoo04a, Ave04].

4.1.4   Other astrophysical neutrino sources

Many other candidate neutrino sources have been proposed in the literature. Galactic compact objects like supernova remnants, X-ray binaries, pulsar wind nebulae, etc. have been studied (for a review, see [Bed04]). However,
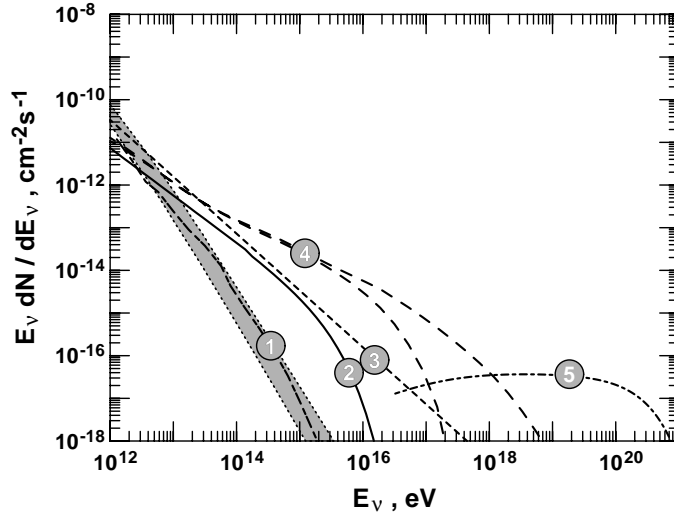
Fig. 4.3.— Fluxes of ν_μ from potential point-like sources [Sta05]. The shaded region indicates the atmospheric neutrino flux within 1° from the source. Upper end is for horizontal and lower one for vertical neutrinos. The labels refer to: 1) the Solar corona neutrinos. 2) the flux expected from the supernova remnant IC443 if the γ-rays detected by EGRET are all of hadronic origin. 3) the expected flux if the TeV γ-ray outburst of the Blazar Mrk 501 is of hadronic origin. 4) the minimum and maximum fluxes expected from the core region of the object 3C273. 5) the flux predicted for the jet of 3C279.

a one-year detection of ten neutrino events of energy larger than 100 TeV coming from a source at distance of 5 kpc in a 0.1 km^2 area would require a source luminosity $\mathcal{L}(E > 100 \text{ TeV}) \simeq 10^{36}$ erg/s, namely almost three orders of magnitude larger than the bolometric luminosity of the Sun. This large value of the luminosity strongly limits galactic source candidates, while such objects are ideal targets for gamma-ray telescopes. Since the neutrino channel is not absorption limited, the presence of powerful engines in the universe makes the prospects for extragalactic neutrino astronomy much more promising. Among the plethora of candidates proposed [Lea00], the most popular are GRB [Wax97, Vie98, Bot98, Hal02] and AGN [Ste91, Nel92, Sza94], particularly those of blazar type [Pro96, Ato01, Ner02], briefly discussed in Section 1.2.
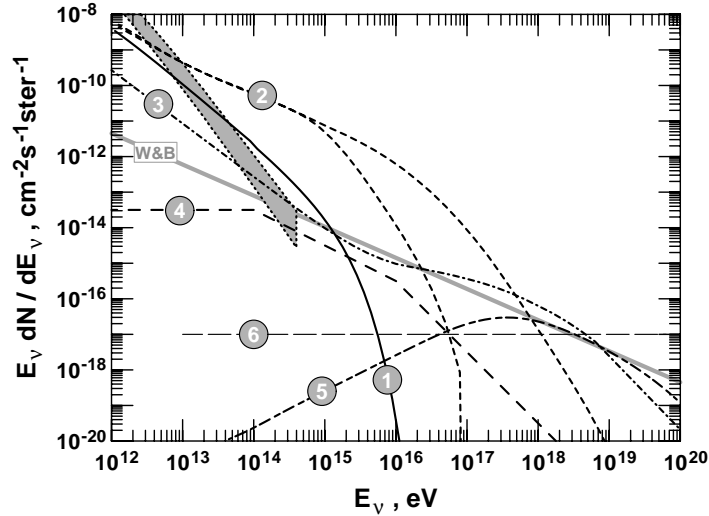
Fig. 4.4.— Diffuse fluxes from unresolved neutrino sources [Sta05]. The shaded area indicates the vertical and horizontal fluxes of atmospheric neutrinos. The Waxman-Bahcall bound is indicated with W&B. The labels refer to: 1) the flux expected from the central Galaxy if all diffuse γ-rays detected by EGRET were created by cosmic ray interactions with matter. 2) the flux from AGN cores. 3) the flux from AGN jets, where pp interactions are added to the high energy photo-production interactions. 4) the flux from GRB in the assumption that GRBs are sources of the ultrahigh energy cosmic rays. 5) the nominal Cosmogenic neutrino flux using the luminosity and cosmological evolution model from the Waxman-Bahcall limit. 6) the flux needed by the Z-burst model to become the production mechanism for UHECR.

4.1.5   Exotica

The vast majority of matter in the universe is dark with its assumed particle nature not yet revealed. The lightest supersymmetric particle, or other Weakly Interacting Massive Particles (WIMPs) proposed as particle candidates for cold dark matter, should become gravitationally trapped in the Sun, Earth or GC. They annihilate, generating high energy neutrinos observable in neutrino telescopes [Beg97, Gon99, Ell00, Fen01, Eig01, Bar02, Cir05]. A neutrino rate from the Sun or the inner Galaxy higher than the predicted one could then indicate DM annihilation. This explains why, despite the relatively low Solar corona and Galactic diffuse neutrino fluxes, it is desirable to obtain realistic estimate of their expected fluxes and uncertainty.

Another class of dark matter candidates are super-heavy particles with masses $m_X \sim 10^{13}$ GeV, that may generate the UHECRs by decay or anni-

hilation as well as solve the dark matter problem. These would also produce a substantial neutrino flux [Ber97, Bik98, Sar01, Bab02]. Extremely high energy neutrinos are also predicted in a wide variety of top-down scenarios invoked to produce cosmic rays, including decaying monopoles, vibrating cosmic strings [Gan96, Ber99] and Hawking radiation from primordial black holes [Haw74, Hal95, Bug01].

In Figure 4.3 we summarize the expected $\nu_\mu + \bar\nu_\mu$ fluxes predicted for five potential "point-like" sources, while Fig. 4.4 shows several diffuse astrophysical neutrino fluxes.

4.2 Detection techniques

Most models for HEν production discussed in Section 4.1 predict that in order to begin neutrino astronomy at $E \gtrsim 100$ GeV the size of the device needed is in the range of a Gigaton effective target volume. For the detection of solar neutrinos or neutrinos from core collapse SN, the appropriate technology includes radiochemical detection and large underground instruments. For the foreseeable future, costs for adequate sensitivity and engineering problems will limit such detectors to a megaton at most. The particle-detection method needed for HEν telescopes requires then a remote sensing technique for the neutrino interactions and a very low-cost target/detection medium. The ideal choice it to exploit natural media as targets and detect tracks at some substantial impact parameter from the sensor. The only means yet identified that satisfy these requirements are summarized in Table 4.1 and will be discussed in more detail in the following. The status of ongoing experimental projects will instead be presented in Section 4.3. Before that, however, in Section 4.2.1 we will briefly review the interaction properties of neutrinos at high energies, relevant for all kinds of experiments.

4.2.1 Neutrino interactions at high energies

At MeV energies, elastic scattering (ES) or quasi-elastic (QE) processes like

$$\nu + e \quad \rightarrow \quad \nu + e \text{ (ES)} \tag{4.13}$$

$$\bar\nu_e + p \quad \rightarrow \quad e^+ + n \text{ (QE)} \tag{4.14}$$

are usually employed to detect neutrinos. However, they are of little interest for neutrino telescopes (for an exception, see the discussion on the SN detection possibilities in Secs. 4.2.2 and 5.1), since a neutrino passing through

Radiation	Medium	Threshold	Atten. Length	Spectral region
Cherenkov light	Lake water	~ 10 GeV	~ 20 m	400–500 nm
	Deep ocean	~ 10 GeV	~ 40 m	350–500 nm
	Polar ice	~ 10 GeV	~ 20 m	300–500 nm
Cherenkov radio	Polar ice	> 5 PeV	~ 1 km	0.1–1 GHz
	Moon	> 100 EeV		1–2 GHz
Acoustic	Water	> 1 PeV	~ 5 km	10–20 kHz
	Ice	$> \mathcal{O}(\text{PeV})$	few km?	10–30 kHz
	Salt domes	$> \mathcal{O}(\text{PeV})$	few km?	10–50 kHz
EAS particles	Atmosphere	~ 10 PeV	> 1 km	100 MeV
N_2 fluorescence	Atmosphere	$\sim$ EeV	~ 10 km	337 nm
EAS radar	Atmosphere	$>$EeV	~ 100 km?	30–100 MHz

Table 4.1: Techniques proposed for large neutrino detectors, adapted from [Lea00].

matter at high energy primarily interacts via charged-current (CC) deep inelastic scattering (DIS) off nucleons of the target,

$$\nu_l + N \rightarrow l + X, \tag{4.15}$$

where l is a charged lepton, N is a nucleon, and X is a hadronic cascade, with a relatively small spatial extent (order of meters in water or ice). At high energies, the leptons will carry about half of the neutrino's energy, with a directional mismatch with respect to the primary neutrino of about

$$\sqrt{\langle \theta^2 \rangle} \simeq \sqrt{m_N/E_\nu} \simeq 1° \sqrt{\text{TeV}/E_\nu}\,, \tag{4.16}$$

as easily derived from the kinematical considerations. Note that, since CC reactions dominate, the identification of the charged lepton flavour would allow to measure the flavour content of the incoming flux. Showers are also produced by the neutral-current (NC) reactions,

$$\nu_l + N \rightarrow \nu_l + X, \tag{4.17}$$

though the lower cross section of NC events (about a factor 3) makes them less interesting for detection. In Fig. 4.5 we show the behaviour of relevant partial and total cross sections.
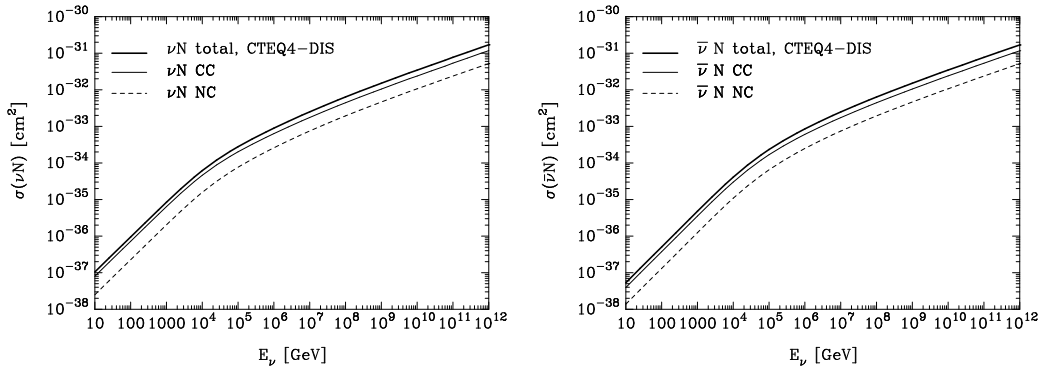
Fig. 4.5.— Cross sections for $\nu_\ell N$ (left panel) and $\bar{\nu}_\ell N$ (right panel) at high energies, according to the CTEQ4–DIS parton distributions: the dashed line refers to the NC, the thin solid line to the CC, the thick line to the total (CC+NC) cross section [Gan98].

The only other reaction of interest is the Glashow resonance,

$$\bar{\nu}_e + e^- \rightarrow W^- \rightarrow \left\{ \begin{array}{l} \bar{\nu}_l + l^- \\ \text{hadrons} \end{array} \right. , \tag{4.18}$$

that proceeds via real W^- production (the branching ratio for each of the three leptonic channels is about 10.7%). This process has a peak cross section of

$$\sigma_{\bar{\nu}_e + e^- \rightarrow W^-} \simeq 4.7 \times 10^{-31} \text{cm}^2 \tag{4.19}$$

at the lab energy of $E_\nu = m_W^2/2m_e \simeq 6.3$ PeV, but such large cross section rapidly falls off due to the small width of the resonance, $\Gamma_W \simeq 2.1$ GeV. Nonetheless, this effect might allow interesting observations, one of which will be briefly discussed in Sec. 5.1. In the following, we will analyze how these interactions can be used to detect neutrinos with a variety of techniques.

4.2.2 Optical Cherenkov technique

Optical Cherenkov detection is the most well-established technique for HEν telescopes. Atmospheric neutrinos of energy up to 10^{14} eV have been detected by these telescopes, and limits on astrophysical ones up to 10^{16} eV have been established. The technique relies on the observation of the Cherenkov radiation from secondary particles produced by neutrinos interacting inside large volumes of highly transparent ice or water instrumented with a lattice of PMTs. Cherenkov radiation can be understood as the decay process $Q \rightarrow Q+\gamma$ of a charged particle Q in a medium. If the particle's velocity exceeds the velocity of the light propagation in the medium, the above-mentioned decay

process is kinematically allowed. Since the dispersion equation relating the wavenumber vector $\mathbf{k}$ to the energy ω of the photons in a medium of index of refraction n is $|\mathbf{k}| = n\,\omega$, the effective mass-square $\omega^2 - |\mathbf{k}|^2$ is negative for $n > 1$, i.e. photons are space-like excitation. Charged particles of velocity β will radiate as long as $\beta > 1/n$, leaving a light wake of constant angle $\theta_c = \arccos(1/n\beta)$, until close to Cherenkov threshold, which involves only the last few centimeters of range. Note that Cherenkov radiation accounts for less than 10^{-4} of the ionization energy loss. Yet, this allows a powerful detection tool, depending on the optics of the medium, since very sensitive detectors permit detection from tens of meters of lateral distance from the particle trajectory.

The most important optical properties of the natural media used as targets are the absorption length and the effective scattering length. Interestingly, the ocean and deep ice are in opposite optical regimes, the ocean water being absorption-limited and the ice being scattering-limited. Thus, the deep oceans are better suited for the detection of large neutrino-induced cascades, and to lower the threshold. Detection is possible at distances out to hundreds of meters before directional information is lost. Deep ice has the advantages of smaller background light and greater absorption lengths, and thus offers better calorimetry if one knows the vertex. Basically, optical Cherenkov telescopes detect the secondary particle showers initiated by NC interactions of $\nu_{e,\mu,\tau}$ and CC interactions of $\nu_{e,\tau}$ as well as the leading secondary muon tracks initiated by ν_μ only. At high energy, the tagging of τ tracks becomes possible, as well as the identification of $\bar{\nu}_e$ showers due to the Glashow resonance around 6.3 PeV. At lower energies, detection of $\bar{\nu}_e$ QE process in a huge burst following SN explosion is also possible (see Fig. 4.6).

High energy electron neutrinos deposit a significant fraction of their energy into the hadronic shower due to the fragments of the target, while a subdominant electromagnetic shower is initiated by the leading final state electron. The identification of the hadronic/leptonic nature of the showers is at present very challenging from the experimental point of view. A typical shower has a lenght of few meters and a diameter of about 10 cm in ice or water, while economic reasons require a much larger spacing of the PMTs. A cascade event represents then, to a good approximation, a point source of Cherenkov photons radiated by the shower particles. These trigger the PMTs at the single photoelectron level over a spherical volume whose radius is about 130 m at 10 TeV and grows by roughly 50 m per decade in energy. The measurement of the radius of the sphere in the lattice of PMTs determines the energy and turns neutrino telescopes into total energy calorimeters (see Fig. 4.7). Because the shower and its accompanying Cherenkov light pool are not totally symmetric but elongated in the direction of the leading elec-
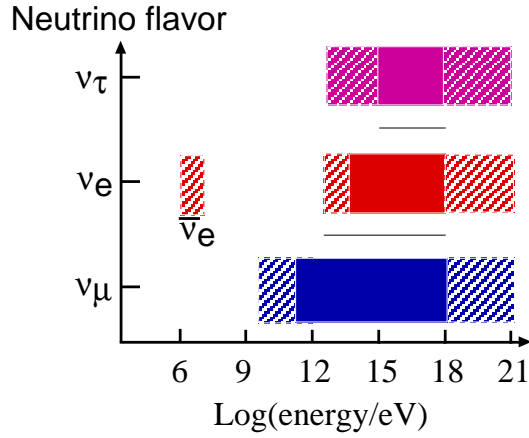
Fig. 4.6.— Although Optical Cherenkov telescopes detect neutrinos of any flavour, at TeV–EeV energies they can identify their flavour and measure their energy in the ranges shown (valid for IceCube) [Hal02]. Filled areas: particle identification, energy, and angle. Shaded areas: energy and angle.

tron, its direction can be reconstructed. Pointing is however far inferior to what can be achieved in muon track detection, and estimated to be precise to $\mathcal{O}(10°)$ at most. On the other hand, compared to ν_μ, energy reconstruction is superior ($\Delta E / E \simeq 30\%$) and the background of atmospheric neutrinos is significantly reduced since at higher energies muons, which generate most of the atmospheric ν_e, no longer decay.

For rough estimates of event rates, one can assume for simplicity an instrumented cubic volume of side L. To a first approximation, a neutrino incident on a side of area L^2 will be detected provided it interacts within the detector volume, i.e. within the instrumented distance L. That probability is

$$P = 1 - \exp(-L/\lambda_\nu) \simeq L/\lambda_\nu \,, \qquad (4.20)$$

with $\lambda_\nu = (\rho N_A \sigma_\nu)^{-1}$. Here ρ is the density of the ice or water, N_A Avogadro's number and σ_ν the neutrino cross section. A neutrino flux ϕ (neutrinos per cm^2 per second) crossing a detector with cross section area $A \simeq L^2$ facing the incident beam, will produce

$$N = ATP\phi \qquad (4.21)$$

events after a time T. In practice, the quantities A, P and ϕ depend on the neutrino energy and N is obtained by a convolution over the neutrino energy above the detector threshold. The "effective" telescope area A is not strictly equal to the geometric cross section of the instrumented volume facing the incoming neutrino because even neutrinos interacting outside the instrumented
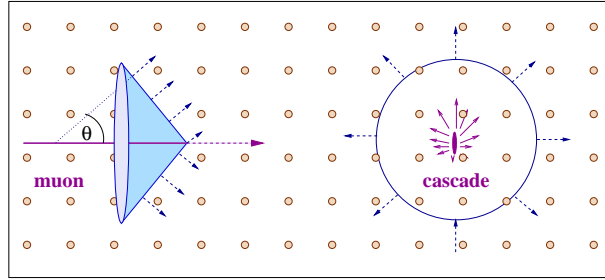
Fig. 4.7.— Sketch of detection of muon tracks (left) and cascades (right) [McD03].

volume may produce a sufficient amount of light inside the telescope to be detected. A is therefore determined as a function of the incident neutrino direction by simulating the entire detector, including the trigger.

The formalism presented applies to neutrino cascades. For muon neutrinos, any neutrino producing a secondary muon that reaches the telescope and has sufficient energy to trigger it, will be detected. Muons range out over kilometers at TeV energy, to tens of kilometers at EeV energy, producing showers along their track by bremsstrahlung, pair production and photonuclear interactions, which all generate Cherenkov radiation. As the energy of the muon degrades along its track, the energy of the secondary showers diminishes and the distance from the track over which the associated Cherenkov light can trigger a PMT becomes smaller. The geometry of the lightpool surrounding the muon track over which single photo-electron are produced is therefore a kilometer-long cone with gradually decreasing radius (Fig.4.7). Because the muon range is larger than the telescope size, neutrinos can be detected far outside the instrumented volume; the probability is obtained by the substitution in Eq. (4.20)

$$L \to R_\mu. \tag{4.22}$$

Here R_μ is the muon range, i.e. the distance a muon travels before its energy drops below the energy threshold E_μ^{thr}, and is given by

$$R_\mu \simeq \frac{1}{\beta} \ln \left[\frac{\alpha + \beta E_\mu}{\alpha + \beta E_\mu^{\text{thr}}} \right] . \tag{4.23}$$

where $\alpha \simeq 2.0 \times 10^{-6}$ TeV cm^2/g and $\beta \simeq 4.2 \times 10^{-6}$ cm^2/g.

The effective aperture for muons is larger than the instrumented area and the angular resolution is in the sub-degree regime. However, the energy measurement for muon tracks is only indirect unlike the case for showers, and because of the stochastic nature of muon energy loss, the measurement is only sensitive to the logarithm of the energy, resulting in $\Delta E/E \simeq 50\%$.

The discovery of the close-to-maximal mixing of μ and τ neutrinos has motivated the search for τ neutrinos from astrophysical sources. The production of ν_τ in hadronic interactions or photo-production in the heavenly bean dump is suppressed relative to ν_e and ν_μ by roughly five orders of magnitude. In the absence of oscillations, ν_τ of astrophysical origin are undetectable. Moreover, the ν_τ, unlike the ν_e and ν_μ, are not absorbed in the Earth due to the charged current "regeneration" effect: ν_τ with energies exceeding 1 PeV pass through the Earth and emerge with an energy of roughly 1 PeV. The mechanism is simple [Hal98]: a ν_τ interacting in the Earth will produce another ν_τ of lower energy, either directly in a NC interaction or via the decay of a tau lepton produced in a CC interaction. High energy ν_τ will thus cascade down to PeV energy where the Earth is transparent. A ν_τ will be detected in a neutrino telescope provided the tau lepton it produces reaches the instrumented volume within its lifetime. Therefore we have to replace in Eq. (4.20)

$$L \to \gamma c\tau = E/mc\tau \,, \qquad (4.24)$$

where m, τ and E are the mass, lifetime and energy of the tau, respectively. The product $\gamma c\tau$ for tau leptons grows linearly with energy and exceeds the range of the muon around 1 EeV. At low energy, the shower signature of a ν_τ is hardly distinguishable from the one of a ν_e, but tau neutrinos of sufficiently high energy can be identified in several ways. The most striking signature is the so-called double bang event [Gai95] in which the production and decay of a τ lepton are detected as two separated showers inside the telescope. It may also be possible to identify "lollypop" events in which a ν_τ creates a long minimum-ionizing track that enters the detector and ends in a huge burst when the τ lepton decays to a final state with hadrons or an electron. The parent τ track can be identified by the reduced catastrophic energy loss compared to a muon of similar energy. Note, however, that in the vicinity of 10 PeV the probability to detect and identify a ν_τ as a double-bang is only 10% of that for detecting a ν_μ of the same energy. At lower and higher energies the likelihood of detecting a double-bang falls rapidly. Further details on the flavour-tagging capabilities of neutrino telescopes can be found in [Bea03a].

4.2.3 Coherent radio-pulse technique

Already in 1962, G. Askaryan proposed that a compact particle shower will emit a coherent Cherenkov radio signal [Ask62]. Subsequent theoretical work in the 1980's [Mar86, Zhe88] and the 1990's [Zas92] supported this prediction. The experimental verification came in 2001 [Sal01], with subsequent measurements confirming the frequency and polarization properties of the

emitted radiation [Gor04]. The emission of a coherent radio signal only happens if a charge asymmetry appears in the particle shower developping in a dense medium. This asymmetry is due to the combined effects of positron annihilation and Compton scattering of electrons at rest. There is about 20% excess of electrons over positrons in such a particle cascade, which moves as a compact bunch a few cm wide and about 1 cm thick at the velocity above the speed of light in the medium. The frequency dependence of Cherenkov radiation emitted is $dP \propto \nu d\nu$. In addition, for radiation with wavelength much larger than the cascade diameter, the radiated signal will add coherently and thus be proportional to the square of shower energy. A radio signal emitted by a particle shower in a material such as ice is coherent up to few GHz, is linearly polarized, and lasts only about a nanosecond. In ice as well as in salt domes, attenuation lengths of several kilometers can be obtained, depending on the frequency band, the temperature of the ice, and the salt quality. For example, neutrinos with energy of 10^{19} eV interacting in the ice produces a radio pulse with a peak strength of 10^{-3} V m^{-1} MHz^{-1} at a distance of 1 km. For energies above a few tens of PeV, radio detection in ice or salt might be competitive or superior to optical detection. For a recent phenomenological study see [Alv05b].

4.2.4   Acoustic technique

Another category of techniques makes use of the acoustic pulse produced by the expansion of the medium when heat is deposited by the particle cascade, an inefficient process with energy transfer efficiency of about 10^{-9}. When a particle cascade is generated from a neutrino interaction (or any other cause), the energy is deposited into the medium via ionization losses and other processes, and within a fraction of a nanosecond is converted to heat. The heat dissipates only very slowly, so the bulk effect is a step-function expansion of the region in which the energy was deposited. This in turn generates a bipolar acoustic pulse. Transverse to the cascade, typically 10 m long in water and a few centimeters wide, the radiation is coherent and adds, much like a stack of dipole antennas. The speed of sound in water is 1.5 km s^{-1}, and the signal power peaks around 20 kHz. The beam pattern is a disk transverse to the neutrino direction with angular thickness of about a degree. The magnitude of the pulse depends on the bulk coefficient of thermal expansion, the density and specific heat of the medium, and the speed of sound. The attenuation length of sea water is a few kilometers (compared to a few tens of meters for light) and given a large initial signal, huge detection volumes can be achieved, a very appealing feature when considering the large aperture required to detect the cosmogenic neutrino flux. With efficient noise

rejection, acoustic detection might be competitive with optical detection at multi-PeV energies [Lea78]. The use of other media, such as salt domes or ice, has been considered as well, and is expected to work rather well. Applications in ice and salt are favorable in comparison to water due to the much higher expected signal strength, e.g. about ten times greater in ice [Pri05] with the further advantage that solids supports shear-waves [Hal90], and observing both compressional and shear waves would give the range.

4.2.5 Extensive air shower detection

At the EeV energy scale, the fact that HEν produce extensive air showers opens the possibility of another detection technique. Some advantages arise at the highest energies: First, the cross section for neutrino interactions continues to rise, faster than hadronic interactions, so neutrinos interact more often (the interaction length is 115±25 km water equivalent at 10^{20} eV). Second, many models for neutrino production indicate that neutrino fluxes may be similar in magnitude to primary cosmic-ray fluxes at these energies. Third, the deposited energy becomes macroscopically detectable, as is the case with EAS produced by ordinary charged cosmic rays of these energies. Such showers extend over kilometer distances and can be detected with relatively simple particle counters at the Earth's surface, although to get a usable rate at 10^{20} eV one needs to cover at least 1000 km^2. Alternatively, the showers can be observed by fluorescence eyes monitoring the dark night sky (see Sec. 1.3.2).

The main challenge lies in separating showers initiated by neutrinos by those induced by hadrons, photons, or penetrating muons produced in the first interaction of the primary. It was already suggested in the 1960s that this could be done at high zenith angles [Ber69] because the atmosphere slant depth is quite large[2]. Neutrinos, having very small cross sections, can interact at any point along their trajectories while most of the air showers induced by protons, nuclei or photons are absorbed before reaching ground level. The signature for neutrino events is thus inclined showers that interact deep in the atmosphere. The most problematic aspect to establish a positive signal is the discrimination against electromagnetic showers initiated deep in the atmosphere by muons themselves from EAS originated by ordinary cosmic rays of large energy. The shape and thickness of the shower front could however be used to discriminate ν-induced and μ-induced showers.

Fluorescence detection is more robust, as one can examine the longitudi-

---

[2]Straight downward, the atmosphere constitutes about 1000 g/cm^2, or more than ten strong interaction lengths. However, near the horizon (say at 85°) it is 30 times thicker.
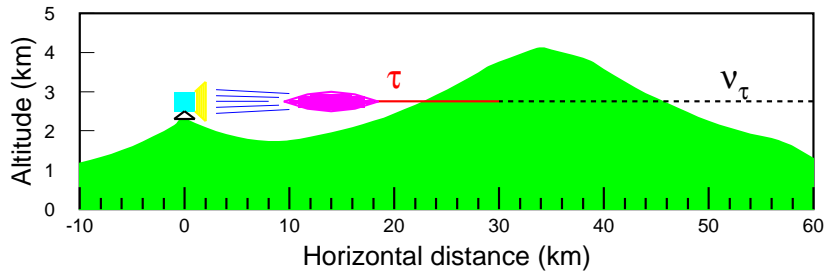
Fig. 4.8.— Cartoon illustration of a conversion $\nu_\tau \rightarrow \tau$ inside a mountain [Hou02].

nal shower development. In the future, this technique might be extended to space-based observatories, by flying large mirrors with light detectors that look down on the atmosphere. A much larger area can be searched from this privileged site than from any site on the Earth's surface. The negative aspects are the higher energy threshold and the associated cost of space activities.

An even better sensitivity might be obtained for ν_τ scratching the Earth and interacting close to the array ("Earth-skimming" neutrinos). Only ν_τ lead to large detectable shower rates in the high energy range of interest. This is due to the combined effect of the lepton lifetime, its energy loss and the neutrino cross section. The charged τ lepton produced in the interaction can escape the rock around the array, in contrast to electrons, and in contrast to muons it decays after a short path into hadrons [Fag01]. If this decay happens above the array or in the field of view of the fluorescence telescopes, the decay cascade can be recorded. Provided the experimental pattern allows for clear identification, the acceptance for these signals can be large. For the optimal energy scale of 1 EeV, the sensitivity might reach $10^{-8}E_\nu^{-2}$ GeV^{-1} cm^{-2} s^{-1} sr^{-1}. A variation of this idea is to search for τ lepton cascades which are produced by horizontal PeV ν_τ hitting a mountain and then decay in a valley between target mountain and an "observer" mountain (Fig. 4.8). Finally, even for EAS experiments some sensitivity exists to the flavour content of the neutrino fluxes. A practical quantity that could be used is the ratio of quasi-horizontal showers to Earth-skimming events [Anc05b].

Further information on the EAS technique for neutrino detection are available in the review [Zas05]. A recently proposed variation to the EAS method uses radar to detect the ionization trail left by EASs, in the same way that meteorites are detected [Gor00], and may offer promising perspectives for the future (see Sec. 1.3.2 and Refs. therein).

4.3 Current and planned experiments

The idea of using Cherenkov radiation for large neutrino detectors arose shortly after the neutrino was discovered. The development in this field was stimulated originally by the DUMAND project close to Hawaii (1976), which was cancelled in 1995. The breakthrough came from the other pioneering experiment located at a depth of 1100 m in the Siberian Lake Baikal. The BAIKAL collaboration was the first to deploy three strings—as necessary for full spatial reconstruction [Bel97]—and also reported the first atmospheric neutrinos detected underwater [Bak00]. The NT-200 instrument, comprising 192 PMTs on 4 strings, has been recently upgraded (NT200+ [Ayn05]).

With respect to its size, NT-200 has been surpassed by the AMANDA detector [And99]. Rather than water, AMANDA uses the 3 km thick ice layer at the geographical South Pole, proving the viability of this technology [And01]. Holes are drilled with hot water, and strings with PMTs are frozen into the ice. With 677 PMTs at 19 strings, most at depths between 1500 and 2000 m, the present AMANDA-II array reaches an area of a few 10^4 m^2 for 1 TeV muons. AMANDA-II may be the first detector with a realistic discovery potential with respect to extraterrestrial high energy neutrinos, even though it is smaller than the km^3 size generally predicted to be required for clear observation of such signals. Limits obtained from the analysis of data taken with the smaller ten-string detector AMANDA-B10 in 1997 are similar to or below those limits which have been obtained by underground detectors over more than a decade of data taking. The limit [Ahr03] on the diffuse flux from unresolved sources with an assumed E^{-2} spectrum is $8 \times 10^{-7} E_\nu^{-2}$ GeV^{-1} cm^{-2} s^{-1} sr^{-1}, slightly below the loosest theoretical bounds [Man01] and a factor of two below the corresponding Baikal limit. AMANDA limits on point sources in the Northern sky [Ahr04] complement the limits obtained from detectors in the Northern hemisphere for the Southern sky. Based on the experience from AMANDA, a cubic kilometer detector, IceCube [Ahr02], is being deployed at the South Pole. It will consist of 4800 PMTs on 80 vertical strings, with 125 m inter-string-distances and a 16 m spacing between the PMTs along a string. The telescope is expected to be fully operational in a few years [Ice05]. Two projects for large neutrino telescopes are under construction in the Mediterranean, ANTARES [Mon02] and NESTOR [Gri01]. Both have assessed the relevant physical and optical parameters of their sites and have deployed prototype arrays of about a dozen PMTs, although they follow different deployment schemes and array designs. The NESTOR group plans to deploy a tower of several floors, each carrying 12 PMTs at 16 m long arms. The ANTARES detector will consist of 12 strings, each equipped with 30 triplets of PMTs. This detector will have an

area of about 2×10^4 m^2 for 1 TeV muons—similar to AMANDA-II—and is planned to be fully deployed in 2006. An additional initiative, NEMO, has finished a series of site explorations at a location 70 km from Sicily and is now in the phase of prototype studies for a cubic kilometer detector [Sap05]. The different efforts are going to converge towards a single project for a km^3-detector, and a coordination network called KM3NeT already exists [Kat06].

Several experiments have already utilized the Askaryan effect to search for HEν. A prototype Cherenkov radio detector called RICE is operating at the geographical South Pole [Kra01]. Twenty receivers and emitters are buried at depths between 120 and 300 m. From the non-observation of very large pulses, a limit of about $10^{-5}E_\nu^{-2}$ GeV^{-1} cm^{-2} s^{-1} sr^{-1} has been derived for energies above 100 PeV. Another project, FORTE in the Greenland ice cap [Leh03], has obtained interesting limits at higher energies. The Goldstone Lunar Ultra-high Energy Neutrino Experiment (GLUE) has searched instead for radio emission from extremely-high energy cascades induced by neutrinos or cosmic rays skimming the moon surface [Gor03]. Using two NASA antennas, an upper limit of $5 \times 10^{-5}E_\nu^{-2}$ GeV^{-1} cm^{-2} s^{-1} sr^{-1} at 100 EeV has been obtained. The forthcoming generation of radio-detection experiments is dominated by ANITA (ANtarctic Impulsive Transient Array), which is an array of radio antennas planned to be flown at a balloon on an Antarctic circumpolar path in 2006 [Sil04, DuV05, Baw05]. From 35 km altitude it may record the radio pulses from neutrino interactions in the thick ice cover and monitor a really huge volume. The expected sensitivity from a 45 day flight is almost $10^{-8}E_\nu^{-2}$ GeV^{-1} cm^{-2} s^{-1} sr^{-1} at 10 EeV, thus reaching enough sensitivity to test current models of cosmogenic neutrinos in the energy range from 0.1 to 100 EeV. Following laboratory studies at SLAC, efforts to simulate a realistic radio array in a rock salt dome have been performed as well (SalSA, Salt dome Shower Array [Gor04]). This R&D project study for radio detection in natural salt domes promises to improve the sensitivity limits by three orders of magnitude with respect to existing ones [Gor01].

Acoustic detection efforts are at an earlier stage with respect to other techniques, with one limit published thus far from 10^{22} to 10^{25} eV [Vad05]. Several groups are working in R&D programs to characterize background sources, and to develop specific hardware for acoustic detection [Nie05, Kag05]. At present, the only running experiments use existing sonar arrays for submarine detection. The most advanced is AUTEC, a project using a very large hydrophone array of the US Navy, close to the Bahamas [Leh01], with an array of 52 hydrophones over an area of 250 km^2. Due to the sparse instrumentation, it is expected to trigger only on events above 100 EeV.

A very appealing possibility for the future are hybrid Cherenkov-acoustic (or Cherenkov-radio-acoustic) neutrino telescopes. It may be possible to

bootstrap the large effective volumes of acoustic and radio detection with the optical method by building a hybrid experiment that can detect a large rate of radio or acoustic events, a fraction of which are also detected by an optical detector. Present initiatives are ongoing in NESTOR, ANTARES, AMANDA/IceCube, and NEMO [Spi02, Lah05] This synergic strategy is pictorially represented in Fig. 4.9, which reports the energy ranges for the different techniques. Optical Cherenkov detectors are in the range to overlap with the underground detectors used e.g. for atmospheric neutrino studies, but also with the other techniques aiming at exploring the high energy window.
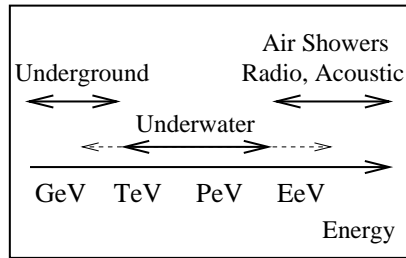

Fig. 4.9.— Energy range of the various detection techniques, the dashed lines showing the maximal sensitivity of Optical Cherenkov detectors, while solid lines the optimal range [McD03].

The Fly's Eye collaboration and more recently the AGASA collaboration have practiced the search mode of horizontal air showers [Bal85b, Hay00]. AGASA derived an upper limit of the order of 10^{-5} in the units given above, only one order of magnitude above optimistic predictions for AGN jets and for topological defects. At supra-EeV energies, large extensive air shower arrays like the AUGER detector in Argentina [Zas04] or the Telescope Array [Sas02] may search for horizontal air showers due to neutrino interactions deep in the atmosphere. The optimum sensitivity for this method is at 1–100 EeV, the effective detector mass is between 1 and 20 Gigatons, and the estimated sensitivity is of the order of $10^{-7}E_\nu^{-2}$ GeV^{-1} cm^{-2} s^{-1} sr^{-1}. According to a recent calculation, AUGER fluorescence detectors have a significant chance to detect at least one Earth-skimming neutrino in a decade, even in conservative scenarios for the cosmogenic neutrino flux [Mie05]. Heading to higher energies leads to space-based detectors monitoring huge volumes. The projects EUSO [Boa05] and OWL [Cli99] intend to launch large aperture optical detectors to 500 km height. They would look down upon the atmosphere and search for fluorescence signals due to neutrino interactions. The monitored mass would be up to ten Teratons, with an energy threshold of about
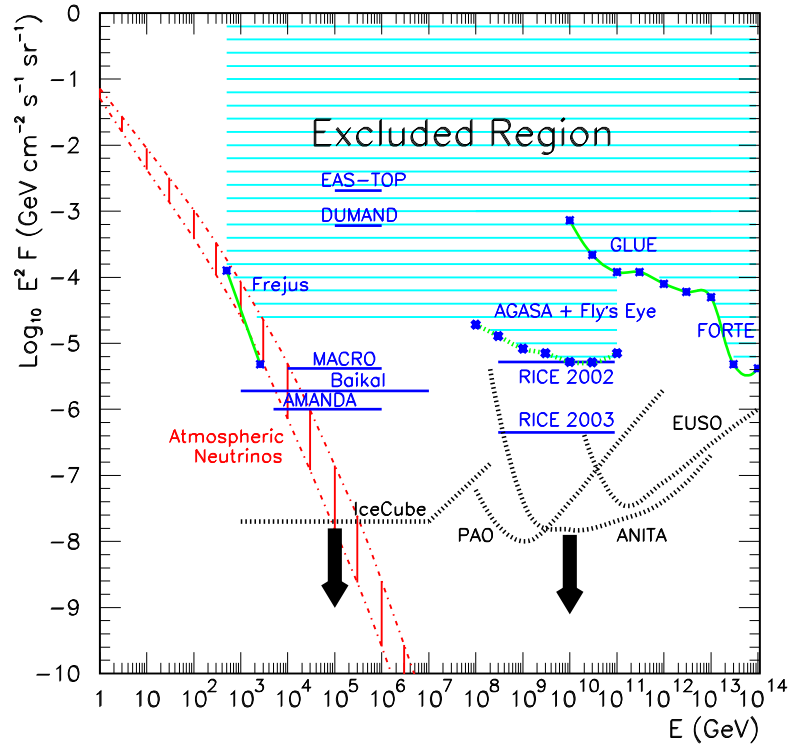
Fig. 4.10.— The horizontal solid lines indicate current 90% C.L. upper limits on the neutrino fluxes $\propto E^{-2}$ as reported by several experiments. The $*-*-*$ lines indicate observational bounds on the all-flavours HEν flux. Also shown (thick dotted lines) are the expected 90% C.L. sensitivity of IceCube in 1 yr of operation, the projected sensitivities of 1 yr running of Auger and EUSO, and of 45 days of ANITA running. The region between the falling dashed-dotted lines indicates the flux of atmospheric neutrinos. Plot from [Tor04], where a full list of references is available.

10^{10} GeV. In Fig. 4.10 we summarize the existing or expected sensitivities to neutrino fluxes.

Chapter 5

Neutrino oscillations at neutrino telescopes

In this Chapter, we describe a particle-physics application of observations at neutrino telescopes. These instruments have been conceived primarily for astrophysical purposes, and hopefully they will shed light on issues like the sources of cosmic rays or astrophysical acceleration mechanisms [Ahl05]. However, the high energies and the long distances to the expected sources, together with their flavour-distinction capability will allow to improve bounds on physics beyond the standard model as well. Anomalous cross sections at high CM energies [Anc05c], violation of the equivalence principle and Lorentz invariance [Goz05], decoherence induced by quantum gravity effects [Hoo04b, Anc05a], neutrino decays [Bea02, Bea03c] may all be probed at neutrino telescopes with an improvement of several orders of magnitude with respect to present limits.

In the following, however, we will concentrate on the possible contribution of neutrino telescopes to the "hot topic" of neutrino oscillations [Rew04]. This is a relatively new field in high energy neutrino (astro-) physics, but several works have recently emphasized possible applications of neutrino telescopes. We will review some of these proposals in Section 5.1, while in Section 5.2 we will illustrate the possibility to perform measurements sensitive to θ_{13} and δ_{CP} at neutrino telescopes by using a peculiar Galactic source that might have been detected in cosmic rays. Extensions of these ideas to other astrophysical situations are outlined in Section 5.3.

93

5.1   Introduction

If neutrinos are massive and individual lepton numbers are not conserved, neutrino flavour eigenstates $\{\nu_e, \nu_\mu, \nu_\tau\}$ are expressed in terms of the mass eigenstates $\{\nu_1, \nu_2, \nu_3\}$ of mass respectively m_1, m_2, m_3 via a unitary mixing matrix $V \equiv U\Phi$ as

$$
\begin{pmatrix} \nu_e \\ \nu_\mu \\ \nu_\tau \end{pmatrix} = V \begin{pmatrix} \nu_1 \\ \nu_2 \\ \nu_3 \end{pmatrix}. \tag{5.1}
$$

The unitary matrix U is the leptonic mixing matrix analogous to the CKM mixing matrix for quarks, that can be written in the canonical form [PDG04]

$$
U = \begin{pmatrix} c_{12}c_{13} & s_{12}c_{13} & s_{13}e^{-i\delta_{\mathrm{CP}}} \\ -s_{12}c_{23}-c_{12}s_{23}s_{13}e^{i\delta_{\mathrm{CP}}} & c_{12}c_{23}-s_{12}s_{23}s_{13}e^{i\delta_{\mathrm{CP}}} & s_{23}c_{13} \\ s_{12}s_{23}-c_{12}c_{23}s_{13}e^{i\delta_{\mathrm{CP}}} & -c_{12}s_{23}-s_{12}c_{23}s_{13}e^{i\delta_{\mathrm{CP}}} & c_{23}c_{13} \end{pmatrix} \tag{5.2}
$$

(here $c_{ij} = \cos\theta_{ij}$ and $s_{ij} = \sin\theta_{ij}$). The matrix Φ is of the form

$$
\Phi = \mathrm{diag}\left(e^{i\phi_1/2}, e^{i\phi_2/2}, 1\right), \tag{5.3}
$$

where ϕ_1 and ϕ_2 are CP-violating phases that for Majorana neutrinos are physical, entering for example the amplitudes of neutrinoless double beta decays or lepton number violating decays like $\mu \to e\gamma$. However, ϕ_1 and ϕ_2 do not influence the neutrino oscillation phenomenology, so that for our purposes $\Phi = \mathbf{1}$. Neutrino flavour oscillation phenomena are governed by six independent parameters: Two mass-squared differences, $\Delta m_{21}^2 \equiv m_2^2 - m_1^2$ and $\Delta m_{32}^2 \equiv m_3^2 - m_2^2$, three mixing angles, θ_{12}, θ_{23}, and θ_{13}, and a possible CP-violating phase δ_{CP}. The angles θ_{ij} can all be made to lie in the first quadrant by a redefinition of the field phases, while $0° \leq \delta_{\mathrm{CP}} < 360°$. By definition $m_1 \leq m_2$, but the sign of Δm_{32}^2 is physical, and the two cases $\Delta m_{32}^2 > 0$ and $\Delta m_{32}^2 < 0$ are referred to as normal and inverted hyerarchy, respectively.

The current experimental situation is that the solar neutrino data are consistent with a flavour oscillation of the initial ν_e driven by a mass-squared difference $\Delta m_\odot^2 = \Delta m_{21}^2 \simeq 7.1 \times 10^{-5}\,\mathrm{eV}^2$ and mixing angle $\theta_\odot = \theta_{12} \simeq 32.5°$, while the atmospheric neutrino data are explained by oscillations mainly between ν_μ and ν_τ with $\Delta m_{\mathrm{atm}}^2 = \Delta m_{32}^2 \simeq 2.6 \times 10^{-3}\,\mathrm{eV}^2$ and $\theta_{\mathrm{atm}} = \theta_{23} \simeq 45°$, i.e. close to maximal mixing [PDG04]. Present uncertainties of 10–20% in the values of the above parameters will significantly reduce after the next round of laboratory experiments. While the determination of the mixing parameters controlling the solar and atmospheric neutrino oscillations has already entered the precision era, there exists currently only an upper limit for θ_{13}

mainly from the CHOOZ reactor experiment, $\sin^2 2\theta_{13} < 0.1$ [Apo02]. The mixing angle θ_{13} characterizes how strong atmospheric and solar oscillations are coupled and therefore also determines the strength of CP violation effects in neutrino oscillations. The phase δ_{CP} is at present completely unconstrained. Both θ_{13} and δ_{CP} are observable in solar and atmospheric neutrino oscillation experiments only as subleading, genuine three-flavour effects that are masked mainly by systematic uncertainties. There are strong experimental efforts to measure θ_{13} in the near future by dedicated experiments [Ans04], but the detection of a non-zero δ_{CP} appears unlikely for the next generation of facilities [Hub04], and probably has to await the construction of long-baseline experiments using second-generation super-beams or perhaps even a neutrino factory. Therefore, any new signature of these parameters both in laboratory and astroparticle experiments would be welcome. We will come back on this topic in Sections 5.2 and 5.3.

A first interesting consequence of neutrino oscillations for the HEν flux is the appearance of a large fraction of ν_τ because of the large (if not maximal) mixing with the muon neutrinos, which are copiously produced in the pion decay chain. Note that the prompt ν_τ production by charmed meson decays is heavily suppressed by a factor of $\mathcal{O}(10^{-5})$, so primary ν_τ from astrophysical sources are virtually unobservable. Notice also that the CC interaction $\nu_\tau N \to \tau X$ has a threshold of about 3.5 GeV, and the oscillation length for the atmospheric mass splitting $\Delta m^2_{\mathrm{atm}}$ is

$$L_{\mathrm{osc}} \equiv \frac{4\pi E_\nu}{\Delta m^2_{\mathrm{atm}}} \simeq 10^3 \left(\frac{E_\nu}{\mathrm{GeV}}\right) \mathrm{km}, \tag{5.4}$$

suggesting that ν_τ appearance requires long-baseline experiments. On the other hand, the large distances involved for any astrophysical source easily allow full mixing of ν_μ with ν_τ. This is the case of the solar corona neutrinos (Sec. 4.1.1) for which a rate of about five τ leptons above 100 GeV per year in a km^3 detector was estimated [Het99]. The problem is that a clean identification of τ's can only be performed in neutrino telescopes at PeV energies, where unfortunately the solar corona flux is strongly attenuated by absorptions in the Sun. However, the Galactic diffuse flux (Sec. 4.1.2) does not suffer this problem, and indeed it was shown in [Ath01b] that almost one τ event per year per steradian for two separable and contained showers with $E \sim 10^6$ GeV should be detected in a km^3 volume neutrino telescope, virtually background-free from guaranteed sources (see Fig. 5.1). Notice that the above-mentioned event rate is quite conservative, since contributions from extragalactic sources are expected as well. At the moment direct evidence for the oscillation of the atmospheric flux into ν_τ is missing. A clean ν_τ-event detection would then have some importance, and is indeed the main goal of
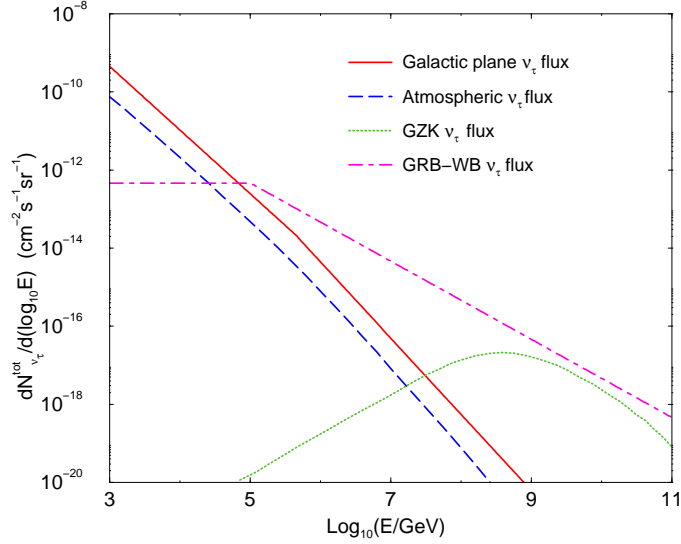
accelerator experiments like OPERA [Pes04].

Fig. 5.1.— Galactic plane, horizontal atmospheric and GZK high energy tau neutrino flux assuming of neutrino oscillations [Ath02]. For comparison, tau neutrino flux in a fireball model of GRB is also shown [Wax97]. The energy range shown covers all the presently envisaged high energy (tau) neutrino detectors.

Another interesting channel to probe neutrino mixing at telescopes has been recently discussed [Bha05]. The basic idea is to exploit the isospin asymmetry accompanying $p\gamma$ neutrino production close to the Δ-threshold (Sec. 4.1). The fractional amounts of neutrinos of various flavours $\mathcal{F}_\nu \equiv \{\nu_e, \bar\nu_e, \nu_\mu, \bar\nu_\mu, \nu_\tau, \bar\nu_\tau\}$ is $\mathcal{F}_\nu^{p\gamma} \simeq \{\frac{1}{3}, 0, \frac{1}{3}, \frac{1}{3}, 0, 0\}$ for $p\gamma$ sources, while for pp production one has $\mathcal{F}_\nu^{pp} \simeq \{\frac{1}{6}, \frac{1}{6}, \frac{1}{3}, \frac{1}{3}, 0, 0\}$. A combination of the two gives $\mathcal{F}_\nu^{\text{tot}} \simeq \{\frac{2-x}{6}, \frac{x}{6}, \frac{1}{3}, \frac{1}{3}, 0, 0\}$, with $x = 0$ corresponding to pure $p\gamma$ mechanism, which is expected to be dominant for extragalactic sources. If we limit our attention to the $\bar\nu$ flavours, it is clear that they have a flux ratio $\{\phi_e : \phi_\mu : \phi_\tau\} = \{\frac{x}{6} : \frac{1}{3} : 0\}$. As long as $x \ll 1$, this provides an almost pure state in flavour basis, which is an ideal tool for neutrino mixing studies. Note that if one considers the summed $\nu + \bar\nu$ ratio, one obtains the flavour content $\{\frac{1}{3} : \frac{2}{3} : 0\}$, oscillating approximately into $\{\frac{1}{3} : \frac{1}{3} : \frac{1}{3}\}$ almost independently from the details of neutrino mixing parameters [Ath00], provided that the μ–τ sector is (close to) maximally mixed. Optical Cherenkov telescopes can distinguish between ν and $\bar\nu$ only in the case of the Glashow resonance pro-
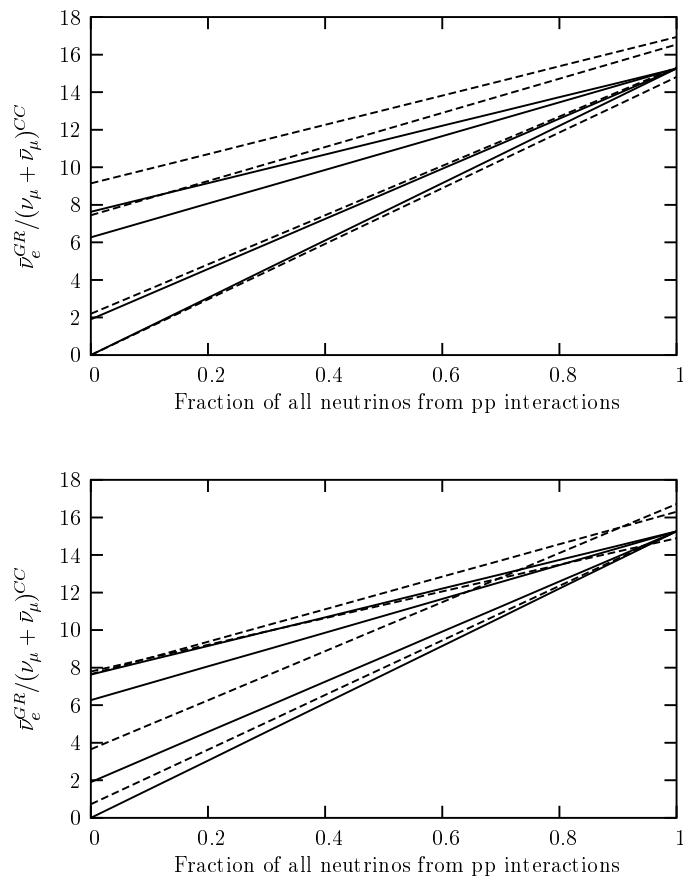
Fig. 5.2.— The number ratio of Glashow resonance events to $(\nu_\mu + \bar{\nu}_\mu)$ CC-events in a water or ice based detector as a function of the fraction x of $(\nu + \bar{\nu})$'s that originate from pp interactions at the source [Bha05]. In both plots, the lines from bottom to top are for $\theta_{12} = 0°$, $15°$, $32.5°$, and $45°$. In the top panel, $\theta_{13} = 0°$ is assumed, and the solid (dashed) lines show the case $\theta_{23} = 45°$ ($\theta_{23} = 40°$). In the bottom panel, $\theta_{23} = 45°$ is assumed, and the solid (dashed) lines show the case $\theta_{13} = 0°$ ($\theta_{13} = 9°$).

cess $\bar{\nu}_e + e^- \to W^-$. The ratio R_G of such events to the ν_μ plus $\bar{\nu}_\mu$ CC tracks in the same energy bin is then a very useful observable. It was shown to have a significant sensitivity both to the parameter x and to the mixing angles, in particular to θ_{12} [Bha05]. Unfortunately, a partial degeneracy between θ_{12} and x exists, but interesting constraints on the mixing angles might still obtain, especially if one can perform this measurement for a well characterized source.

We have not yet mentioned observables sensitive to the neutrino mass splittings. There are very few chances of performing such observations: If only vacuum oscillations are involved, the preferred values for the mass splittings imply that the oscillation lengths for any high energy neutrino source are much smaller than the distances involved, for any reasonable energy. Note that this statement could change if exotic mass-splittings exist in the neutrino sector. One possibility discussed in the literature is the one of "Pseudo-Dirac neutrinos" [Bea03b]. Even in the standard scenario, however, one exception is provided by the Solar corona neutrinos. The oscillation lengths for the Sun-Earth distance are matched for $E_\nu^\odot \simeq 4.9\,\mathrm{TeV}$ and $E_\nu^{\mathrm{atm}} \simeq 130\,\mathrm{TeV}$ respectively. The relatively low statistics expected has not motivated further analysis of such a source, however. Alternatively, the mass splittings might determine the phenomenology of matter effects (for an introduction see [Kuo89]), but they are typically unimportant for HEν telescopes. One possible exception is the case of Galactic SN neutrinos, that would allow to use neutrino telescopes to probe the mass hierarchy by detecting MeV-range neutrinos [Dig03]. IceCube, the km^3 Cherenkov neutrino telescope in construction at the South Pole, is highly sensitive to a Galactic SN neutrino burst (see Fig. 4.6). The Cherenkov light corresponding to the total energy deposited by the SN neutrinos in the ice can be measured relative to background fluctuations with a statistical precision much better than 1%. If the SN is viewed through the Earth, the matter effect on neutrino oscillations can change the signal by more than 5%, depending on the flavour-dependent source spectra and the neutrino mixing parameters. Therefore, IceCube together with another high-statistics experiment like Hyper-Kamiokande can detect the Earth effect, an observation that would identify specific neutrino mixing scenarios that are difficult to pin down with long-baseline experiments. In particular, the normal mass hierarchy can be clearly detected if the third mixing angle is not too small, i.e. $\sin^2\theta_{13} \gtrsim 10^{-3}$. The small flavour-dependent differences of the SN neutrino fluxes and spectra that are found in state-of-the-art simulations suffice for this purpose. A HEν telescope will be probably built in the Northern hemisphere, probably in the Mediterranean sea, within the next decade. For any astronomical survey, it is in fact necessary to achieve the total coverage of the sky. One might wonder that previous considerations could apply to a co-detection between two km^3 telescopes. Unfortunately, the water-based techniques forecast for a Northern observatory prevent such a possibility. The much higher noise level induced by radioactive salts prevents this kind of telescopes to observe a SN signal.

In general, the flux flavour ratios[1] ϕ_β^D arriving at the detector are given

---

[1]Henceforth, we denote with $\phi_\alpha^{(D)}$ the combined flux of ν_α and $\bar{\nu}_\alpha$.

in terms of the probabilities $P_{\alpha\beta} \equiv P(\nu_\alpha \to \nu_\beta)$ as $\phi_\beta^D = \sum_\alpha P_{\alpha\beta}\phi_\alpha$, where ϕ_α are the flux ratios at the source. Matter effects in the propagation of neutrinos are negligible because of the extremely low densities of interstellar and intergalactic medium, and often they are of no importance at the production site as well. In the following, we will then consider pure vacuum oscillations. Another simplification is that the Galactic and cosmic distances far exceed the experimentally known oscillation lengths, even at ultra-PeV energies. This implies that the interference terms sensitive to the mass splittings and to the sign of $\delta_{\rm CP}$ (i.e., the CP-violating terms) average out. Moreover, since $P(\bar\nu_\alpha \to \bar\nu_\beta, \delta_{\rm CP}, \mathcal{V}) = P(\nu_\alpha \to \nu_\beta, -\delta_{\rm CP}, -\mathcal{V})$ [Akh04], in the limit in which the matter potential $\mathcal{V}$ vanishes and no sensitivity to the sign of $\delta_{\rm CP}$ remains, the same probability formulae apply to the neutrino and anti-neutrino channels, $P_{\alpha\beta} = P_{\bar\alpha\bar\beta}$.
Therefore, one obtains

$$P_{\alpha\beta} = \delta_{\alpha\beta} - 2\sum_{j>k} {\rm Re}(U_{\beta j}U_{\beta k}^* U_{\alpha j}^* U_{\alpha k}), \qquad (5.5)$$

where $U(\theta_{12}, \theta_{23}, \theta_{13}, \delta_{\rm CP})$ is the neutrino mixing matrix of Eq. (5.2) and greek (latin) letters are used as flavour (mass) indices. Useful approximations to Eq. (5.5), obtained as first order expansion in the small quantity $\sin\theta_{13}$, are

$$
\begin{aligned}
P_{ee} &\simeq 1 - \frac{1}{2}\sin^2 2\theta_{12}, &(5.6)\\
P_{e\mu} &\simeq \frac{1}{2}\sin^2 2\theta_{12}\cos^2\theta_{23} + \frac{\sigma_{13}}{2}\sin 2\theta_{12}\cos 2\theta_{12}\sin 2\theta_{23},\\
P_{e\tau} &\simeq \frac{1}{2}\sin^2 2\theta_{12}\sin^2\theta_{23} - \frac{\sigma_{13}}{2}\sin 2\theta_{12}\cos 2\theta_{12}\sin 2\theta_{23},\\
P_{\mu\mu} &\simeq 1 - 2\cos^2\theta_{23} \times\\
&\qquad \left[\sin^2\theta_{23} + \frac{1}{4}\sin^2 2\theta_{12}\cos^2\theta_{23} + \frac{\sigma_{13}}{2}\sin 2\theta_{12}\cos 2\theta_{12}\sin 2\theta_{23}\right],\\
P_{\mu\tau} &= 1 - P_{\mu\mu} - P_{e\mu},\\
P_{\tau\tau} &= 1 - P_{\mu\tau} - P_{e\tau} = P_{\mu\mu} + P_{e\mu} - P_{e\tau},
\end{aligned}
$$

where $\sigma_{13} \equiv \sin\theta_{13}\cos\delta_{\rm CP}$ represents the only term responsible for truly three-neutrino mixing effects at the first order.

5.2   Galactic beta beams

In the following, we propose to use high energy neutrinos produced by decaying neutrons as a probe of θ_{13} and $\delta_{\rm CP}$ at neutrino telescopes. It is fascinating

that nature may provide in a very cheap way almost pure flavour neutrino beams that, similarly to proposed beta-beam factories [Zuc02], might help to deepen our knowledge of the neutrino mixing parameters.

Neutron primaries have been invoked to explain an excess of high energy cosmic rays from two regions in the Galactic plane [Anc03b, Crk04]. This signal, in a limited energy range around 10^{18} eV, has been observed by several experiments with different techniques. The AGASA Collaboration found a correlation of the arrival directions of CRs with the Galactic plane at the $4\,\sigma$ level [Hay98]. This excess, which is roughly 4% of the diffuse flux, is concentrated towards the Cygnus region, with a second hot spot towards the GC [Tes01]. Such a signal has been independently confirmed by the Fly's Eye Collaboration [Bir98] and by a re-analysis of the SUGAR data [Bld00].

Complementary evidence for a cosmic accelerator in the Cygnus region comes from the detection of an extended TeV γ-ray source by the HEGRA experiment [Aha02, Aha05]. Also, X-ray or radiowave emission could not be detected by CHANDRA or VLA [But03], thus favoring a hadronic accelerator. Similarly, multi-TeV γ-rays from the vicinity of the GC have been detected by HESS [Aha04], and recently confirmed by MAGIC [Alb05].

The excess from the Cygnus and GC region is seen at $E \simeq 10^{18}$ eV, i.e. at energies where charged cosmic rays suffer large deflections in the GMF so that only a neutral primary can produce a directional signal. Another evidence for neutrons as primaries is that the signal appears just at that energy where the neutron lifetime allows neutrons to propagate over distances of several kpc.

Neutrons can be generated as secondaries either in collisions of high energy protons on ambient photons and protons, or in the photo-dissociation of nuclei. In the first case, the flux of $\bar{\nu}_e$ from neutron decays would be negligible compared to the neutrino flux from pion decays. The oscillation phenomenology and signature for such a "standard" GC source were already considered in [Crk99]. In contrast, photo-dissociation of nuclei produces a pure $\bar{\nu}_e$ initial flux.

There are several arguments in favor of the dominance of heavy nuclei in the diffuse Galactic CR flux around 10^{18} eV. The end of the Galactic CR spectrum is expected to consist of heavy nuclei, because the GMF confines more easily CRs with small rigidity. Subtracting the spectrum expected for extragalactic CRs from the measured CR spectrum, [Ber04] found evidence that the transition between Galactic and extragalactic CRs happens around a few $\times 10^{17}$ eV. In this case, the total diffuse CR flux between 1 and 10×10^{17} eV consists mainly of galactic iron nuclei and extragalactic protons. Another method to determine the transition energy is to study the chemical composition of the CR flux [Wat04]. At present, these measurements are not

conclusive but point to a dominantly heavy component in the CR flux at least up to about 10^{18} eV and a possible transition to extragalactic protons at higher energies (see Fig. 1.5). Such a higher transition energy would also ease the difficult luminosity requirements needed for extragalactic ultra-high energy cosmic ray sources [Ste05]. Around and above the transition energy, the unconfined flux from Galactic point sources should become visible.

In the following we use as our basic assumption that nuclear photo-dissociation is the origin of the decaying neutrons. In order for our argument to work, we have to assume that other neutrino sources that contaminate the pure $\bar{\nu}_e$ initial flux are negligible. Following the treatment of [Tor04], we outline in the next Section how such a neutron-dominated source of neutrinos could be realized in the Cygnus star formation region, or in any other similar astrophysical environment, and we will estimate the event rate at IceCube.

5.2.1   A model for the Cygnus source

Antineutrinos take only a very small part of the energy of the parent neutron, of the order of $(m_n - m_p - m_e)/2\, m_n \lesssim 10^{-3}$. Hence, to estimate the event rate of TeV antineutrinos at a neutrino telescope, the relevant nucleus population at the source has an energy per nucleon $E_{N,\mathrm{PeV}} \sim 1$ PeV. Nuclei with Lorentz factor of the order of 10^6 are synthesized in all supernovae. Hadronic interactions with the HII population of density < 30 cm^{-3} [But03] and photo-disintegration processes provide the flux of PeV neutrons. In this energy regime, the target photons at photo-disintegration threshold energies are in the ultraviolet, $E_\gamma \sim 5$ eV. This includes the entire emission spectrum of the O stars and about 60% of photons from B stars (with average temperature 28000 K). From the photon emission rate F_{UV} the number density n_{UV} at the surface of a sphere of radius R from the core center is given by

$$\frac{1}{4} n_{\mathrm{UV}}\; c = \frac{F_{\mathrm{UV}}}{4\pi R^2}\;. \tag{5.7}$$

For the O-star population, the photon emission rate in the Lyman region is found to be $F_{\mathrm{L}} \approx 10^{51}$ photons s^{-1} [Kno00]. The Lyman emission corresponds to 60% of the entire O star spectrum. Furthermore, as mentioned above, 60% of the B star spectrum is also active for photo-disintegration in this energy region, and the B star population is about 20 times greater than that of the O stars [Kno00]. Now, from the H-R diagram [Has03] one can infer that the energy luminosity of a B-star is about 10% that of an O star. Additionally, the B star temperature is about 50% the O star temperature, giving a number luminosity ratio of about 0.2. For photo-disintegration resulting in PeV nucleons, the relevant photon density in the core of the

Cygnus OB2 association is then $n_{UV} \simeq 230 \, \text{cm}^{-3}$. The nucleus mean free path is about $35 \, \text{kpc}$, corresponding to a collision time $\tau = 10^5 \, \text{yr}$. Thus, the collision rate for photo-disintegration in the core region is comparable to the hadronic interaction rate. This estimate takes into account a hadronic cross section $\sigma_{Fep} \simeq A^{0.75} \, \sigma_{pp} \simeq 6 \times 10^{-25} \, \text{cm}^2$, and the generous upper limit of the nucleon density $30 \, \text{cm}^{-3}$ [Tor03b].

Since one is interested in neutrinos, it is still necessary to compare the production rate for charged pions in the hadronic case to the overall rate for generating neutrons. To assess this ratio, in [Tor04] high energy event simulations were used showing spectator nucleon and pion spectra for Fe-N/p-N collisions at 10^{15}–10^{16} eV [Kna96, Kna97]. Allowing for sizeable differences in hadronic interaction models, the secondary populations are roughly 35% $\pi^{\pm}$, 45% γ, 10% nucleons, and 10% K [Kna97]. In the energy range yielding PeV neutrons, only about 30% of the rapidity plateau contributes charged pions above 2 TeV. Since only half of the nucleons are neutrons, one arrives at a ratio

$$\frac{\pi^{\pm}(> 2 \text{ TeV})}{n(\sim \text{ PeV})} \simeq 3 \tag{5.8}$$

from the hadronic interactions.

However, photo-disintegration also takes place in the outer regions of the OB association as long as: i) the density of the optical photons propagating out from the core allows a reaction time which is smaller than the age of the cluster, 2.5 Myr [Kno01] and ii) the diffusion front of the nuclei has passed the region in question. From Eq. (5.7) one estimates an average photon density $n_{UV} \gtrsim 25 \, \text{cm}^{-3}$ out to 30 pc, which gives a reaction time of about 10^6 yr. The diffusion time ($\simeq 1.2$ Myr) is a bit smaller than the age of the cluster, and somewhat higher than the reaction time, allowing about 90% of the nuclei to interact during the lifetime of the source. Thus, the production rate of neutrons via photo-disintegration is amplified by a volume factor of 27 over the rate in the 10 pc core. The net result is that the PeV neutron population is about an order of magnitude greater than that of the TeV charged pions [Anc03b].

With this in mind, one can assess the prospects for a new multi-particle astronomy. Neutrons as directional pointers plus antineutrinos as inheritors of directionality. The basic formula that relates the neutron flux at the source $(\text{d}F_n/\text{d}E_n)$ to the antineutrino flux observed at Earth $(\text{d}F_{\overline{\nu}}/\text{d}E_{\overline{\nu}})$ is [Anc03b]

$$
\begin{aligned}
\frac{\text{d}F_{\overline{\nu}}}{\text{d}E_{\overline{\nu}}}(E_{\overline{\nu}}) \;=\; & \int \text{d}E_n \, \frac{\text{d}F_n}{\text{d}E_n}(E_n) \left[1 - \exp\left(-\frac{D \, m_n}{E_n \, \tau_n} \right) \right] \int_0^Q \text{d}\epsilon_{\overline{\nu}} \, \frac{\text{d}P}{\text{d}\epsilon_{\overline{\nu}}}(\epsilon_{\overline{\nu}}) \\
& \times \; \int_{-1}^{1} \frac{\text{d}\cos\overline{\theta}_{\overline{\nu}}}{2} \, \delta\left(E_{\overline{\nu}} - \frac{E_n \, \epsilon_{\overline{\nu}}}{m_n}(1 + \cos\overline{\theta}_{\overline{\nu}}) \right) .
\end{aligned}
\tag{5.9}
$$

The variables appearing in Eq. (5.9) are the antineutrino and neutron energies in the lab ($E_{\bar{\nu}}$ and E_n), the antineutrino angle with respect to the direction of the neutron momentum in the neutron rest frame ($\overline{\theta}_{\bar{\nu}}$), and the antineutrino energy in the neutron rest-frame ($\epsilon_{\bar{\nu}}$). The last three variables are not observed by a neutrino-detector, and so are integrated over. The observable $E_{\bar{\nu}}$ is held fixed. The delta-function relates the neutrino energy in the lab to the three integration variables. Note that $E_{\bar{\nu}} = \Gamma_n(\epsilon_{\bar{\nu}} + \beta\epsilon_{\bar{\nu}}\cos\overline{\theta}_{\bar{\nu}}) = E_n\epsilon_{\bar{\nu}}(1 + \cos\overline{\theta}_{\bar{\nu}})/m_n$, where $\Gamma_n = E_n/m_n$ is the Lorentz factor, and (as usual) $\beta \simeq 1$ is the particle's velocity in units of c. The parameters appearing in Eq. (5.9) are the neutron mass and rest-frame lifetime (m_n and $\overline{\tau}_n$), and the distance to the neutron source (D). The quantity $\mathrm{d}F_n/\mathrm{d}E_n$ is the neutron flux that would be observed from the Cygnus region in the absence of neutron decay. Finally, $dP/d\epsilon_{\bar{\nu}}$ is the normalized probability that the decaying neutron in its rest-frame produces a $\bar{\nu}_e$ with energy $\epsilon_{\bar{\nu}}$. Setting the beta-decay neutrino energy $\epsilon_{\bar{\nu}}$ equal to its mean value $\epsilon_0 \simeq (m_n - m_p)[1 - m_e^2/(m_n - m_p)^2]/2 = 0.55$ MeV, we have $\mathrm{d}P/\mathrm{d}\epsilon_{\bar{\nu}} = \delta(\epsilon_{\bar{\nu}} - \epsilon_0)$. Note that the delta-function in the neutron frame gives rise to a flat spectrum for the neutrino energy in the lab for fixed neutron lab-energy $E_n = \Gamma_n m_n$,

$$\frac{\mathrm{d}P}{\mathrm{d}E_{\bar{\nu}}} = \int_{-1}^{1} \frac{\mathrm{d}\cos\overline{\theta}_{\bar{\nu}}}{2}\left(\frac{\mathrm{d}\epsilon_{\bar{\nu}}}{dE_{\bar{\nu}}}\right)\left(\frac{\mathrm{d}P}{\mathrm{d}\epsilon_{\bar{\nu}}}\right) = \frac{1}{2\,\Gamma_n\,\epsilon_0}\,, \qquad (5.10)$$

with $0 \leq E_{\bar{\nu}} \leq 2\,\Gamma_n\,\epsilon_0$. The maximum neutrino energy in the neutron rest frame is $Q \equiv m_n - m_p - m_e = 0.71$ MeV, and the minimum neutrino energy is zero in the massless limit. The expression in parentheses in Eq. (5.9) is the decay probability for a neutron with lab energy E_n, traveling a distance D. In general, when considering a source distribution, one should integrate over the volume. Assuming the Cygnus OB2 complex at the average distance of 1.7 kpc and normalizing to the observed "neutron" excess around 10^{18} eV leads to about 20 antineutrino events at IceCube per year [Anc03b].

5.2.2 Effect of the oscillations and detection in IceCube

For the energies of interest, 10^{12} eV $\lesssim E \lesssim 10^{15}$ eV, the CC interactions of ν_e and ν_τ are in principle only distinguishable by the different muon content in electromagnetic and hadronic showers. In practice, this is an experimental challenge and we consider ν_e and ν_τ as indistinguishable in a neutrino telescope. By contrast, in ν_μ CC interactions the long range of muons ensures that the muon track is always visible and allows the identification of these events. Finally, all flavours undergo the same, indistinguishable NC interactions. This interaction contributes however only about 25% to the total cross

section [Gan98]. Moreover, in this case the energy of the primary is underestimated by a factor 3–4, further suppressing the relative importance of NC interactions because of the steeply falling energy spectrum. In the following, we neglect therefore NC interaction and consider the combined $\bar{\nu}_e$ and $\bar{\nu}_\tau$ flux $\phi_e^D + \phi_\tau^D$ and the $\bar{\nu}_\mu$ flux ϕ_μ^D as our two observables. For a neutron beam source, the ratio of observed track to shower events R can be expressed in terms of oscillation probabilities $P_{\alpha\beta}$ as

$$R \equiv \frac{\phi_\mu^D}{\phi_e^D + \phi_\tau^D} = \frac{P_{e\mu}}{P_{ee} + P_{e\tau}} = \frac{P_{e\mu}}{1 - P_{e\mu}}, \tag{5.11}$$

where in the last step we used the unitarity condition $P_{ee} + + P_{e\mu} + P_{e\tau} = 1$. Actually, the above defined quantity R is the ratio of observed track to shower events only in the limit in which sub-leading NC events are neglected, and if both channels are detected with the same efficiency. This is however a technical point inessential to our considerations, since it could be easily accounted for in refined predictions and for a specific experimental setup.

To obtain a feeling for the dependence of the fluxes on θ_{13} and $\delta_{\rm CP}$, we give an expansion of $P_{e\beta}$ up to second order in θ_{13} where we use $\theta_{12} = 30°$ and $\theta_{23} = 45°$,

$$\begin{aligned}
P_{ee} &\simeq \frac{5}{8} - \frac{5}{4}\theta_{13}^2 \,, \\
P_{e\mu} &\simeq \frac{3}{16} + \frac{\sqrt{3}}{8}\theta_{13}\cos\delta_{\rm CP} + \frac{5\theta_{13}^2}{8} \,, \\
P_{e\tau} &\simeq \frac{3}{16} - \frac{\sqrt{3}}{8}\theta_{13}\cos\delta_{\rm CP} + \frac{5\theta_{13}^2}{8} \,.
\end{aligned} \tag{5.12}$$

As expected, the survival probability P_{ee} (or equivalently ϕ_e^D) does not depend on $\delta_{\rm CP}$ and the unitarity relation $\sum_\beta P_{e\beta} = 1$ holds at each order in θ_{13}. Moreover, the $\bar{\nu}_\mu$ and $\bar{\nu}_\tau$ fluxes depend on $\delta_{\rm CP}$ only via the quantity $\cos\delta_{\rm CP}$. Note that the independence of P_{ee} from θ_{23} and $\delta_{\rm CP}$, as well as the relation $P_{e\mu} = P_{e\tau}(\theta_{23} \to \theta_{23} + \pi/2)$ that shows up in the opposite signs of the $\cos\delta_{\rm CP}$ terms in Eq. (5.12) hold exactly [Akh04]. Although the approximate relations Eq. (5.12) are useful to grasp the main features of the dependence of the fluxes ϕ_α^D on θ_{13} and $\delta_{\rm CP}$, in the following we will use the exact expressions given in Eq. (5.5). We also fix the value of the solar mixing angle to $\theta_{12} = 32.5°$ [Rew04].

Of course, the flux ratio R as the only observable does not allow for the simultaneous measurement of θ_{13} and $\delta_{\rm CP}$. For the sake of clarity, we first explore the sensitivity of R to the value of θ_{13}, fixing $\delta_{\rm CP} = 0°$. In Fig. 5.3, we show the expected ratio R as a function of θ_{13} for three representative

values of θ_{23}. This ratio varies by 25–50% in the interval $0° \leq \theta_{13} \leq 10°$ and differs in the extreme by a factor of three from the standard value, $\phi_\mu^D/(\phi_e^D + \phi_\tau^D) = 1/2$, that is also shown for comparison.
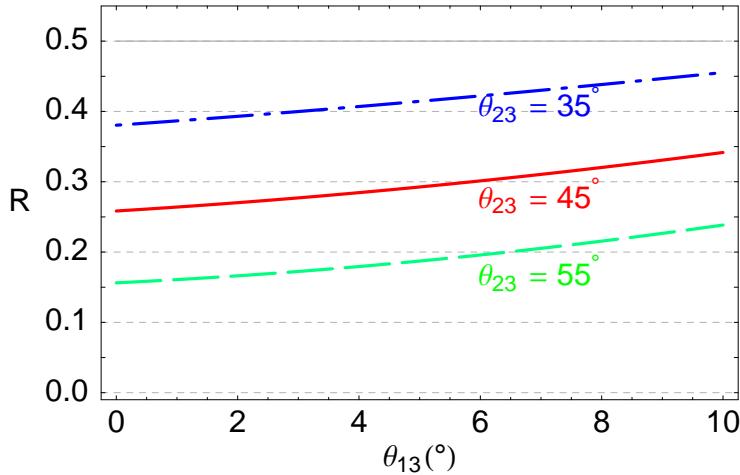

Fig. 5.3.— Flux ratio R at Earth as a function of θ_{13} for $\theta_{23} = 35°$ (blue, dot-dashed curve), $\theta_{23} = 45°$ (red, solid curve), $\theta_{23} = 55°$ (green, dashed curve), for initial fluxes $\{\phi_e : \phi_\mu : \phi_\tau\} = \{1 : 0 : 0\}$ at the source and $\delta_{CP} = 0°$. The ratio $R = 0.5$ expected for standard astrophysical sources is shown for comparison.

If the next generation of oscillation experiments measures θ_{13}, a neutrino telescope may even aim to constrain the leptonic CP-phase. In Fig. 5.4, we show the expected ratio R as a function of δ_{CP} for three values of θ_{13}. We have chosen the best fit value $\theta_{23} = 45°$. In this case the ratio varies maximally by about 35% in the interval $0° \leq \delta_{CP} < 180°$ and differs in the extreme by a factor two from the standard value $1/2$. If we use instead $\theta_{23} = 35°$ (55°), the only change would be an overall shift of the three curves by $\Delta R \simeq +0.1$ (-0.1).

The excellent angular resolution of $0.7°$ expected for IceCube applies only for ν_μ CC tracks, while for ν_e and ν_τ events the resolution is only about $25°$ [Bea03a]. According to the estimate in [Anc03b], one expects roughly 1.5 atmospheric ν_μ background events per year at $E > 1$ TeV in a window of $1° \times 1°$, i.e. about 2.3 yr^{-1} events in a $0.7°$ radius around the Cygnus region. This number has to be compared with the 4 $\bar{\nu}_\mu$ signal events assuming $\theta_{23} = 45°$ and $\theta_{13} = 0$. A $2\,\sigma$ detection of the $\bar{\nu}_\mu$ flux is then within 1 yr capability of IceCube. Rescaling this background number to a cone of $25°$ opening angle, one expects about 2900 ν_μ background events and 145
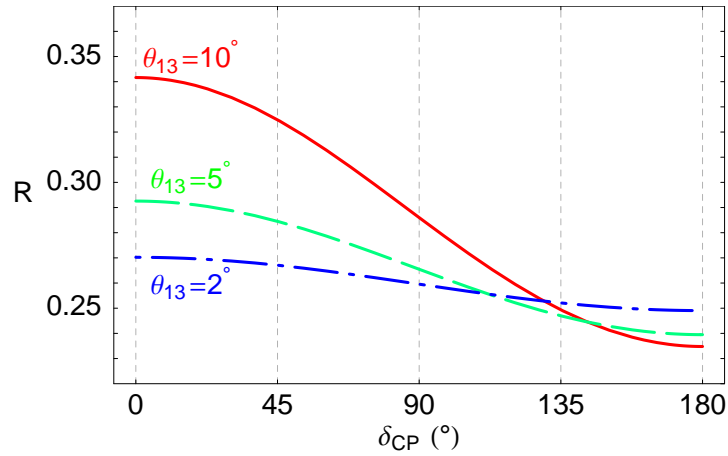
Fig. 5.4.— Flux ratio R at Earth as a function of δ_{CP} for $\theta_{13} = 10°$ (red, solid curve), $\theta_{13} = 5°$ (green, dashed curve), and $\theta_{13} = 2°$ (blue, dot-dashed curve), for $\theta_{23} = 45°$ and initial fluxes $\{\phi_e : \phi_\mu : \phi_\tau\} = \{1 : 0 : 0\}$ at the source.

background showers. Here we used the fact that the atmospheric neutrino background has a flavour ratio of $\{\phi_e : \phi_\mu : \phi_\tau\} \simeq \{0.05 : 1 : 0\}$ in the energy range of interest, 10^{11} eV $\lesssim E \lesssim 10^{14}$ eV [Bea04]. The resulting statistical fluctuation of the background shower number is $\sqrt{N} \simeq 12$. Thus integrating one year the $\simeq 16$ yr^{-1} rate from Cygnus one expects a $1.3\,\sigma$ signal hint, or equivalently a $4.2\,\sigma$ measurement in a decade.

Obviously, the poor angular resolution for ν_e and ν_τ events is the most serious obstacle to improve this measurement. If however a future neutrino telescope would be able to increase the shower resolution to, say, $10°$, then the same estimate would lead to a $3.3\,\sigma$ detection already in one year of data taking. Theoretical predictions for the neutron spectrum at the source could also be used to optimize the detection strategy. To fit the anisotropy data without introducing a cutoff, the AGASA collaboration required in [Hay98] a source spectrum with $\propto E^{-3}$ or steeper, while the spectral index of the model in [Anc03b] is 3.1. The atmospheric neutrino flux falls with a similar slope: its spectral index is in the range 3–3.7, being steeper at higher energies. Thus, if the $\bar{\nu}_e$ spectrum would be truly harder than the atmospheric neutrino background, the signal to background ratio could be improved by an increase of the threshold energy. Notice also that experimentally, the energy spectrum of the signal events could be more easily measured using the shower events [Bea04].

What happens to our previous estimates if we add some contamination from conventional pion decay? If the nuclei photo-dissociation mechanism is the

correct explanation for the neutron signal, realistic models like the one presented in Sec. 5.2.1 for the Cygnus region would led to 10% flux pollution. In this case, a shift as low as 0.01–0.02 is expected in the flux ratio R, within the expected experimental statistical error. An accidental pion contamination of the same order of the expected signal would lead to shifts of about $+0.1$ in R. The parameter estimate would then be challenging, but significant constraints on the parameter space would be still possible, in particular when neutrino telescopes data could be combined with complementary information from terrestrial experiments. Finally, we want to add a remark on the case when neutrons are generated mainly in pp or $p\gamma$ collisions. Since the normalization of the $\bar{\nu}_e$ flux from neutron decay is based on the 4% anisotropy in the CR data, the number of events in IceCube from neutron decay does not depend on the specific generation mechanism. However, when neutrons are produced in pp or $p\gamma$ collisions, additionally a much larger flux of neutrinos from pion decays with $\left\{\phi_e^D : \phi_\mu^D : \phi_\tau^D\right\} \simeq \left\{\frac{1}{3} : \frac{1}{3} : \frac{1}{3}\right\}$ is expected. Obviously, the background for the θ_{13} and $\delta_{\rm CP}$ searches discussed here would therefore drastically increase, while the detection of these Galactic point sources by neutrino telescopes would become much easier. A much larger flux and a flavour ratio $\phi_\mu^D/(\phi_e^D + \phi_\tau^D) \simeq 1/2$ in IceCube would be a smoking gun for the dominance of the pp or $p\gamma$ collision mechanism. Although less exciting from the point of view of neutrino physics, such a measurement would have important consequences for the astrophysical source diagnostics as well as for CR composition studies around 10^{18} eV.

5.3 A canonical flavour ratio for high energy neutrinos?

The standard paradigm of flavour content at HEν telescopes is that neutrinos originate mainly from pion decays. This suggests a flavour composition of $\{\phi_e : \phi_\mu : \phi_\tau\} \simeq \left\{\frac{1}{3} : \frac{2}{3} : 0\right\}$ at the source. Presently favored ranges for mixing parameters imply oscillated fluxes at the detector ϕ_α^D approximately in the ratios $\left\{\frac{1}{3} : \frac{1}{3} : \frac{1}{3}\right\}$, almost independently from the details of neutrino mixing parameters [Ath00]. Astrophysical uncertainties and the expected low statistics would not justify deeper studies. This qualitative argument probably explains why the potential for neutrino mixing studies has remained largely unexplored.

However, the possibility to exploit the flavour content of neutrino fluxes for astrophysical diagnostics has been recently analyzed in greater detail. A change in neutrino flavour fluxes was recently shown to be important for

diagnostics of gamma ray bursts (GRB) [Kas05]. As another example, the fraction of neutrinos produced in high energy accelerators via the strongly isospin-asymmetric $p\gamma$ process (as opposed to pp inelastic scattering) might also be measurable, at least around energies of 6.3 PeV [Bha05]. The discussion of the previous Section also shows that sensitivity to sources like Galactic-plane neutron beams can also be achieved, and implies non-trivial effects of the mixing parameters on the observable flavour content. However, though physically plausible, this source is not guaranteed. The very existence of a significant anisotropy—at least towards the GC—is currently debated, in the light of the negative results of an analysis of preliminary Auger data [Let05].

In the following, we generalize previous considerations arguing that: i) There could be neutron beam sources invisible to cosmic ray (an-)isotropy observations, and only detectable indirectly at neutrino telescopes. ii) Other candidate targets useful for neutrino mixing studies at neutrino telescopes also exist, like muon-damped ν_μ sources from pion decays, that were recently discussed [Kas05]. We shall motivate that both classes of sources could be not only identified at neutrino telescopes, but also used to infer non-trivial information on certain neutrino mixing parameters in a *model-independent way*, i.e. irrespective of astrophysical uncertainties. The argument still holds when presently allowed ranges for the other mixing parameters are taken into account. In particular, we shall show how a robust lower bound on θ_{23} could be established, and thus a value of $\theta_{23} > 45°$ identified. Note that this information is non-trivial. The present 2σ range is $36° \leq \theta_{23} \leq 52°$ [Fog05] and a deviation from maximal mixing would be important for flavour symmetries and neutrino mass models [Dor04, Anu04]. Of course, our considerations could be invalidated if exotic mechanisms like neutrino decays are effective [Bea02], but such scenarios seem to be at least disfavored by cosmological bounds [Had05, Bll05].

In Section 5.3.1 we treat generic neutron beam sources and focus on the octant of θ_{23} as a model-independent parameter possibly accessible at neutrino telescopes. Similar considerations are developed for a pure ν_μ beam from pion decay. In Section 5.3.2 we conclude.

5.3.1   Neutron and muon-damped beam sources

Neutrino fluxes detectable at neutrino telescopes, i.e. at $E \gtrsim$ 0.1–1 TeV, might well originate in the decay of few PeV neutrons from sources which have characteristics similar to the ones detailed in Section 5.2, but whose neutron spectrum cuts off at energies $E \ll 10^{18}$ eV. Since the decay length of a neutron is $d_n \simeq 10$ pc (E_n/PeV), and typical galactic distances are of

order 10 kpc, such a source would not show up as a cosmic ray anisotropy. The decay protons would rapidly lose directional information via deflection in the GMF. The dominance of nuclei in the Galactic cosmic ray spectrum is likely starting just above 10^{15} eV, and the spectrum of galactic cosmic rays is expected to extend at least up to few $\times 10^{17}$ eV (see e.g. [Ber04, All05b] and Section 3.1 in [Kac05]): A situation suitable to the neutron beam production is conceivable in many regions of our Galaxy. Of course, such "hidden" neutron beams could only be revealed by neutrino observations, and are thus constrained only by the direct observational upper bounds at neutrino telescopes. Nonetheless, any standard pion-decay source would produce neutrinos with a ratio $R \simeq 0.5$ or larger. By observing a ratio R significantly lower than 0.5, one could claim both the discovery of an invisible neutron beam and put constraints on the neutrino mixing parameters, since any background[2] should push R to higher values. The extremes of the ratio R of Eq. (5.11) for a fixed
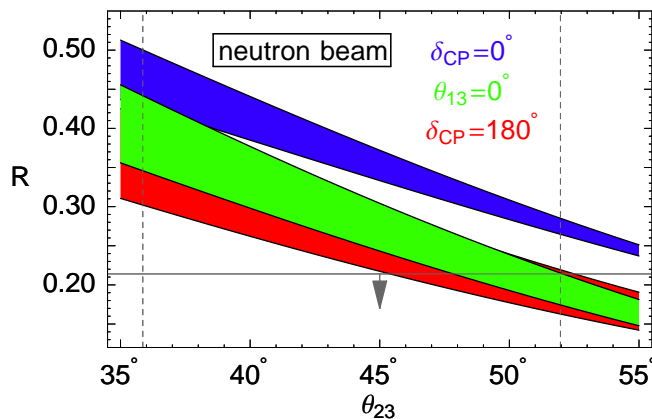
Fig. 5.5.— The ratio R of Eq. (5.11) for a neutron beam source vs. θ_{23}. The bands show the effect of the uncertainty on θ_{12}, and the trivial case $\{\theta_{13} = 0°\}$ is plotted together with the limiting cases $\{\theta_{13} = 10.3°, \delta_{CP} = 0°\}$ and $\{\theta_{13} = 10.3°, \delta_{CP} = 180°\}$. Dashed vertical lines enclose the allowed range for θ_{23}. The ranges shown are the 95% C.L. according to Ref. [Fog05]. The region below the solid horizontal line requires $\theta_{23} > 45°$.

θ_{12} and θ_{23} are obtained for the maximally allowed value of θ_{13} and the cases $\cos \delta_{CP} = \pm 1$, as the linear approximation of Eq. (5.6) suggests. In Fig. 5.5 it is clearly shown that, also including current 2σ uncertainties on mixing parameters, observations of an extremely low value for R, say $R \leq 0.21$, could

---

[2]Throughout the Section, we refer to other fluxes as "background" whenever they do not share the same flavour content of the source under consideration.

only be reconciled with a mixing angle $\theta_{23} > 45°$.

Until now we have focused on neutron beams from Galactic sources, because they are well motivated targets having a chance of detection. On the other hand, it should be stressed that extra-galactic sources that have suitable conditions also exist. Even when one turns to the most reliable of all extra-galactic neutrino sources, the cosmogenic neutrino flux, one easily realizes that at energies around 10^{16} eV a secondary peak almost purely made of $\bar{\nu}_e$ should be present [Eng01]. This peak is formed after neutron decays, both in the case of proton and heavy nuclei primaries. In the latter case a relatively larger contribution is expected because of the additional free-neutrons produced in photo-dissociations [Ave04, Hoo04a], see Fig. 5.6. In normal astrophysical sources, the photon target spectrum often extends for decades in energy, and the pion neutrino flux forming via photo-hadronic processes on the longer wavelength photons is expected to dominate the $\bar{\nu}_e$ from neutron flux produced on shorter wavelengths, shifting the neutron decay dominance peak to energies of no interest for neutrino telescopes. For extra-galactic nuclei, instead, the reactions on CMB photons are by far dominant and the secondary $\bar{\nu}_e$ peak is expected to show up. Of course, this flux is so low that a detection is challenging, and may be prevented even in principle by the larger contributions from canonical diffuse fluxes from other extra-galactic sources.

We now turn to another class of sources producing a non-trivial flavour content at neutrino telescopes, i.e. sources optically thick to muons (lifetime 2.2×10^{-6} s) but not to pions (lifetime 2.6×10^{-8} s), which would mainly emit neutrinos in the flavour ratios $\{0 : 1 : 0\}$. Such flavour content arises in specific astrophysical models [Rac98]. In addition, for any concrete example of accelerating engine, a transition from $\left\{\frac{1}{3} : \frac{2}{3} : 0\right\}$ to $\{0 : 1 : 0\}$ is expected in some energy range. This follows from the competition between growing decay path-length ($\lambda_{\text{decay}} \propto E$) and decreasing energy-loss distance with energy. For standard AGN models the transition energy is expected to be quite high, around 10^6 TeV, but it might be as low as about 10 TeV for GRB. Such a phenomenon could also offer interesting perspectives for GRB diagnostics [Kas05]. Again, the effect of mixing angles in this case is non-trivial. The flavour ratio at the Earth for a $\{0 : 1 : 0\}$ source would depend only on the ν_μ survival probability as

$$R \equiv \frac{\phi_\mu^D}{\phi_e^D + \phi_\tau^D} = \frac{P_{\mu\mu}}{1 - P_{\mu\mu}}, \qquad (5.13)$$

where we used the unitarity condition $P_{\mu e} + P_{\mu\tau} = 1 - P_{\mu\mu}$.

In Fig. 5.7 we show that any observation of a ratio $R \gtrsim 0.78$ would not only point to a muon-damped source, but would also constrain the octant
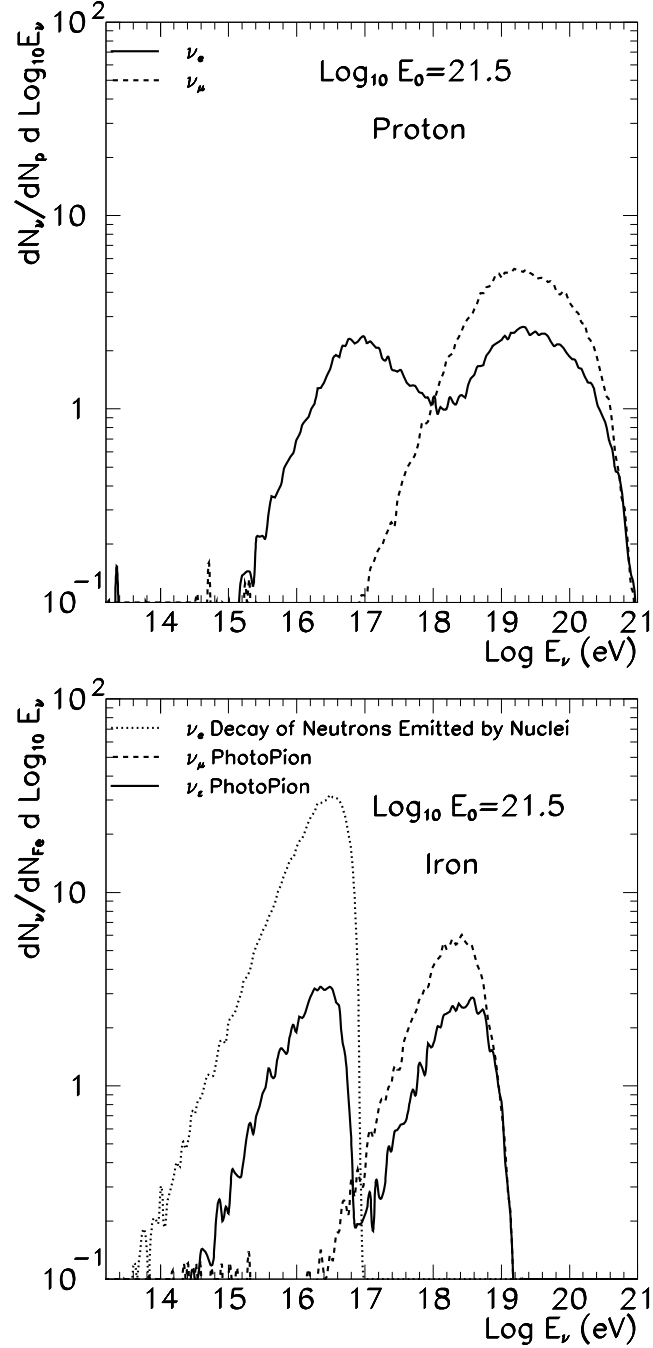
Fig. 5.6.— Cosmogenic neutrino yield for proton (top) and iron (bottom) [Ave04]. The energy considered is $10^{21.5}$ eV, and the propagation distance 300 Mpc. Different lines indicate the different origin of the neutrinos: the solid lines are $\nu_e + \bar{\nu}_e$ and the dashed lines are $\nu_\mu + \bar{\nu}_\mu$ all produced by photopion interactions. The dotted line is for $\bar{\nu}_e$ produced in the decay of neutrons emitted by the nuclei in photo-disintegration processes.
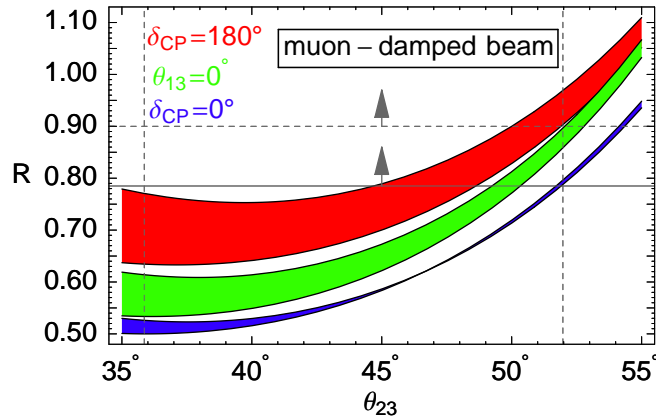
Fig. 5.7.— Same as Fig. 5.5, for a source optically thick to muons, but not to pions. The region above the solid horizontal line requires $\theta_{23} > 45°$, the one above the dashed horizontal line in addition requires a non-vanishing $\{\theta_{13}, \delta_{CP}\}$ sector.

of θ_{23}, i.e. $\theta_{23} > 45°$. This result is irrespective of the uncertainties on the other mixing parameters, as well as of known backgrounds from (undamped) pion chain or even neutron beams, which could only contribute to lower the value of R. Note also that in both Figs. 5.5 and 5.7, special regions in the parameter space exist that are only compatible with very specific values of the mixing parameters, and in particular θ_{13} and δ_{CP}. For example, if one establishes independently that $\theta_{23} < 45°$, a detected value of $R \gtrsim 0.7$ would only be compatible with a relatively large θ_{13} and a non-vanishing δ_{CP}.

To give a quantitative example, for a benchmark flux of muon neutrinos of $E^2 dN_\mu/dE = 10^{-7}\,\mathrm{GeV\ cm^{-2}\ s^{-1}}$, IceCube should be able to determine the flavour ratio at the 15% level after 1 yr [Bea03a], being thus sufficiently sensitive to detect the effects described above. Moderately lower fluxes could be compensated by a larger integration time.

Remarkably, any kind of extraterrestrial flux, even a diffuse one, can be studied as a function of E to identify an energy range with peculiar flavour ratios. Moreover, adding information from forthcoming laboratory experiments would improve the chances to identify the effect of $\theta_{23} > 45°$ at neutrino telescopes.

5.3.2 Conclusion

We have argued that the role of neutrino mixing at high energy neutrino telescopes is not trivial, and that forthcoming observations are potentially

interesting for neutrino mixing phenomenology. If sources like neutron or pion beams exist, we showed that: i) They can be unambiguously identified at neutrino telescopes. ii) They may allow a model-independent determination of crucial qualitative features of neutrino mixing parameters, like the octant of θ_{23} or the existence of a non-vanishing $\{\theta_{13}, \delta_{\mathrm{CP}}\}$ sector.

From a complementary perspective, accurate laboratory measurements of neutrino mixing parameters are of primary importance to perform astrophysical diagnostics: Since the flux flavour ratios depend on mixing angles, degeneracies with astrophysical parameters may arise. For example, although the main emphasis in [Bha05] was on the sensitivity of the ratio R_G to θ_{12} (which is relatively well determined from solar neutrino experiments), we remark that varying θ_{13} in the allowed experimental range can have an impact as large as 15% on R_G. This effect alone might affect the extraction of astrophysical parameters.

Throughout this Section, we have conservatively assumed that only the ratio R can be measured at neutrino telescopes. At energies larger than a few PeV, and in particular around the 6.3 PeV where the observable R_G can be used, one might expect to measure or to constrain the τ flavour fraction as well, since ν_τ-specific signatures such as lolly-pop or double bang events can be detected [Bea03a]. It is clear that the chance for a multi-channel observation offers a more powerful tool.

We conclude that the usual assumption of a canonical flavour equipartition at neutrino telescopes is too simplistic: Peculiar astrophysical sources may offer complementary constraints to laboratory measurements or, conversely, a more accurate experimental determination of mixing parameters may help to shed light on the properties of cosmic accelerators. After the pioneering era of the discovery of the solar neutrino deficit and of the atmospheric neutrino anomaly, observations at the highest energies will be sensitive to new astrophysical sources, that might still offer opportunities for neutrino oscillation studies.

Chapter 6

Discussion and conclusion

*Veniet tempus quo ista quæ nunc latent in lucem dies extrahat
et longioris ævi diligentia.[...] Veniet tempus quo posteri nostri
tam aperta nos nescisse mirentur.*

Seneca, Naturales Quæstiones, VII, XXV, 62 A.D.

The field of UHECRs is entering a new era, no longer plagued by the lack of
statistics, and hopefully improved in the control of the systematics, thanks
to hybrid techniques and to the validation of hadronic interaction models
at forthcoming accelerators. The Pierre Auger Observatory, whose Southern
site is almost completed, will unambiguously test the existence of the GZK-
suppression in the UHECR spectrum. New physics would almost certainly be
needed if the GZK-feature is absent as suggested by the AGASA data. Even
if the GZK suppression is found, however, the importance of UHECRs for
fundamental physics can not be excluded, yet. The possibility to use UHE
cosmic rays to study particle interactions at CM energies much larger than
in any planned accelerator will be linked to another question on which Auger
is expected to shed light: Is UHECR astronomy possible?

In the first part of this thesis, we have discussed the chance to use the
Galactic magnetic field as a spectrograph to discriminate among source mod-
els and primaries of UHECRs. Our findings are two-fold. On the one hand, the
regular GMF is so poorly known that it is hard to draw model-independent
conclusions. On the other hand, we showed that already with current statis-
tics one could discriminate among GMF field models and primary charges,
provided one has a clue to the astrophysical sources of UHECRs. Even more
important, in the next decade radio-astronomical surveys like the Square
Kilometer Array [SKA04] will finally provide a satisfactory mapping of the
GMF. The statistics collected in ten years by Auger and Telescope Array,
together with the characterization of the GMF, should offer powerful tools

for a major improvement in our knowledge of the cosmos. Interestingly, we found that a database of the same size is required to compare large scale anisotropies in UHECR arrival distribution with astronomical catalogues of the local universe. The hypothesis that UHECRs are mainly protons and trace the baryonic distribution in the universe should then be testable within one decade, provided that the extragalactic magnetic fields are not too strong.

The physics of neutrinos is entering the precision era where laboratory sources from reactors or accelerators are progressively replacing the natural ones (solar and atmospheric neutrinos) for the detailed determination of mixing angles and mass splittings. On the other hand, with the improved capabilities of present and future neutrino detectors, new natural sources are likely to be discovered or better characterized. The recent detection of geo-neutrinos leads the way [Ark05]. Valid theoretical reasons exist to expect that the diffuse supernova neutrino background is on the verge of detection [Sri05], not to speak about the breakthrough that the observation of neutrinos from a galactic core-collapse supernova might have for a huge number of astroparticle issues. In particular in the latter case, the potential to constrain—or even detect—non-standard physics effects is enormous and has been deeply analyzed in the literature [Raf02]. Supernova neutrino detection can also offer insights on "standard" neutrino oscillations, like a determination of the mass hierarchy or constraints on the yet unmeasured mixing angle θ_{13} [Raf05]. A parallel development is expected with the opening of a new observational window in astrophysics by the next generation of high energy neutrino telescopes [Lea00]. The first km^3-telescope, IceCube, will be completed in a few years and it will have the sufficient sensitivity to detect extraterrestrial high energy neutrinos. The ANITA balloon, aiming at the radio-Cherenkov detection of the cosmogenic neutrino flux, is flying in 2006-2007. These instruments are expected to finally shed light on several open problems in cosmic ray and gamma-ray astrophysics, but the possibility to exploit them to constrain exotic physics has been largely explored as well. In the second part of this thesis, we have analyzed the potential of neutrino telescopes for neutrino mixing phenomenology, finding interesting perspectives to determine the octant of θ_{23} or the existence of a non-vanishing $\{\theta_{13}, \delta_{CP}\}$ sector, exploiting peculiar sources like muon-damped or neutron beams.

Past astronomical revolutions suggest that new observational windows often offer interesting and unexpected consequences for fundamental physics. The thermal universe has been discovered in the 19th century, and widely explored by the 20th century astrophysics. We are now in the position to unveil the mysteries of non-thermal phenomena discovered in the 20th century, eventually transforming astronomy, the oldest science, into a frontier field of research for the exploration of fundamental physics at the highest energies.

Abbreviations

AGN	—	Active galactic nuclei
ASS	—	Axisymmetrical
BSS	—	Bisymmetrical
CC	—	Charged-current
C.L.	—	Confidence level
CM	—	Center-of-mass
CMB	—	Cosmic microwave background
CR	—	Cosmic ray
DIS	—	Deep inelastic scattering
EAS	—	Extensive air showers
EGMF	—	Extra-galactic magnetic field
ES	—	Elastic scattering
GC	—	Galactic center
GMF	—	Galactic magnetic field
GRB	—	Gamma ray bursts
GZK	—	Greisen-Zatsepin-Kuzmin
HEν	—	High energy neutrino
lab	—	Laboratory
LSS	—	Large scale structures
NC	—	Neutral-current
PAO	—	Pierre Auger Observatory
PMT	—	Photo-multipliers tubes
QE	—	Quasi-elastic scattering
R.A.	—	Right ascension
SN	—	Supernova
UHECR	—	Ultra-high energy cosmic ray
1 PeV	—	10^{15} eV
1 EeV	—	10^{18} eV

Acknowledgments

No work is a one-man enterprise: Many people and institutions have contributed to this thesis. My work has only been possible thanks to the support of the Max-Planck-Institut for Physics of Munich—where I have spent most of last three years—and of Manfred Lindner at the Institut T30d of the Physics Department of the TUM, who has also offered me the opportunity of a stimulating teaching experience. I express my gratitude to all the members of these institutions that with advice, support, patience, and kindness helped me to progress on the path of Science.

In my research activity, foremost I am indebted to Georg Raffelt, for the opportunities he offered me and for his constant advice in so many ways, as well as for the proofreading and valuable suggestions on this manuscript. Besides the uncountable number of things I have learned, his bright example of scientific creativity, always joined with profound professional ethics, will accompany me for the rest of my life.

I thank Michael Kachelrieß for introducing me to current issues in the field of ultra-high energy cosmic rays. For any question and doubt, I found Michael's door wide open, and his proofreading and suggestions were important for improving the manuscript.

Also I would like to thank all the people with whom I have collaborated. In particular I am grateful to the members of the astroparticle group of Naples, for encouragement and support, and for the warm atmosphere they managed to create around me. If I felt at home, it is also thanks to them.

A special thank to Alessandro Mirizzi, for his suggestions in the field of neutrino physics, for the long discussions and his proofreading, but above all for his friendship!

I am also grateful to all the "inhabitants" of the MPI theory division that have shared with me weeks or months, for creating a friendly and stimulating environment. A special mention to the experimental colleagues and friends of the MAGIC group at MPI. For discussions about physics and beyond, for DVD-sessions, for surviving India, for all the help and the smiles, thank you!

Of fundamental importance were all those friends and my family who

helped and encouraged me throughout all the years. In particular, for their love and support in any possible way I owe my deepest thanks to my parents. While I was in Munich, some members of my family lived wonderful or terrible moments, some passed away, and a new member has added. I regret that I could not be with you during many crucial days. This work is dedicated to you all, and in particular to those of you I will miss forever. If I am proud of being the person I am, it is thanks to your feelings for me.

For being still there, deep in my life and my heart, for your encouragement and patience, for coloring the days with your joy and sweetness, and for everything you did for me, words cannot express my love for you, Vera.

Bibliography

[Abb03] R. Abbasi *et al.* [HiRes Collaboration], "Search for global dipole enhancements in the HiRes-I monocular data above 10**18.5-eV," Astropart. Phys. **21**, 111 (2004) [astro-ph/0309457].

[Abb04a] R. U. Abbasi *et al.* [The High Resolution Fly's Eye Collaboration (HiRes)], "Study of small-scale anisotropy of ultrahigh energy cosmic rays observed in stereo by HiRes," Astrophys. J. **610**, L73 (2004) [astro-ph/0404137].

[Abb04b] R. U. Abbasi *et al.* [The High Resolution Fly's Eye Collaboration (HiRes)], "A search for arrival direction clustering in the HiRes-I monocular data above 10**19.5-eV," Astropart. Phys. **22**, 139 (2004) [astro-ph/0404366].

[Abb05] R. U. Abbasi *et al.* [HiRes Collaboration], "Search for cross-correlations of ultra-high-energy cosmic rays with BL Lacertae objects," astro-ph/0507120.

[Abu00] T. Abu-Zayyad *et al.*, "The Prototype High-Resolution Fly's Eye Cosmic Ray Detector," Nucl. Instrum. Meth. A **450**, 253 (2000).

[Ade05] J. K. Adelman-McCarthy *et al.* [SDSS Collaboration], "The Fourth Data Release of the Sloan Digital Sky Survey," astro-ph/0507711.

[Afa96] B. N. Afanasiev,*et al.*, 1996 *in Proc. Int. Symp. on Extremely High Energy Cosmic Rays : Astrophysics and Future Observatories* (ed. M.Nagano, Institute for Cosmic Ray Research, Univ. of Tokyo) p.32.

[Agl94] M. Aglietta *et al.* [EAS-TOP Collaboration], "The Limit to the UHE extraterrestrial neutrino flux from the observations of horizontal air showers at EAS-TOP," Phys. Lett. B **333**, 555 (1994).

[Aha02] F. A. Aharonian *et al.*, "An unidentified TeV source in the vicinity of Cygnus OB2," Astron. Astrophys. **393**, L37 (2002) [astro-ph/0207528].

[Aha04] F. Aharonian *et al.* [The HESS Collaboration], "Very high energy gamma rays from the direction of Sagittarius A*," Astron. Astroph. **425**, L13-L17 (2004) [astro-ph/0408145].

[Aha05] F. Aharonian *et al.*, "The unidentified TeV source (TeVJ2032+4130) and surrounding field: Final HEGRA IACT-System results," astro-ph/0501667.

[Ahl05] M. Ahlers *et al.*, "Neutrinos as a diagnostic of cosmic ray galactic / extra-galactic transition," Phys. Rev. D **72**, 023001 (2005) [astro-ph/0503229].

[Ahr02] J. Ahrens *et al.* [The IceCube Collaboration], "IceCube: The next generation neutrino telescope at the South Pole," Nucl. Phys. Proc. Suppl. **118**, 388 (2003) [astro-ph/0209556].

[Ahr03] J. Ahrens *et al.*, "Limits on diffuse fluxes of high energy extraterrestrial neutrinos with the AMANDA-B10 detector," Phys. Rev. Lett. **90**, 251101 (2003) [astro-ph/0303218].

[Ahr04] J. Ahrens *et al.* [AMANDA Collaboration], "Search for extraterrestrial point sources of neutrinos with AMANDA-II," Phys. Rev. Lett. **92**, 071102 (2004) [astro-ph/0309585].

[Akh04] E. K. Akhmedov, R. Johansson, M. Lindner, T. Ohlsson and T. Schwetz, "Series expansions for three-flavor neutrino oscillation probabilities in matter," JHEP **0404**, 078 (2004) [hep-ph/0402175].

[Alb05] J. Albert *et al.* [MAGIC Collaboration], "Observation of gamma rays from the galactic center with the MAGIC telescope," astro-ph/0512469.

[All05a] D. Allard, E. Parizot, E. Khan, S. Goriely and A. V. Olinto, "UHE nuclei propagation and the interpretation of the ankle in the cosmic-ray spectrum," Astron. Astroph. **443** (2005) L29-L32 [astro-ph/0505566].

[All05b] D. Allard, E. Parizot and A. V. Olinto, "On the transition from Galactic to extragalactic cosmic-rays: spectral and composition features from two opposite scenarios," astro-ph/0512345.

[Alv01] J. Alvarez-Muniz, R. Engel and T. Stanev, "UHECR propagation in the Galaxy: clustering versus isotropy," Astrophys. J. **572**, 185 (2001) [astro-ph/0112227].

[Alv05a] J. Alvarez-Muniz and T. Stanev, "The large scale structure of the galactic magnetic field and high energy cosmic ray anisotropy," astro-ph/0507273.

[Alv05b] J. Alvarez-Muniz, E. Marques, R. A. Vazquez and E. Zas, "Coherent radio pulses from showers in different media: A unified parameterization," astro-ph/0512337.

[Anc96] L. A. Anchordoqui, M. T. Dova, L. N. Epele and J. D. Swain, "Effect of the 3-K background radiation on ultrahigh energy cosmic rays," Phys. Rev. D **55**, 7356 (1997) [hep-ph/9704387].

[Anc01] L. A. Anchordoqui, H. Goldberg, S. Reucroft, G. E. Romero, J. Swain and D. F. Torres, "The mysterious ultrahigh energy cosmic ray clustering," Mod. Phys. Lett. A **16**, 2033 (2001) [astro-ph/0106501].

[Anc02] L. Anchordoqui, T. Paul, S. Reucroft and J. Swain, "Ultrahigh energy cosmic rays: The state of the art before the Auger observatory," Int. J. Mod. Phys. A **18**, 2229 (2003) [hep-ph/0206072].

[Anc03a] L. A. Anchordoqui, C. Hojvat, T. P. McCauley, T. C. Paul, S. Reucroft, J. D. Swain and A. Widom, "Full-sky search for ultrahigh-energy cosmic ray anisotropies," Phys. Rev. D **68**, 083004 (2003) [astro-ph/0305158].

[Anc03b] L. A. Anchordoqui, H. Goldberg, F. Halzen and T. J. Weiler, "Galactic point sources of TeV antineutrinos," Phys. Lett. B **593**, 42 (2004) [astro-ph/0311002].

[Anc04] L. Anchordoqui, M. T. Dova, A. Mariazzi, T. McCauley, T. Paul, S. Reucroft and J. Swain, "High energy physics in the atmosphere: Phenomenology of cosmic ray air showers," Annals Phys. **314**, 145 (2004) [hep-ph/0407020].

[Anc05a] L. A. Anchordoqui, H. Goldberg, M. C. Gonzalez-Garcia, F. Halzen, D. Hooper, S. Sarkar and T. J. Weiler, "Probing Planck scale physics with IceCube," Phys. Rev. D **72**, 065019 (2005) [hep-ph/0506168].

[Anc05b] L. Anchordoqui, T. Han, D. Hooper and S. Sarkar, "Exotic neutrino interactions at the Pierre Auger observatory," Astropart. Phys, in press [hep-ph/0508312].

[Anc05c] L. A. Anchordoqui, J. L. Feng and H. Goldberg, "Particle physics on ice: Constraints on neutrino interactions far above the weak scale," Phys. Rev. Lett., in press [hep-ph/0504228].

[And99] E. Andres *et al.*, "The AMANDA neutrino telescope: Principle of operation and first results," Astropart. Phys. **13**, 1 (2000) [astro-ph/9906203].

[And01] E. Andres *et al.*, "Observation of high-energy neutrinos using Cherenkov detectors embedded deep in Antarctic ice," Nature **410**, 441 (2001).

[Ans04] K. Anderson *et al.*, "White paper report on using nuclear reactors to search for a value of theta(13)," hep-ex/0402041.

[Ant03] T. Antoni *et al.* [KASCADE Collaboration], "The Cosmic ray experiment KASCADE," Nucl. Instrum. Meth. A **513**, 490 (2003).

[Ant05] T. Antoni *et al.* [The KASCADE Collaboration], "KASCADE measurements of energy spectra for elemental groups of cosmic rays: Results and open problems," Astropart. Phys. **24**, 1 (2005) [astro-ph/0505413].

[Anu04] S. Antusch, P. Huber, J. Kersten, T. Schwetz and W. Winter, "Is there maximal mixing in the lepton sector?," Phys. Rev. D **70**, 097302 (2004) [hep-ph/0404268].

[Apo02] M. Apollonio *et al.*, "Search for neutrino oscillations on a long baseline at the CHOOZ nuclear power station," Eur. Phys. J. C **27**, 331 (2003) [hep-ex/0301017].

[Ara03] Y. Arai *et al.*, "The Telescope Array experiment: An overview and physics aims," Proc. 28$^{\text{th}}$ ICRC - Tsukuba, Japan (2003).

[Arc03] G. Archbold *et al.*, Proc. 28$^{\text{th}}$ ICRC - Tsukuba, Japan (2003).

[Ark05] T. Araki *et al.*, "Experimental investigation of geologically produced antineutrinos with KamLAND," Nature **436**, 499 (2005).

[Ask62] G. A. Askaryan, JETP 14, 441 (1962); JETP 21, 658 (1965)

[Ath00] H. Athar, M. Jezabek and O. Yasuda, "Effects of neutrino mixing on high-energy cosmic neutrino flux," Phys. Rev. D **62**, 103007 (2000) [hep-ph/0005104].

[Ath01a] H. Athar, G. L. Lin and J. J. Tseng, "Muon pair production by electron photon scatterings," Phys. Rev. D **64**, 071302 (2001) [hep-ph/0104185].

[Ath01b] H. Athar, K. m. Cheung, G. L. Lin and J. J. Tseng, "High-energy cosmic-ray tau neutrino flux from the Milky Way," Astropart. Phys. **18**, 581 (2003) [hep-ph/0112222].

[Ath02] H. Athar, "High energy astrophysical tau neutrinos: The expectations," Nucl. Phys. Proc. Suppl. **122**, 305 (2003) [hep-ph/0210244].

[Ato01] A. Atoyan and C. D. Dermer, "High-energy neutrinos from photomeson processes in blazars," Phys. Rev. Lett. **87**, 221102 (2001) [astro-ph/0108053].

[Ave00] M. Ave *et al.* [Haverah Park Collaboration], "New constraints from Haverah Park data on the photon and iron fluxes of UHE cosmic rays," Phys. Rev. Lett. **85**, 2244 (2000) [astro-ph/0007386].

[Ave01] M. Ave, J. Knapp, J. Lloyd-Evans, M. Marchesini and A. A. Watson, "The energy spectrum of cosmic rays above 3 x 10**17-eV as measured with the Haverah Park Array," Astropart. Phys. **19**, 47 (2003) [astro-ph/0112253].

[Ave02] M. Ave, L. Cazon, J. A. Hinton, J. Knapp, J. LLoyd-Evans and A. A. Watson, "Mass composition of cosmic rays in the range 2 x 10**17 - 3 x 10**18 measured with the Haverah Park Array," Astropart. Phys. **19**, 61 (2003) [astro-ph/0203150].

[Ave03] M. Ave, J. Knapp, M.. Marchesini, M. Roth and A. A. Watson, Proc. 28$^{\text{th}}$ ICRC - Tsukuba, Japan (2003).

[Ave04] M. Ave, N. Busca, A. V. Olinto, A. A. Watson and T. Yamamoto, "Cosmogenic neutrinos from ultra-high energy nuclei," Astropart. Phys. **23**, 19 (2005) [astro-ph/0409316].

[Ayn05] V. Aynutdinov *et al.* [Baikal Collaboration], "The Baikal neutrino experiment: From NT200 to NT200+," Proc. 29$^{\text{th}}$ ICRC - Pune, India (2005) [astro-ph/0507709].

[Bab02] C. Barbot and M. Drees, "Production of ultra-energetic cosmic rays through the decay of super-heavy X particles," Phys. Lett. B **533**, 107 (2002) [hep-ph/0202072].

[Bak00] V. Balkanov *et al.*, "An upper limit on the diffuse flux of high energy neutrinos obtained with the Baikal detector NT-96," Astropart. Phys. **14**, 61 (2000).

[Bak01] V. Balkanov *et al.* [BAIKAL Collaboration], "Baikal experiment: Status report," Nucl. Phys. Proc. Suppl. **110**, 504 (2002) [astro-ph/0112446].

[Bal85a] R. M. Baltrusaitis *et al.*, "The Utah Fly's Eye Detector," Nucl. Instrum. Meth. A **240**, 410 (1985).

[Bal85b] R. M. Baltrusaitis *et al.*, "Limits On Deeply Penetrating Particles In The > 10**17-Ev Cosmic Ray Flux," Phys. Rev. D **31**, 2192 (1985).

[Bar02] V. D. Barger, F. Halzen, D. Hooper and C. Kao, "Indirect search for neutralino dark matter with Phys. Rev. D **65**, 075022 (2002), [hep-ph/0105182].

[Baw05] S. W. Barwick *et al.* [ANITA Collaboration], "Constraints on cosmic neutrino fluxes from the ANITA experiment," astro-ph/0512265.

[Bea02] J. F. Beacom, N. F. Bell, D. Hooper, S. Pakvasa and T. J. Weiler, "Decay of high-energy astrophysical neutrinos," Phys. Rev. Lett. **90**, 181301 (2003) [hep-ph/0211305].

[Bea03a] J. F. Beacom, N. F. Bell, D. Hooper, S. Pakvasa and T. J. Weiler, "Measuring flavor ratios of high-energy astrophysical neutrinos," Phys. Rev. D **68**, 093005 (2003) [Erratum-ibid. D **72**, 019901 (2005)] [hep-ph/0307025].

[Bea03b] J. F. Beacom, N. F. Bell, D. Hooper, J. G. Learned, S. Pakvasa and T. J. Weiler, "Pseudo-Dirac neutrinos, a challenge for neutrino telescopes," Phys. Rev. Lett. **92**, 011101 (2004) [hep-ph/0307151].

[Bea03c] J. F. Beacom, N. F. Bell, D. Hooper, S. Pakvasa and T. J. Weiler, "Sensitivity to Theta(13) and delta in the decaying astrophysical neutrino scenario," Phys. Rev. D **69**, 017303 (2004) [hep-ph/0309267].

[Bea04] J. F. Beacom and J. Candia, "Shower power: Isolating the prompt atmospheric neutrino flux using electron neutrinos," JCAP **0411**, 009 (2004) [hep-ph/0409046].

[Bec96] R. Beck, A. Brandenburg, D. Moss, A. Shukurov, D. Sokoloff, "Galactic Magnetism: Recent Developments and Perspectives," Ann. Rev. Astron. Astrophys. **34**, 155 (1996).

[Bec00] R. Beck, "Galactic and extragalactic magnetic fields," in "The Astrophysics of Galactic Cosmic Rays", eds. R. Diehl *et al.*, Space Science Reviews, Kluwer [astro-ph/0012402].

[Bed04] W. Bednarek, G. F. Burgio and T. Montaruli, "Galactic discrete sources of high energy neutrinos," New Astron. Rev. **49**, 1 (2005) [astro-ph/0404534].

[Beg97] L. Bergstrom, J. Edsjo and P. Gondolo, "Indirect neutralino detection rates in neutrino telescopes," Phys. Rev. D **55**, 1765 (1997) [hep-ph/9607237].

[Beg98] L. Bergstrom, "Particle dark matter and its indirect detection," New Astron. Rev. **42**, 245 (1998).

[Bel97] I. A. Belolaptikov *et al.* [BAIKAL Collaboration], "The Baikal underwater neutrino telescope: Design, performance, and first results," Astropart. Phys. **7**, 263 (1997).

[Bem05] D. R. Bergman [the HiRes Collaboration], "Fitting the HiRes spectra," Proc. 29th ICRC - Pune, India (2005) [astro-ph/0507484].

[Ber69] V. S. Beresinsky and G. T. Zatsepin, "Cosmic Rays At Ultrahigh-Energies (Neutrino?)," Phys. Lett. B **28**, 423 (1969).

[Ber75] V. S. Berezinsky and A. Yu. Smirnov, Astrophys. Space Sci. **32**, 461 (1975); V. S. Berezinsky, in Proc. of "Neutrino-77", Baksan , USSR, ed. M.A.Markov **1**, 177 (1977).

[Ber88] V. S. Berezinskii and S. A. Grigor'eva, "A bump in the ultra-high energy cosmic ray spectrum" Astron. Astrophys. **199**, 1 (1988).

[Ber90] V.S. Berezinsky *et al.*, "Astrophysics of Cosmic Rays", Nort-Holland (1990)

[Ber92] V. S. Berezinsky, T. K. Gaisser, F. Halzen and T. Stanev, "Diffuse radiation from cosmic ray interactions in the galaxy," Astropart. Phys. **1**, 281 (1993).

[Ber97] V. Berezinsky, M. Kachelrieß and A. Vilenkin, "Ultra-high-energy cosmic rays without GZK cutoff," Phys. Rev. Lett. **79**, 4302 (1997), [astro-ph/9708217].

[Ber99] V. S. Berezinsky and A. Vilenkin, "Ultra high-energy neutrinos from hidden-sector topological defects," Phys. Rev. D **62**, 083512 (2000), [hep-ph/9908257].

[Ber04] V. S. Berezinsky, S. I. Grigorieva and B. I. Hnatyk, "Extragalactic UHE proton spectrum and prediction for iron-nuclei flux at 10**8-GeV to 10**9-GeV," Astropart. Phys. **21**, 617 (2004) [astro-ph/0403477].

[Ber05] V. Berezinsky, A. Z. Gazizov and S. I. Grigorieva, "Dip in UHECR spectrum as signature of proton interaction with CMB," Phys. Lett. B **612**, 147 (2005) [astro-ph/0502550].

[Bes05a] P. N. Best *et al.*, "The host galaxies of radio-loud AGN: mass dependencies, gas cooling and AGN feedback," *MNRAS* **362**, 25 (2005) [astro-ph/0506269].

[Bes05b] P. N. Best, G. Kauffmann, T. M. Heckman and Z. Ivezic, "A sample of radio-loud AGN in the Sloan Digital Sky Survey," *MNRAS* **362**, 9 (2005) [astro-ph/0506268].

[Bet05] X. Bertou [Pierre Auger Collaboration], "Performance of the Pierre Auger Observatory surface array," Proc. 29$^{\text{th}}$ ICRC - Pune, India (2005) [astro-ph/0508466].

[Beu85] K. Beuermann, G. Kanbach, E. M. Berkhuijsen, "Radio structure of the Galaxy - Thick disk and thin disk at 408 MHz," Astron. Astrophys. **153**, 17 (1985).

[Bha98] P. Bhattacharjee and G. Sigl, "Origin and propagation of extremely high energy cosmic rays," Phys. Rept. **327**, 109 (2000) [astro-ph/9811011].

[Bha05] P. Bhattacharjee and N. Gupta, "Probing neutrino mixing angles with ultrahigh energy neutrino telescopes," hep-ph/0501191.

[Bik98] M. Birkel and S. Sarkar, "Extremely high-energy cosmic rays from relic particle decays," Astropart. Phys. **9**, 297 (1998), hep-ph/9804285.

[Bir93] D. J. Bird *et al.* [Fly's Eye Collaboration], "Evidence for correlated changes in the spectrum and composition of cosmic rays at extremely high-energies," Phys. Rev. Lett. **71**, 3401 (1993).

[Bir98] D. J. Bird *et al.* [HIRES Collaboration], "Study of broad scale anisotropy of cosmic ray arrival directions from 2 x 10^{17} eV to 10^{20} eV from Fly's Eye data," Astrophys. J. **511**, 739 (1999) [astro-ph/9806096].

[Bla40] P. M. S. Blackett and A. C. B Lovell, Proc. Roy. Soc. (London) Ser. A **177**, 183 (1940).

[Bld00] J. A. Bellido, R. W. Clay, B. R. Dawson and M. Johnston-Hollitt, "Southern hemisphere observations of a 10^{18} eV cosmic ray source near the direction of the galactic centre," Astropart. Phys. **15**, 167 (2001) [astro-ph/0009039].

[Bll05] N. F. Bell, E. Pierpaoli and K. Sigurdson, "Cosmological signatures of interacting neutrinos," astro-ph/0511410.

[Bln00] M. Blanton, P. Blasi and A. V. Olinto, "The GZK feature in our neighborhood of the universe," Astropart. Phys. **15**, 275 (2001) [astro-ph/0009466].

[Boa05] S. Bottai [EUSO Collaboration], "EUSO and neutrino detection," Nucl. Phys. Proc. Suppl. **143**, 381 (2005).

[Bol97] J. W. Bolesta *et al.*, "A search for very high energy neutrinos from active galactic nuclei," astro-ph/9705198.

[Bon05] C. Bonifazi *et al.* [The Pierre Auger collaboration], "Angular resolution of the Pierre Auger Observatory," Proc. 29$^{\text{th}}$ ICRC - Pune, India (2005).

[Bot98] M. Bottcher and C. D. Dermer, 37kb) "High Energy Gamma Rays from Ultrahigh Energy Protons in Gamma Ray Bursts", Astrophys. J. Lett. 499, L131, [astro-ph/9801027].

[Bug01] E. V. Bugaev and K. V. Konishchev, "Extragalactic neutrino background from PBHs evaporation," astro-ph/0103265.

[But03] Y. Butt *et al.*, "CHANDRA/VLA follow-up of TeV J2032+4131, the only unidentified TeV gamma-ray source," Astrophys. J. **597**, 494 (2003) [astro-ph/0302342].

[Can05] J. Candia, "Detectable neutrino fluxes due to enhanced cosmic ray densities in the galactic center region," JCAP **0511**, 002 (2005) [astro-ph/0505346].

[Cas90] G. L. Cassiday *et al.*, "A Coarse Grain Search for Anisotropy in the Arrival Directions of Cosmic Rays Above 10**17-Ev," Astrophys. J. **351**, 454 (1990).

[Chi91] N. Chiba *et al.*, "Akeno giant air shower array (AGASA) covering 100-km**2 area," Nucl. Instrum. Meth. A **311**, 338 (1992).

[Cho92] M. J. Chodorowski, A. Zdziarski and M. Sikora, "Reaction rate and energy-loss rate for photopair production by relativistic nuclei" Astrophys. J. **400**, 181 (1992).

[Cir05] M. Cirelli, N. Fornengo, T. Montaruli, I. Sokalski, A. Strumia and F. Vissani, "Spectra of neutrinos from dark matter annihilations," Nucl. Phys. B **727**, 99 (2005) [hep-ph/0506298].

[Cla57] G. W. Clark, J. Earl, W. L. Kraushaar, J. Linsley, B. B. Rossi, and F. Scherb, Nature **180**, 353 (1957).

[Cli99] D. B. Cline and F. W. Stecker, "Exploring the ultrahigh energy neutrino universe," astro-ph/0003459.

[Col03] A. A. Collister and O. Lahav, "ANNz: estimating photometric redshifts using artificial neural networks," Publ. Astron. Soc. Pac. **16**, 345 (2004) [astro-ph/0311058].

[Com32] A.H. Compton, "Variation of the Cosmic Rays with Latitude," Phys. Rev. **41**, 111 (1932)

[Cor92] S. C. Corbato *et al.*, "Hires: A High Resolution Fly's Eye Detector," Nucl. Phys. Proc. Suppl. **28B**, 36 (1992).

[Crk99] R. M. Crocker, F. Melia and R. R. Volkas, "Oscillating neutrinos from the galactic center," Astrophys. J. Suppl. **130**, 339 (2000) [astro-ph/9911292].

[Crk04] R. M. Crocker *et al.*, "The AGASA / SUGAR anisotropies and TeV gamma rays from the galactic center: A possible signature of extremely high-energy neutrons," Astrophys. J. **622**, 892 (2005) [astro-ph/0408183]; "Neutrinos from the galactic center in the light of HESS," Astrophys. J. **622**, L37 (2005) [astro-ph/0411471].

[Cro92] J. W. Cronin, Nucl. Phys. Proc. Suppl. **28B**, 213 (1992); see also http://www.auger.org/.

[Dag89] R. D. Dagkesamansky and I. M. Zheleznykh, JETP Lett. 50, 223 (1989).

[Dav88] Davis, M., Meiksin, A., Strauss, M. A., da Costa, L. N., & Yahil, A. "On the universality of the two-point galaxy correlation function," Astrophys. J. **333**, L9 (1988).

[Dig03] A. S. Dighe, M. T. Keil and G. G. Raffelt, "Detecting the neutrino mass hierarchy with a supernova at IceCube," JCAP **0306**, 005 (2003) [hep-ph/0303210].

[Dol03] K. Dolag, D. Grasso, V. Springel and I. Tkachev, "Mapping deflections of Ultra-High Energy Cosmic Rays in Constrained Simulations of Extragalactic Magnetic Fields," JETP Lett. **79**, 583 (2004) [Pisma Zh. Eksp.

Teor. Fiz. **79**, 719 (2004)] [astro-ph/0310902]; See also "Constrained simulations of the magnetic field in the local universe and the propagation of UHECRs," JCAP **0501**, 009 (2005) [astro-ph/0410419].

[Dom93] G. Domokos, B. Elliott and S. Kovesi-Domokos, "Cosmic neutrino production in the Milky Way," J. Phys. G **19**, 899 (1993).

[Dor04] I. Dorsner and A. Y. Smirnov, "Neutrino masses and mixing: Singular mass matrices and quark lepton symmetry," Nucl. Phys. B **698**, 386 (2004) [hep-ph/0403305].

[Dov03] M. T. Dova, M. E. Mancenido, A. G. Mariazzi, T. P. McCauley and A. A. Watson, "New constraints on the mass composition of cosmic rays above 10**17-eV from Volcano Ranch measurements," [astro-ph/0312463].

[DuV05] M. A. DuVernois *et al.*, "Radio Detection of UHE Neutrinos with the Antarctic Impulsive Transient Antenna (ANITA) Experiment: Data and Analysis"Proc. 29th ICRC - Pune, India (2005).

[Edg78] D. M. Edge, A. M. Pollock, R. J. Reid, A. A. Watson and J. G. Wilson, "A Study Of The Arrival Direction Distribution Of High-Energy Particles As Observed From The Northern Hemisphere," J. Phys. G **4**, 133 (1978).

[Efi91] N.N. Efimov *et al.* [Yakutsk Collaboration], "The Energy Spectrum and Anisotropy of primary cosmic rays at energy $E(0) > 10^{17}$ eV observed in Yakutsk", in Proceedings of *Astrophysical Aspects of the Most Energetic Cosmic Rays*, (World Scientific, Singapore, 1991).

[Efs88] Efstathiou, G., Ellis, R. S., & Peterson, B. S. 1988, *MNRAS*, 232, 431

[Egg03] K. Eggert, "The TOTEM/CMS forward experiment at the LHC," Nucl. Phys. Proc. Suppl. **122**, 447 (2003).

[Eig01] G. Eigen, R. Gaitskell, G. D. Kribs and K. T. Matchev, "Indirect investigations of supersymmetry," hep-ph/0112312.

[Ell00] J. R. Ellis, T. Falk, G. Ganis and K. A. Olive, "Supersymmetric dark matter in the light of LEP and the Tevatron collider," Phys. Rev. D **62**, 075010 (2000), [hep-ph/0004169].

[Eng01] R. Engel, D. Seckel and T. Stanev, "Neutrinos from propagation of ultra-high-energy protons," Phys. Rev. D **64**, 093010 (2001), [astro-ph/0101216].

[Eng05] R. Engel "Very High Energy Cosmic Rays and Their Interactions", astro-ph/0504358.

[Epe98] L. N. Epele, S. Mollerach and E. Roulet, "On the disintegration of cosmic ray nuclei by solar photons," JHEP 03 (1999) 017, [astro-ph/9812130].

[Eva03] N. W. Evans, F. Ferrer and S. Sarkar, "The clustering of ultra-high energy cosmic rays and their sources," Phys. Rev. D **67**, 103005 (2003) [astro-ph/0212533].

[Fag01] D. Fargion, "Upward and horizontal tau airshowers by UHE nu," hep-ph/0111289.

[Fal02] H. Falcke and P. Gorham, "Detecting radio emission from cosmic ray air showers and neutrinos with a digital radio telescope," Astropart. Phys. **19**, 477 (2003) [astro-ph/0207226].

[Fal04] H. Falcke, P. Gorham and R. J. Protheroe, "Prospects for radio detection of ultra-high energy cosmic rays and neutrinos," New Astron. Rev. **48**, 1487 (2004) [astro-ph/0409229].

[Fal05] H. Falcke *et al.* [The LOPES Collaboration], "Detection and imaging of atmospheric radio flashes from cosmic ray air showers," Nature **435**, 313 (2005) [astro-ph/0505383].

[Far98] G. R. Farrar and P. L. Biermann, "Correlation between compact radio quasars and ultra-high energy cosmic rays," Phys. Rev. Lett. **81**, 3579 (1998) [astro-ph/9806242].

[Far99] G. R. Farrar and P. L. Biermann, "Reply to comment on 'Correlation between compact radio quasars and ultra-high energy cosmic rays'," Phys. Rev. Lett. **83**, 2472 (1999) [astro-ph/9901315].

[Far05a] G. R. Farrar, "A cluster of ultrahigh energy cosmic rays," astro-ph/0501388.

[Far05b] G. R. Farrar, A. A. Berlind and D. W. Hogg, "Foreground and source of a cluster of ultra-high energy cosmic rays," astro-ph/0507657.

[Faz04] A. R. Fazely [The IceCube Collaboration], "IceCube: The cubic kilometer neutrino telescope at the south pole," astro-ph/0406125. See also `http://icecube.wisc.edu`

[Fen01] J. L. Feng, K. T. Matchev and F. Wilczek, "Prospects for indirect detection of neutralino dark matter," Phys. Rev. D **63**, 045024 (2001), [astro-ph/0008115].

[Fer49] E. Fermi, "On the Origin of the Cosmic Radiation" Phys. Rev. **75**, 1169 (1949).

[Fin04] C. B. Finley and S. Westerhoff, "On the evidence for clustering in the arrival directions of AGASA's ultrahigh energy cosmic rays," Astropart. Phys. **21**, 359 (2004) [astro-ph/0309159].

[Fin05] C. B. Finley and S. Westerhoff [HiRes Collaboration], "Search for cross-correlations of ultra-high-energy cosmic rays with BL Lacertae objects," astro-ph/0507465.

[Fis95] K.B. Fisher *et al.*, "The IRAS 1.2 Jy Survey: Redshift Data", Astrophys. J. Suppl. **100**, 69 (1995).

[Fog05] G. L. Fogli, E. Lisi, A. Marrone and A. Palazzo, "Global analysis of three-flavor neutrino masses and mixings," hep-ph/0506083.

[Fri00] P. Frick, R. Stepanov, A. Shukurov and D. Sokoloff, "Structures in the RM sky," *MNRAS* **325**, 649 (2001) [astro-ph/0012459].

[Gai90] T.K. Gaisser, "Cosmic Rays and Particle Physics," Cambridge University Press (1990).

[Gai95] T. K. Gaisser, F. Halzen and T. Stanev, "Particle astrophysics with high-energy neutrinos," Phys. Rept. **258**, 173 (1995) [Erratum-ibid. **271**, 355 (1996)] [hep-ph/9410384].

[Gan96] R. Gandhi, C. Quigg, M. H. Reno and I. Sarcevic, "Detecting neutrinos from AGNs and topological defects with neutrino telescopes," hep-ph/9609516.

[Gan98] R. Gandhi, C. Quigg, M. H. Reno and I. Sarcevic, "Neutrino interactions at ultrahigh energies," Phys. Rev. D **58**, 093009 (1998) [hep-ph/9807264].

[Ger60] N.M. Gerasimova and G.T. Zatsepin, Sov.Phys. JETP 11, 899 (1960)

[Gob02] D. S. Gorbunov, P. G. Tinyakov, I. Tkachev and S. V. Troitsky, "Evidence for a connection between γ-ray and highest-energy cosmic ray emissions by BL Lacs," Astrophys. J. **577**, L93 (2002) [astro-ph/0204360].

[Gob04] D. S. Gorbunov, P. G. Tinyakov, I. I. Tkachev and S. V. Troitsky, "Testing the correlations between ultra-high-energy cosmic rays and BL Lac type objects with HiRes stereoscopic data," JETP Lett. **80**, 145 (2004) [Pisma Zh. Eksp. Teor. Fiz. **80**, 167 (2004)] [astro-ph/0406654].

[Gol00] H. Goldberg and T. J. Weiler, "Directional clustering in highest energy cosmic rays," Phys. Rev. D **64**, 056008 (2001) [astro-ph/0009378].

[Gon99] P. Gondolo and J. Silk, "Dark matter annihilation at the galactic center," Phys. Rev. Lett. **83**, 1719 (1999) [astro-ph/9906391].

[Gor00] P. W. Gorham, "On the possibility of radar echo detection of ultra-high energy cosmic ray and neutrino induced extensive air showers," Astropart. Phys. **15**, 177 (2001) [hep-ex/0001041].

[Gor01] P. Gorham, D. Saltzberg, A. Odian, D. Williams, D. Besson, G. Frichter and S. Tantawi, "Measurements of the suitability of large rock salt formations for radio detection of high energy neutrinos," Nucl. Instrum. Meth. A **490**, 476 (2002) [hep-ex/0108027].

[Gor03] P. W. Gorham, C. L. Hebert, K. M. Liewer, C. J. Naudet, D. Saltzberg and D. Williams, "Experimental Limit on the Cosmic Diffuse Ultra-high Energy Neutrino Flux," Phys. Rev. Lett. **93**, 041101 (2004) [astro-ph/0310232].

[Gor04] P. W. Gorham *et al.*, "Accelerator measurements of the Askaryan effect in rock salt: A roadmap toward Teraton underground neutrino detectors," Phys. Rev. D **72**, 023002 (2005) [astro-ph/0412128].

[Goz05] M. C. Gonzalez-Garcia, F. Halzen and M. Maltoni, "Physics reach of high-energy and high-statistics Icecube atmospheric neutrino data," Phys. Rev. D **71**, 093010 (2005) [hep-ph/0502223].

[Gre56] K. Greisen, Progr. Cosmic Rays 3 (1956), 1.

[Gre66] K. Greisen, "End To The Cosmic Ray Spectrum?," Phys. Rev. Lett. **16**, 748 (1966).

[Gri01] P. K. F. Grieder [NESTOR Collaboration], "The NESTOR neutrino telescope," Nuovo Cim. **24C**, 771 (2001). G. Aggouras *et al.*, "A measurement of the cosmic-ray muon flux with a module of the NESTOR neutrino telescope," Astropart. Phys. **23**, 377 (2005).

[Had05] S. Hannestad and G. Raffelt, "Constraining invisible neutrino decays with the cosmic microwave background," Phys. Rev. D **72**, 103514, (2005) [hep-ph/0509278].

[Hal90] F. Halzen, J.G. Learned, T. Stanev, "Astrophys. in Antarctica", Bartol, AIP Conf. Proc. 198:39. New York: AIP (1990)

[Hal95] F. Halzen, B. Keszthelyi and E. Zas, "Neutrinos from primordial black holes," Phys. Rev. D **52**, 3239 (1995), [hep-ph/9502268].

[Hal98] F. Halzen and D. Saltzberg, "Tau neutrino appearance with a 1000-Megaparsec baseline," Phys. Rev. Lett. **81**, 4305 (1998) [hep-ph/9804354].

[Hal02] F. Halzen and D. Hooper, "High-energy neutrino astronomy: The cosmic ray connection," Rept. Prog. Phys. **65**, 1025 (2002) [astro-ph/0204527].

[Han94] J. L. Han and G. J. Qiao, "The magnetic field in the disk of our Galaxy,", Astron. Astrophys. **288**, 759 (1994).

[Han97] J. L. Han, R. N. Manchester, E. M. Berkhuijsen, R. Beck, "Antisymmetric rotation measures in our Galaxy: evidence for an A0 dynamo," Astron. Astrophys. **322**, 98 (1997).

[Han99] J. L. Han, R. N. Manchester, G. J. Qiao, "Pulsar rotation measures and the magnetic structure of our Galaxy," *MNRAS* **306**, 371 (1999).

[Han01] J. Han, "Magnetic fields in our Galaxy: How much do we know? (II) Halo fields and the global field structure," in "Astrophysical Polarized Backgrounds", American Institute of Physics, edited by S. Cecchini *et al.*, p. 96 (2002) [astro-ph/0110319].

[Han02] J. L. Han, R. N. Manchester, G. J. Qiao and A. G. Lyne, "The large-scale Galactic magnetic field structure and pulsar rotation measures," in "Radio Pulsars", [astro-ph/0211197].

[Har99] D. Harari, S. Mollerach and E. Roulet, "The toes of the ultra high energy cosmic ray spectrum," JHEP **9908**, 022 (1999) [astro-ph/9906309].

[Har00] D. Harari, S. Mollerach and E. Roulet, "Signatures of galactic magnetic lensing upon ultra high energy cosmic rays," JHEP **0002**, 035 (2000) [astro-ph/0001084].

[Har02a] D. Harari, S. Mollerach, E. Roulet and F. Sanchez, "Lensing of ultra-high energy cosmic rays in turbulent magnetic fields," JHEP **0203** (2002) 045 [astro-ph/0202362].

[Har02b] D. Harari, S. Mollerach and E. Roulet, "Astrophysical magnetic field reconstruction and spectroscopy with ultra high energy cosmic rays," JHEP **0207** (2002) 006 [astro-ph/0205484].

[Has03] M. M. Hanson, "A Study of Cyg OB2: Pointing the Way Towards Finding Our Galaxy's Super Star Clusters," Astrophys. J. **597**, 957 (2003) [astro-ph/0307540].

[Haw74] S. W. Hawking, "Black Hole Explosions," Nature **248**, 30 (1974).

[Hay96] N. Hayashida *et al.*, "Possible Clustering Of The Most Energetic Cosmic Rays Within a Limited Space Angle Observed By The Akeno Giant Air Shower Array," Phys. Rev. Lett. **77**, 1000 (1996).

[Hay98] N. Hayashida *et al.* [AGASA Collaboration], "The anisotropy of cosmic ray arrival directions around 10^{18} eV," Astropart. Phys. **10**, 303 (1999) [astro-ph/9807045].

[Hay00] N. Hayashida *et. al.* [AGASA Collaboration], "Updated AGASA event list above 4*10**19-eV," astro-ph/0008102.

[Hei84] W. Heitler, "The Quantum Theory of Radiation", Dover New York, 1984.

[Het99] C. Hettlage, K. Mannheim and J. G. Learned, "The sun as a high energy neutrino source," Astropart. Phys. **13**, 45 (2000) [astro-ph/9910208].

[Hil84] A.M. Hillas, Ann. Rev. Astron. Astrophys. **22**, 425 (1984).

[Hit49] W. A. Hiltner, "On the Presence of Polarization in the Continuous Radiation of Stars. II," Astrophys. J. **109**, 471 (1949).

[Hof99] C. M. Hoffman, "Comment on 'Correlation between compact radio quasars and ultrahigh energy cosmic rays'," Phys. Rev. Lett. **83**, 2471 (1999) [astro-ph/9901026].

[Hoo04a] D. Hooper, A. Taylor and S. Sarkar, "The impact of heavy nuclei on the cosmogenic neutrino flux," Astropart. Phys. **23**, 11 (2005) [astro-ph/0407618].

[Hoo04b] D. Hooper, D. Morgan and E. Winstanley, "Probing quantum decoherence with high-energy neutrinos," Phys. Lett. B **609**, 206 (2005) [hep-ph/0410094].

[Hou02] G.W.S. Hou and M.A. Huang, "Expected performance of a neutrino telescope for seeing AGN/GC behind a mountain," astro-ph/0204145.

[Hub04] P. Huber, M. Lindner, M. Rolinec, T. Schwetz and W. Winter, "Prospects of accelerator and reactor neutrino oscillation experiments for the coming ten years," Phys. Rev. D **70**, 073014 (2004) [hep-ph/0403068].

[Ice05] IceCube Collaboration, "The IceCube collaboration: Contributions to the 29th international cosmic ray conference (ICRC 2005), Pune, India, Aug. 2005," astro-ph/0509330.

[Ing96a] G. Ingelman and M. Thunman, "Particle Production in the Interstellar Medium," hep-ph/9604286.

[Ing96b] G. Ingelman and M. Thunman, "High Energy Neutrino Production by Cosmic Ray Interactions in the Sun," Phys. Rev. D **54**, 4385 (1996) [hep-ph/9604288].

[Jar00] T.H. Jarrett *et al.*, "2MASS Extended Source Catalog: Overview and Algorithms," Astron. J., **119**, 2498 (2000).

[Jar04] T.H. Jarrett, "Large Scale Structure in the Local Universe: The 2MASS Galaxy Catalog," Publ. Astron. Soc. Aust., **21**, 396 (2004) [astro-ph/0405069].

[Joh38] Th. H. Johnson,"Cosmic-Ray Intensity and Geomagnetic Effects," Rev. Mod. Phys. **10**, 193 (1938).

[Jun96] G. Jungman, M. Kamionkowski and K. Griest, "Supersymmetric dark matter," Phys. Rept. **267**, 195 (1996) [hep-ph/9506380].

[Kac04a] M. Kachelrieß and D. Semikoz, "Ultra-high energy cosmic rays from a finite number of point sources," Astropart. Phys. **23**, 486 (2005) [astro-ph/0405258].

[Kac04b] M. Kachelrieß, "Status of particle physics solutions to the UHECR puzzle," Comptes Rendus Physique **5**, 441 (2004) [hep-ph/0406174].

[Kac05] M. Kachelrieß, P. D. Serpico and M. Teshima, "The Galactic magnetic field as spectrograph for ultra-high energy cosmic rays," astro-ph/0510444.

[Kag05] T. Karg *et al.* [ANTARES Collaboration], "Development of acoustic devices for ultra-high energy neutrino detectors," astro-ph/0509455.

[Kah05] K. Kasahara *et al.* [TA Collaboration], "The Current Status and Prospect of the TA Experiment," astro-ph/0511177.

[Kar71] S. Karakula, J. .L. Osborne, E. Roberts and W. Tkaczyk, "The Galactic Magnetic Field and Anisotropy of Cosmic Rays above 1017 eV," Proc. 12th ICRC - Hobart, Australia, **1**, 310 (1971).

[Kas05] T. Kashti and E. Waxman, "Astrophysical Neutrinos: Flavor Ratios Depend on Energy," Phys. Rev. Lett. **95**, 181101 (2005) [astro-ph/0507599].

[Kat06] U. F. Katz, "Neutrino telescopy in the Mediterranean sea," astro-ph/0601012. See also the URL: `http://www.km3net.org/`.

[Kna96] J. Knapp, D. Heck and G. Schatz, "Comparison of hadronic interaction models used in air shower simulations and of their influence on shower development and observables," FZKA-5828.

[Kna97] J. Knapp, D. Heck and G. Schatz, "Comparison Of Hadronic Interaction Models Used In Eas Simulations," Nucl. Phys. Proc. Suppl. **52B** (1997) 136.

[Kno00] J. Knodlseder, "Cygnus OB2 - a young globular cluster in the Milky Way," Astron. Astrophys., **360**, 539 [astro-ph/0007442].

[Kno01] J. Knodlseder, M. Cervino, D. Schaerer, P. von Ballmoos and G. Meynet, "The Cygnus X region: a nucleosynthesis laboratory for INTEGRAL," astro-ph/0104074, proceedings of the 4th INTEGRAL workshop (Alicante).

[Kra01] I. Kravchenko *et al.* [RICE Collaboration], "Performance and simulation of the RICE detector," Astropart. Phys. **19**, 15 (2003) [astro-ph/0112372].

[Kro99] Julian H. Krolik, "Active Galactic Nuclei", Princeton University Press (1999).

[Kuo89] T. K. Kuo and J. T. Pantaleone, "Neutrino Oscillations In Matter," Rev. Mod. Phys. **61**, 937 (1989).

[Kus00] A. Kusenko and M. Postma, "Neutrinos produced by ultrahigh-energy photons at high red shift," Phys. Rev. Lett. **86**, 1430 (2001) [hep-ph/0007246].

[Lah05] R. Lahmann *et al.*, "Integration of Acoustic Detection Equipment into ANTARES," astro-ph/0511834.

[LaR05] T. N. LaRosa *et al.*, C. L. Brogan, S. N. Shore, T. J. Lazio, N. E. Kassim and M. E. Nord, "Evidence for a Weak Galactic Center Magnetic Field from Diffuse Low Frequency Nonthermal Radio Emission," Astrophys. J. **626**, L23 (2005) [astro-ph/0505244].

[Law91] M. A. Lawrence, R. J. O. Reid and A. A. Watson [Haverah Park Collaboration], "The Cosmic ray energy spectrum above 4x10**17 eV as measured by the Haverah Park array," J. Phys. G **17**, 733 (1991).

[Lea78] J. G. Learned, "Acoustic Radiation By Charged Atomic Particles In Liquids: An Analysis," Phys. Rev. D **19**, 3293 (1979).

[Lea00] J. G. Learned and K. Mannheim, "High-energy neutrino astrophysics," Ann. Rev. Nucl. Part. Sci. **50**, 679 (2000).

[Leh01] N. G. Lehtinen, S. Adam, G. Gratta, T. K. Berger and M. J. Buckingham, "Sensitivity of an underwater acoustic array to ultra-high energy neutrinos," Astropart. Phys. **17**, 279 (2002) [astro-ph/0104033].

[Leh03] N. G. Lehtinen, P. W. Gorham, A. R. Jacobson and R. A. Roussel-Dupre, "FORTE satellite constraints on ultra-high energy cosmic particle fluxes," Phys. Rev. D **69**, 013008 (2004) [astro-ph/0309656].

[Lem33] G. Lemaitre and M. S. Vallarta, "On Compton's Latitude Effect of Cosmic Radiation," Phys. Rev. **43**, 87 (1933).

[Let05] A. Letessier-Selvon [Pierre Auger Collaboration], "Anisotropy studies around the galactic center at EeV energies with Auger data," Proc. 29th ICRC - Pune, India (2005) [astro-ph/0507331]

[Lin63] Linsley, "Evidence for a Primary Cosmic-Ray Particle with Energy 10**20 eV", Phys. Rev. Lett. **10**, 146 (1963).

[Lin75] J. Linsley, "Fluctuation effects on directional data," Phys. Rev. Lett. **34**, 1530 (1975).

[Lin80] J. Linsley, *Catalog of Highest Energy Cosmic Ray,* (World Data Center of Cosmic Rays, Institute of Physical and Chemical Research, Itabashi, Tokyo) p.3, (1980).

[Lin81] J. Linsley and A. A. Watson, "Validity Of Scaling To 10**20-Ev And High-Energy Cosmic Ray Composition," Phys. Rev. Lett. **46**, 459 (1981).

[Man01] K. Mannheim, R. J. Protheroe and J. P. Rachen, "On the cosmic ray bound for models of extragalactic neutrino production," Phys. Rev. D **63**, 023003 (2001) [astro-ph/9812398].

[Mar86] M. Markov and I. Zheleznykh, Nucl. Instrum. Meth. A **248**, 242 (1986).

[Mau02] D. Maurin, R. Taillet, F. Donato, P. Salati, A. Barrau and G. Boudoul, "Galactic cosmic ray nuclei as a tool for astroparticle physics," astro-ph/0212111.

[McD03] A. B. McDonald, C. Spiering, S. Schonert, E. T. Kearns and T. Kajita, "Astrophysical neutrino telescopes," Rev. Sci. Instrum. **75**, 293 (2004) [astro-ph/0311343].

[Med97] G. A. Medina-Tanco, E. M. de Gouveia Dal Pino and J. E. Horvath, "Deflection of ultra high energy cosmic rays by the galactic magnetic field: From the sources to the detector," Astrophys. J. **492**, 200 (1998) [astro-ph/9707041].

[Med98] G. A. Medina-Tanco and A. A. Watson, "The photodisintegration of cosmic ray nuclei by solar photons: The Gerasimova-Zatsepin effect revisited," Astropart. Phys. **10** (1999) 157 [astro-ph/9808033].

[Med03] G. Medina-Tanco, M. Teshima, and M. Takeda, "Constrains on the Galactic Magnetic Field from the Two-Dimensional Correlation Function of AGASA Events", Proc. 28th ICRC - Tsukuba, Japan (2003).

[Mie05] G. Miele, S. Pastor, and O. Pisanti, "The aperture for UHE tau neutrinos of the Auger fluorescence detector using a Digital Elevation Map," astro-ph/0508038.

[Mon02] T. Montaruli [ANTARES Collaboration], "Status report of the ANTARES project," Nucl. Phys. Proc. Suppl. **110**, 513 (2002) [hep-ex/0201009].

[Nag00] M. Nagano and A. A. Watson, "Observations and implications of the ultrahigh-energy cosmic rays," Rev. Mod. Phys. **72**, 689 (2000).

[Nah05] R. Nahnhauer *et al.* "Acoustic Sensor and Transmitter Development for a Large Volume Neutrino Detection Array in Ice", Proc. 29th ICRC - Pune, India (2005).

[Nel92] L. Nellen, K. Mannheim and P. L. Biermann, "Neutrino production through hadronic cascades in AGN accretion disks," Phys. Rev. D **47**, 5270 (1993) [hep-ph/9211257].

[Ner02] A. Y. Neronov and D. V. Semikoz, "Which blazars are neutrino loud?," Phys. Rev. D **66**, 123003 (2002) [hep-ph/0208248].

[Nie05] V. Niess and V. Bertin, "Underwater acoustic detection of ultra high energy neutrinos," astro-ph/0511617.

[Pal05] S. Palomares-Ruiz, A. Irimia and T. J. Weiler, "Acceptances for Space-Based and Ground-Based Fluorescence Detectors, and Inference of the Neutrino-Nucleon Cross Section above $10^{1}9$ eV," astro-ph/0512231.

[PDG04] S. Eidelman *et al.* [Particle Data Group], Phys. Lett. **B592**, 1 (2004).

[Pee80] Peebles, P. J. E. 1980, "The Large-Scale Structure of the Universe" (Princeton, NJ: Princeton University Press)

[Pes04] H. Pessard [OPERA Collaboration], "The OPERA experiment," hep-ex/0504033.

[Pet97] Bradley M. Peterson, "An Introduction to Active Galactic Nuclei", Cambridge University Press, (1997).

[Pos01] M. Postma, "Neutrinos as a signature of ultrahigh energy photons at high red shift," Phys. Rev. D **64**, 023001 (2001) [hep-ph/0102106].

[Pri05] B. Price, submitted to J. Geophys. Res., Earth Surfaces.

[Pro92] R. J. Protheroe and A. P. Szabo, "High-energy cosmic rays from active galactic nuclei," Phys. Rev. Lett. **69**, 2885 (1992).

[Pro96] R. J. Protheroe, "High energy neutrinos from blazars," astro-ph/9607165.

[Prz03] M. Prouza and R. Smida, "The Galactic magnetic field and propagation of ultra-high energy cosmic rays," Astron. Astrophys. **410**, 1 (2003) [astro-ph/0307165].

[Rac93] J. P. Rachen and P. L. Biermann, "Extragalactic ultrahigh-energy cosmic rays. 1. Contribution from hot spots in FR-II radio galaxies," Astron. Astrophys. **272**, 161 (1993) [astro-ph/9301010].

[Rac96] Jörg-Paul Rachen, "Interaction Processes and Statistical Properties of the Propagation of Cosmic Rays in Photon Backgrounds", PhD dissertation, University of Bonn 1996.

[Rac98] J. P. Rachen and P. Meszaros, "Photohadronic neutrinos from transients in astrophysical sources," Phys. Rev. D **58**, 123005 (1998) [astro-ph/9802280].

[Raf02] G. G. Raffelt, "Physics with supernovae," Nucl. Phys. Proc. Suppl. **110**, 254 (2002) [hep-ph/0201099].

[Raf05] G. G. Raffelt, "Supernova neutrino oscillations," hep-ph/0501049.

[Ran94] R. J. Rand and A. G. Lyne, "New Rotation Measures of Distant Pulsars in the Inner Galaxy and Magnetic Field Reversals," *MNRAS* **268**, 497 (1994).

[Raz05] S. Razzaque, P. Meszaros and E. Waxman, "Enhancement of the anti-nu/e flux from astrophysical sources by two photon annihilation interactions," astro-ph/0509186.

[Rev05] B. Revenu [Pierre Auger Collaboration], "Search for localized excess fluxes in Auger sky maps and prescription results," Proc. 29$^{\text{th}}$ ICRC - Pune, India (2005) [astro-ph/0507600].

[Rew04] For a review of the current status of neutrino oscillations see e.g. the focus issue New J. Phys. **6** (2004) or the Proceedings of "21st Inter. Conf. on Neutrino Physics and Astrophysics (Neutrino 2004)," Nucl. Phys. B (Proc. Suppl.) **143**, 3 (2005).

[Ris05] M. Risse [Pierre Auger Collaboration], "Upper limit on the primary photon fraction from the Pierre Auger observatory," astro-ph/0507402.

[Ros34] B. Rossi "Directional Measurements on the Cosmic Rays Near the Geomagnetic Equator", Phys. Rev. **45**, 212 (1934).

[Rou03] E. Roulet, "Astroparticle theory: Some new insights into high energy cosmic rays," Int. J. Mod. Phys. A **19**, 1133 (2004) [astro-ph/0310367].

[Roy04] S. Roy, "The Galactic Centre region," Bull. Astron. Soc. India **32**, 205 (2004) [astro-ph/0411687].

[Sak05] T. Sako *et al.*, Proc. 29$^{\text{th}}$ ICRC - Pune, India (2005).

[Sal01] D. Saltzberg *et al.*, "Observation of the Askaryan effect: Coherent microwave Cherenkov emission from charge asymmetry in high energy particle cascades," Phys. Rev. Lett. **86**, 2802 (2001) [hep-ex/0011001].

[San79] Sandage, A., Tammann, G. A., & Yahil, A. (1979), "STY luminosity function fitting method", Astrophys. J. **232**, 352.

[Sap05] P. Sapienza, "A km^3 detector in the Mediterranean: Status of NEMO," Nucl. Phys. Proc. Suppl. **145**, 331 (2005).

[Sar01] S. Sarkar and R. Toldra, "The high-energy cosmic ray spectrum from massive particle decay," Nucl. Phys. B **621**, 495 (2002), [hep-ph/0108098].

[Sas02] M. Sasaki and M. Jobashi, "Detecting very high energy neutrinos by the Telescope Array," Astropart. Phys. **19**, 37 (2003) [astro-ph/0204167].

[Sau00] W. Saunders *et al.*, "The PSCz Catalogue," *MNRAS* **317**, 55 (2000) [astro-ph/0001117].

[Sec91] D Seckel, T Stanev, and T K Gaisser, "Signatures of cosmic-ray interactions on the solar surface," Astrophys. J. **382** (1991) 652

[Sec05] D. Seckel and T. Stanev, "Neutrinos: The key to UHE cosmic rays," Phys. Rev. Lett. **95**, 141101 (2005) [astro-ph/0502244].

[She04] J.V. Shebalin "Størmer regions for axisymmetric magnetic multipole fields", Physics of Plasmas, **11**, (2004) 3472.

[Shi03] K. Shinozaki *et al.* [AGASA Collaboration], "Chemical composition of ultra-high energy cosmic rays observed by AGASA," Proc. 28th International Cosmic Ray Conference, Tsukuba, 401 (2003).

[Sig00] G. Sigl, D. F. Torres, L. A. Anchordoqui and G. E. Romero, "Testing the correlation of ultra-high energy cosmic rays with high redshift sources," Phys. Rev. D **63**, 081302 (2001) [astro-ph/0008363].

[Sig04] G. Sigl, F. Miniati and T. A. Ensslin, "Ultra-high energy cosmic ray probes of large scale structure and magnetic fields," Phys. Rev. D **70**, 043007 (2004) [astro-ph/0401084]. See also "Cosmic magnetic fields and their influence on ultra-high energy cosmic ray propagation," Nucl. Phys. Proc. Suppl. **136**, 224 (2004) [astro-ph/0409098].

[Sil04] A. Silvestri *et al.* [The ANITA Collaboration], "Status of ANITA and ANITA-lite," astro-ph/0411007.

[Sin03] S. Singh, C. P. Ma and J. Arons, "Gamma-ray bursts and magnetars as possible sources of ultra high energy cosmic rays: Correlation of cosmic ray event positions with IRAS galaxies," Phys. Rev. D **69**, 063003 (2004) [astro-ph/0308257].

[SKA04] "Science with the Square Kilometre Array", eds. C. Carilli, S. Rawlings, New Astronomy Reviews, Vol.48, Elsevier, December 2004. See also the URL http://www.skatelescope.org/.

[Smi02] A. Smialkowski, M. Giller and W. Michalak, "Luminous infrared galaxies as possible sources of the UHE cosmic rays," J. Phys. G **28**, 1359 (2002) [astro-ph/0203337].

[Sok04] P. Sokolosky, "Introduction to Ultrahigh Energy Cosmic Ray Physics," Westview Press (2004).

[Sol92] D. Sokolov, A. Shukurov and M. Krause, "Pattern recognition of the regular magnetic field in disks of spiral galaxies," Astron. Astrophys. **264**, 396 (1992).

[Som00] P. Sommers, "Cosmic Ray Anisotropy Analysis with a Full-Sky Observatory," Astropart. Phys. **14**, 271 (2001) [astro-ph/0004016].

[Som04] P. Sommers, "Extensive air showers and measurement techniques," Comptes Rendus Physique **5**, 463 (2004).

[Spe03] D. N. Spergel *et al.* [WMAP Collaboration], "First Year Wilkinson Microwave Anisotropy Probe (WMAP) observations: Determination of cosmological parameters," Astrophys. J. Suppl. **148**, 175 (2003) [astro-ph/0302209].

[Spi02] C. Spiering, "High energy neutrino astronomy," Prog. Part. Nucl. Phys. **48**, 43 (2002).

[Sri05] L. E. Strigari, J. F. Beacom, T. P. Walker and P. Zhang, "The concordance cosmic star formation rate: Implications from and for the supernova neutrino and gamma ray backgrounds," JCAP **0504**, 017 (2005) [astro-ph/0502150].

[Sta95] T. Stanev, P. Biermann, J. Lloyd-Evans, J. P. Rachen and A. A. Watson, "The Arrival directions of the most energetic cosmic rays," Phys. Rev. Lett. **75**, 3056 (1995) [astro-ph/9505093].

[Sta97] T. Stanev, "Ultra–High-Energy Cosmic Rays and the Large-Scale Structure of the Galactic Magnetic Field," Astrophys. J. **479**, 290 (1997).

[Sta04] T. Stanev, "High Energy Cosmic Rays," Springer Praxis Books / Astrophysics and Astronomy (2004).

[Sta05] T. Stanev, "High energy neutrinos: Sources and fluxes," astro-ph/0511641.

[Ste79] F. W. Stecker, "Diffuse Fluxes Of Cosmic High-energy Neutrinos," Astrophys. J. **228**, 919 (1979).

[Ste91] F. W. Stecker, C. Done, M. H. Salamon and P. Sommers, "High-energy neutrinos from active galactic nuclei," Phys. Rev. Lett. **66**, 2697 (1991) [Erratum-ibid. **69**, 2738 (1992)].

[Ste05] F. W. Stecker and S. T. Scully, "Lorentz invariance violation and the spectrum and source power of ultrahigh energy cosmic rays," Astropart. Phys. **23**, 203 (2005) [astro-ph/0412495].

[Stø55] C. Stoermer, "The Polar Aurora", Oxford University Press, New York, 1955.

[Stp01] R. Stepanov, P. Frick, A. Shukurov and D. Sokoloff, "Wavelet tomography of the Galactic magnetic field. I. The method," Astron. Astrophys. **391** 361 (2002) [astro-ph/0112507].

[Str04] A. W. Strong, I. V. Moskalenko and O. Reimer, "A new determination of the extragalactic diffuse gamma-ray background from EGRET data," Astrophys. J. **613**, 956 (2004) [astro-ph/0405441].

[Swa33] W. F. G. Swann, "Application of Liouville's Theorem to Electron Orbits in the Earth's Magnetic Field" Phys. Rev. **44**, 224 (1933).

[Swo97] J. Cronin, T.K. Gaisser, and S.P. Swordy, Sci. Amer. **276**, 44 (1997). See also http://astroparticle.uchicago.edu/announce.htm

[Sza94] A. P. Szabo and R. J. Protheroe, "Implications of particle acceleration in active galactic nuclei for cosmic rays and high-energy neutrino astronomy," Astropart. Phys. **2**, 375 (1994) [astro-ph/9405020].

[Tak98] M. Takeda *et al.* [AGASA Collaboration], "Extension of the cosmic-ray energy spectrum beyond the predicted Greisen-Zatsepin-Kuzmin cutoff," Phys. Rev. Lett. **81**, 1163 (1998) [astro-ph/9807193].

[Tak99] M. Takeda *et al.*, "Small-scale anisotropy of cosmic rays above 10**19-eV observed with the Akeno Giant Air Shower Array," Astrophys. J. **522**, 225 (1999) [astro-ph/9902239].

[Tam05] H. Takami, H. Yoshiguchi and K. Sato, "Propagation of ultra-high energy cosmic rays above 10**19-eV in a structured extragalactic magnetic field and galactic magnetic field," Astrophys. J., in press [astro-ph/0506203].

[Teg03] M. Tegmark *et al.* [SDSS Collaboration], "The 3D power spectrum of galaxies from the SDSS," Astrophys. J. **606**, 702 (2004) [astro-ph/0310725].

[Tes01] M. Teshima *et al.*, Proc. 27th ICRC - Hamburg, Germany (2001), 341.

[Tin01a] P. G. Tinyakov and I. I. Tkachev, "Correlation function of ultra-high energy cosmic rays favors point sources," JETP Lett. **74**, 1 (2001) [Pisma Zh. Eksp. Teor. Fiz. **74**, 3 (2001)] [astro-ph/0102101].

[Tin01b] P. G. Tinyakov and I. Tkachev I., "BL Lacertae are sources of the observed ultra-high energy cosmic rays," JETP Lett. **74**, 445 (2001) [Pisma Zh. Eksp. Teor. Fiz. **74**, 499 (2001)] [astro-ph/0102476].

[Tin01c] P. G. Tinyakov and I. Tkachev I., "Tracing protons through the Galactic magnetic field: a clue for charge composition of ultra-high energy cosmic rays," Astropart. Phys. **18**, 165 (2002) [astro-ph/0111305].

[Tin03] P. G. Tinyakov and I. Tkachev I., "Cuts and penalties: comment on "The clustering of ultra-high energy cosmic rays and their sources"," Phys. Rev. D **69**, 128301 (2004) [astro-ph/0301336].

[Tin04] P. G. Tinyakov and I. I. Tkachev, "Deflections of cosmic rays in a random component of the galactic magnetic field," Astropart. Phys. **24**, 32 (2005) [astro-ph/0411669].

[Tor03a] D. F. Torres, S. Reucroft, O. Reimer and L. A. Anchordoqui, "On the cross-correlation between the arrival direction of ultra-high energy cosmic rays, BL Lacertae, and EGRET detections: A new way to identify EGRET sources," Astrophys. J. **595**, L13 (2003) [astro-ph/0307079].

[Tor03b] D. F. Torres, E. Domingo-Santamaria and G. E. Romero, "High-energy γ-rays from stellar associations," Astrophys. J. **601**, L75 (2004) [astro-ph/0312128].

[Tor04] D. F. Torres and L. A. Anchordoqui, "Astrophysical origins of ultrahigh energy cosmic rays," Rept. Prog. Phys. **67**, 1663 (2004) [astro-ph/0402371].

[Tro05] S. V. Troitsky, "Magnetic deflections and possible sources of the ultra-high-energy cosmic rays in the AGASA-HiRes-Yakutsk cluster," astro-ph/0505262.

[Uch99] Y. Uchihori, M. Nagano, M. Takeda, M. Teshima, J. Lloyd-Evans and A. A. Watson, "Cluster analysis of extremely high energy cosmic rays in the northern sky," Astropart. Phys. **13**, 151 (2000) [astro-ph/9908193].

[Vad05] J. Vandenbroucke, G. Gratta and N. Lehtinen, "Experimental study of acoustic ultra-high-energy neutrino detection," Astrophys. J. **621**, 301 (2005) [astro-ph/0406105].

[Ver00] M. P. Veron-Cetty and P. Veron, "A catalogue of Quasars and Active Galactic Nuclei, 9th Edition," ESO Scientific Report (2000).

[Ver03] M.-P. Véron-Cetty and P. Véron, "A catalogue of quasars and active nuclei: 11th edition", Astron. Astrophys. **412**, 399 (2003). The catalogue is available on-line at `http://www.obs-hp.fr/www/catalogues/veron2_11/veron2_11.html`

[Vie98] M. Vietri, "Ultra high-energy neutrinos from gamma ray bursts," Phys. Rev. Lett. **80**, 3690 (1998), [astro-ph/9802241].

[Vir02] A. Virmani, S. Bhattacharya, P. Jain, S. Razzaque, J. P. Ralston and D. W. McKay, "Correlation Of Ultra High Energy Cosmic Rays With Compact Radio Loud Quasars," Astropart. Phys. **17**, 489 (2002) [astro-ph/0010235].

[Wai92] R. J. Wainscoat *et al.*, "A model of the 8-25 micron point source infrared sky," Astrophys. J. Suppl. **83**, 111 (1992).

[Wat04] A. A. Watson, "The mass composition of cosmic rays above 10**17 eV," Nucl. Phys. Proc. Suppl. **136**, 290 (2004) [astro-ph/0408110].

[Wax96] E. Waxman, K. B. Fisher and T. Piran, "The signature of a correlation between > 10**19-eV cosmic ray sources and large scale structure," Astrophys. J. **483**, 1 (1997) [astro-ph/9604005].

[Wax97] E. Waxman and J. N. Bahcall, "High energy neutrinos from cosmological gamma-ray burst fireballs," Phys. Rev. Lett. **78**, 2292 (1997), [astro-ph/9701231].

[Wax98] E. Waxman and J. N. Bahcall, "High energy neutrinos from astrophysical sources: An upper bound," Phys. Rev. D **59**, 023002 (1999) [hep-ph/9807282].

[Wax03] E. Waxman, "Gamma-ray bursts: The underlying model," Lect. Notes Phys. **598**, 393 (2003) [astro-ph/0303517].

[Wdo84] J. Wdowczyk and A. W. Wolfendale, "Galactic Cosmic Rays Above 10**18 eV," J. Phys. G **10**, 1453 (1984).

[Win86a] M. M. Winn *et al.*[SUGAR Collaboration], "The Cosmic Ray Energy Spectrum Above 10**17 eV," J. Phys. G **12**, 653 (1986).

[Win86b] M. M. Winn, J. Ulrichs, L. S. Peak, C. B. Mccusker and L. Horton, "The Arrival Directions Of Cosmic Rays Above 10**17-Ev," J. Phys. G **12**, 675 (1986).

[Yor00] D. York *et al.* "The Sloan Digital Sky Survey: Technical Summary" Astron. J., **120**, 1579 (2000).

[Yos01] S. Yoshida *et al.*, "A search for horizontal air showers induced by extremely high energy cosmic neutrinos observed by Akeno Giant Air Shower Array," Proc. 27$^{\text{th}}$ ICRC - Hamburg, Germany (2001), 1142.

[Yos03] H. Yoshiguchi, S. Nagataki and K. Sato, "A new method for calculating arrival distribution of ultra-high energy cosmic rays above 10**19-eV with modifications by the galactic magnetic field," Astrophys. J. **596**, 1044 (2003) [astro-ph/0307038].

[Yos04a] H. Yoshiguchi, S. Nagataki and K. Sato, "Numerical study on the propagation of ultra-high-energy cosmic rays in the galactic magnetic field," Astrophys. J. **607** (2004) 840.

[Yos04b] H. Yoshiguchi, S. Nagataki and K. Sato, "Statistical significance of small scale anisotropy in arrival directions of ultra-high energy cosmic rays," Astrophys. J. **614**, 43 (2004) [astro-ph/0404411].

[Zas92] E. Zas, F. Halzen and T. Stanev, "Electromagnetic pulses from high-energy showers: Implications for neutrino detection," Phys. Rev. D **45**, 362 (1992).

[Zas04] E. Zas [Auger Collaboration], "The Auger Observatory: Status and potential for neutrino detection," Nucl. Phys. Proc. Suppl. **143**, 373 (2005).

[Zas05] E. Zas, "Neutrino detection with inclined air showers," New J. Phys. **7**, 130 (2005) [astro-ph/0504610].

[Zat51] G.T. Zatsepin, Dokl.Akad.Nauk Ser.Fiz. 80, 577 (1951)

[Zat66] G. T. Zatsepin and V. A. Kuzmin, "Upper Limit Of The Spectrum Of Cosmic Rays," JETP Lett. **4**, 78 (1966) [Pisma Zh. Eksp. Teor. Fiz. **4**, 114 (1966)].

[Zhe88] I. M. Zheleznykh, Proc. Neutrino '88, World Scientific, Boston, ed. J. Schreps, 528.

[Zuc02] P. Zucchelli, "A novel concept for a anti-nu/e / nu/e neutrino factory: The beta beam," Phys. Lett. B **532**, 166 (2002).

[Zwi97] E. Zwiebel and C. Heiles, "Magnetic fields in galaxies and beyond," Nature **385**, 131 (1997).